UNIVERSITY OF THESSALY
DEPARTMENT OF MECHANICAL ENGINEERING

Study of strain-induced transformation in low-alloy TRIP steels

ILIAS I. BELLAS

M. Sc. Thesis

2015

Approved by the members of the Examination Committee

First Examiner (Supervisor)	Dr. Gregory Haidemenopoulos Professor, Department of Mechanical Engineering, University of Thessaly
Second Examiner	Dr. Nikolaos Aravas Professor, Department of Mechanical Engineering, University of Thessaly
Third Examiner	Dr. Alexis Kermanidis Assistant Professor, Department of Mechanical Engineering, University of Thessaly

Abstract

Low alloy TRIP steels belong to the 1st generation of advanced high-strength steels (AHSS) produced mainly in sheets for automotive applications. They possess a multiphase microstructure consisting typically of ferrite, bainite and Retained Austenite (RA). The remarkable combination of strength and ductility/formability of these steels is due to the strain-induced transformation of retained austenite during the forming operations.

The modeling of the strain-induced transformation leads to a better understanding of the parameters involved such as: the chemical composition, austenite particle size and stress triaxiality. A new model was developed in this work, which describes the strain-induced transformation of retained austenite and which, for the first time, takes into account the austenite particle size.

The model was fitted to available experimental data. The stabilizing effect of retained austenite particle size refinement as well as the destabilizing effect of stress triaxiality were revealed. The contribution of stress-assisted transformation and the effect of effect of temperature were also determined.

In addition to modeling, a new technique, magnetic force microscopy (MFM), was applied to determine the evolution austenite grain size during the strain-induced transformation. Magnetic Force Microscopy (MFM) has been proved a reliable technique to identify austenite in the microstructure. The results indicated that larger retained austenite particles transform first at low strains, while smaller particles transform at higher strains.

The results of this thesis can be used to identify possible compositions and process routes for improved performance of these steels.

Acknowledgements

First and foremost, I would like to express my gratitude to my supervising Prof. G. N. Haidemenopoulos. There are no words, which can describe my appreciation to him. His knowledge and way of teaching are the reasons why I have been attracted in the Material's field. He is an excellent teacher and a role model for all of his students. He believed in my potentials and gave me the opportunity to research the interesting field of strain-induced transformation kinetics in low-alloy TRIP steels. I am indebted for his support, advice, inspiration and encouragement during my work and my stay in the department. He has always been by my side and devoted much time in order to help me complete this thesis. I am grateful for honoring me with his trust and giving me the opportunity to research interesting scientific fields. I will always remember the valuable and inspiring discussions I had with him and his well-targeted advices.

I would also like to thank Prof. N. Aravas for his support and the valuable comments on this thesis. He made me understand better the scientific field of mechanics.

I want to thank Prof. A. Kermanidis and his Phd student Peter Christodoulou for their support and guidance and for helping me kindly to perform the interrupted tension tests.

Special regards to Voestalpine Stahl company, which is located in Linz Austria and Dr. Daniel Krizan, for providing us the material for my studies and performing the retained austenite % measurements. Their support was significant.

I want to thank Prof. G. Constantinides of CUT for performing the MFM measurements presented in the present work. His contribution has been of great importance.

My working days in the laboratory of materials have become enjoyable due to the friendly working environment.

I would like to express my gratitude to Prof. Helena Kamoutsi for the assistance and technical support that she kindly provided. She along with my friend and Phd. student of the department Gioula Sarafoglou have always provided me with the technical support and experience needed to deliver the experiments presented in the present work and helped me during the metallography.

I greatly acknowledge the presence of Prof. Anna Zervaki in the laboratory of materials. She has always been very kind to all of the students and she has showed genuine interest on the progress of my work. She encouraged me during this trip and helped me believe in my potentials.

I want to thank the secretary of the department Heleana Pappa for the friendly environment she has created.

I would like to express my gratitude to all of my friends; Thomas, Dimitris, Stamatis, Nikolas, Thanos, John, Bill, George , Chryssa, Ioanna, Gregory, Giannoula, Sven and many other, who I may forget, for their continuous encouragement and friendship through all of these years.

Last but not least, I would like to express my gratitude to my family for their endless love and support; my father, my mother and my brother, who have always been by my side and their love helps me achieve my goals and become a better person.

Table of Contents

List of Figures 9

List of Tables 12

1 Introduction 13

1.1 Objective and scope 13

1.2 Thesis outline 14

2 Literature review 16

2.1 Introduction 16

2.2 Heat treatment of TRIP steels 19

2.3 Mechanical performance 20

2.4 General aspects of martensitic transformation 22

2.5 Driving force for martensitic transformation 24

2.6 Transformation plasticity 25

2.7 Alloying elements in TRIP steels 29

2.8 Factors affecting austenite stability 30

2.8.1 Proportion of phases 30

2.8.2 Stability of retained austenite 31

2.9 Effect of temperature and strain rate on plastic deformation of single – phase face-centered cubic (FCC) metals 36

2.9.1 Effect of temperature and strain rate on flow stress 36

2.9.2 Effect of temperature and strain rate on flow ductility 36

2.10 Modeling of the mechanical constitutive behavior 37

2.11 Conclusions 40

3 Model describing the kinetics of strain-induced transformation of dispersed austenite in low-alloy TRIP steels 41

3.1 Introduction 41

3.2 Model description 43

3.2.1 Martensitic nucleation and potency distribution of nucleation sites 43

3.3 Potency distribution for stress-assisted transformation 45

3.4 Potency distribution for strain-induced transformation 45

3.5 Overall Potency distribution and transformation fraction 46
3.6 Fitting the model to available experimental data 47
3.6.1 Experimental steels 47
3.6.2 Chemical driving force 48
3.6.3 Mechanical driving force 49
3.6.4 Frictional work of interfacial motion 51
3.6.5 Shape parameters and other constants 52
3.6.6 Fitting parameters 53
3.6.7 Effect of austenite composition 53
3.6.8 Effect of temperature 55
3.7 Implications of the model 56
3.7.1 Stress-assisted transformation 56
3.7.2 Effect of austenite particle size 58
3.7.3 Effect of stress triaxiality 59
3.8 Effect of various parameters used in this model 60
3.9 Implementation of the M_s^{σ} model for the calculation of the carbon content in the retained austenite 63
3.9.1 Calculation of the M_s^{σ} temperature 63
3.9.2 Material and heat treatment 65
3.9.3 Calculation of the carbon content of the retained austenite 66
4 Evolution of the austenite grain size during the strain-induced transformation 68
4.1 Introduction 68
4.2 Material 69
4.3 Optical microscopy and etching technique 71
4.4 Magnetic method and volume fraction results 73
4.5 Determination method of the fraction of retained austenite 74
4.6 Results extracted by the MFM 75
4.7 Results 79
5 Modeling of intercritical annealing 80

5.1 Introduction 80
5.2 The model 81
5.3 Results and discussion 83
5.4 Conclusions 90
6 Conclusions and Suggestions for future work 91
6.1 Conclusions 91
6.2 Suggestions for further work 93

List of Figures

Figure 1: Car components manufactured from TRIP steels [1] 17
Figure 2: Total elongation and tensile strength of TRIP steels in comparison with conventional high strength steels [2] 17
Figure 3: Microstructure of TRIP steel 18
Figure 4: Schematic representation of the heat treatment performed for TRIP steels (A: austenite, B: bainite, F: ferrite) [4] 19
Figure 5: Superior elongation observed in a TRIP steel compared to a dual phase steel with similar strength level [5] 20
Figure 6: Dislocations generated in ferrite due to transformation of austenite during deformation [7] 21
Figure 7: Schematic representation of the superior crash-worthiness of TRIP-assisted steels in comparison to other types of steels. The steels are tested with a prestrain of 0% and 5% in each case [8] 21
Figure 8: Schematic representation of the martensitic transformation. (a) the shape change predicted by Bain (b) shear at the interface between austenite and α' martensite (c) twinning at the interface of austenite and α' martensite [9] 22
Figure 9: Lattice distortion and correspondence proposed by BAIN for the FCC→BCC (BCT) martensitic transformation in iron alloys [11] 23
Figure 10: Schematic representation of homogeneous (a) lattice deformation and (b) shuffles [10] 24
Figure 11: Schematic representation of free energy curves of the matrix and martensite phases as a function of temperature [11] 24
Figure 12: Schematic representation of (a) stress assisted and (b) strain-induced martensite volume fraction formed as a function of strain [13] 26
Figure 13: Schematic representation of stress assisted and strain-induced regimes of mechanically induced martensitic transformation [14] 27
Figure 14: The transformation induced martensitic transformation in metastable austenitic stainless steels is enhaced by low temperatures [15] 29
Figure 15: Effect of bainite transformation time on C content in retained austenite [19] 31
Figure 16: Effect of carbon content and plastic strain in the transformation 32
Figure 17: Effect of strain rate on the formation of strain-induced α'-martensite in AISI 304 austenitic stainless steel examined in uniaxial tension [24] 34
Figure 18: Effect of strain rate on the flow curve at different test temperatures [25] 35
Figure 19: Comparison of the results obtained by equation 2.4 with the experimental data. (a) Behavior of material above M_s^{σ}(b) behavior of material bellow M_s^{σ}[28] 38

Figure 20: Comparison of experimental and calculated stress strain curves for 14Ni-7Cr stainless steel studied by Naturani, et al. [29] 39
Figure 21: Models for the strain-induced martensitic transformation kinetics [37] 42
Figure 22: Change of the energy per unit area for three different thicknesses 44
Figure 23: Variation of chemical driving force with temperature 49
Figure 24: Variation of operational sites under applied stress with yield strength for Steel 1 at 20^{o}C 50
Figure 25: Frictional work of interfacial motion as a function of mole fraction of C and Mn in austenite. The two families of curves correspond to the linear and the 2/3 power-law approximation respectively 52
Figure 26: Variation of martensite volume fraction with axial strain. Comparison of model and experimental data: (a) 10^{o}C, (b) 20^{o}C, (c) 65^{o}C for Steels 1, 2, 3 and (d) 20^{o}C for Steels 4/ 10, 4/60, 4/480 54
Figure 27: Variation of martensite volume fraction with axial strain. Comparison of model with experimental data for (a) Steel 1 (b) Steel 2 and (c) Steel 3 55
Figure 28: Variation of critical value of n* for martensitic transformation with temperature for Steels 1, 2 and 3 56
Figure 29: The fraction martensite formed through stress-assisted transformation (f_{SA}) as a function of testing temperature for Steels 1, 2 and 3 57
Figure 30: Variation of operational sites under applied stress 57
Figure 31: Effect of particle size on the curve for a steel with 0.8 mass% C (T=20^{o}C). R is the radius of the spherical austenite particles 58
Figure 32: Effect of stress triaxiality on the curve for a steel with 1 mass% C (T=20^{o}C, R=1μm and R=0.3μm) 59
Figure 33: Variation of additional sites produced by plastic strain with axial strain for Steel 1 for three different values of the parameter k 60
Figure 34: Variation of additional sites produced by plastic strain with axial strain for Steel 1 for three different values of the parameter n 61
Figure 35: Variation of operational sites under applied stress with critical value of for stress-assisted martensitic transformation for Steel 1 62
Figure 36: Variation of operational sites under applied stress with critical value of for stress-assisted martensitic transformation for Steel 1 63
Figure 37: Representation of heat treatment A and B for TRIP steel 700 [30] 65
Figure 38: Tensile specimen geometry 70
Figure 39: Demonstration of pre-strain test experiment 70
Figure 40: Engineering stress-strain curve in TRIP 700 steel 71

Figure 41: Microstructure of TRIP 700 steel (a) in untransformed material (15.8% RA) (b) after 4% deformation (13.7% RA) (c) after 8% deformation (12.1% RA) (d) after 12% deformation (7.1% RA) 72
Figure 42: Deflection (a,c) and Magnetic (b,d) image of a TRIP steel (ε=4%). 2-d (a,b) and 3-d (c,d) visualizations 76
Figure 43: Deflection (a,c) and Magnetic (b,d) image of a TRIP steel (ε=4%). 2-d (a,b) and 3-d (c,d) visualizations 77
Figure 44: Evolution of retained austenite volume fraction (a) and mean grain size (b) as a function of specimen deformation 77
Figure 45: Variation of martensite volume fraction f with axial strain ε. Comparison of model and experimental data at 25^{o}C for TRIP Steel 700 78
Figure 46: Schematic representation of the two stage heat treatment typically applied in TRIP steels [69] 80
Figure 47: Geometrical model for austenite formation during intercritical annealing 81
Figure 48: Concentration profiles for (a) C (c) Mn (e) Si in steel 1 , (b) C (d) Mn and (f) Al in steel 2 across the austenite-ferrite phase boundary during intercritical annealing after 10s, 50s, 90s at 817 ^{o}C. The arrow indicates the direction of movement of the phase boundary during intercritical annealing. Whereas the C is expected to reach equilibrium composition, the substitutional solutes are not 86
Figure 49: Austenite volume fraction as a function of annealing time for (a) steel 1and (b) steel 2 at 1050K (777 ^{o}C), 1070K (797 ^{o}C) and 1090K (817 ^{o}C) 87
Figure 50: Interface velocity as function of annealing 88
Figure 51: Austenite volume fraction as a function of annealing 88
Figure 52: Position of interface as a function of annealing 89
Figure 53: Concentration profiles for (a) C and (b) Mn mass contents in % in steel 1and steel 2, after annealing at 817^{o}C for 90s 90

List of Tables

Table 1: Chemical composition of typical TRIP steels 30
Table 2: Chemical composition (in mass%) of the steels considered in this study 47
Table 3 Values of various parameters used in the model describing the kinetics of evolution of martensite during strain-induced transformation 53
Table 4: Values of various parameters used in the M_S^σ model 64
Table 5: Chemical composition (in mass%) of the steel under consideration 65
Table 6: Tensile properties of TRIP 700 (A) and (B) materials 66
Table 7: Chemical composition (in mass%) of the retained austenite of Steel (A) and (B) for the linear and the 2/3 power low M_S^σ model 66
Table 8: Chemical composition in (%) weight of the steel 69
Table 9: Tensile properties of TRIP steel 700 71
Table 10: Measurments of retained austenite (RA) prior and after pre-strain test 74
Table 11: Results from image grains analysis using the threshold method 77
Table 12: Chemical composition (in mass %) of TRIP steels employed in simulations 84

1 Introduction

1.1 Objective and scope

Improved fuel consumption, weight reduction and high passenger safety are only some of the reasons, which make it essential for the automotive industries to develop steels with enhanced mechanical properties. The development of steels during the last twenty years has shown that TRIP steels constitute a new category of sheet steels, in terms of their high strength and enhanced formability. The Low-alloy Transformation-Induced Plasticity (TRIP) steels, which present great industrial importance, possess a multiphase microstructure, which consists typically of ferrite, bainite and retained austenite. The retained austenite, with a typical volume fraction of 10-15%, is in the form of particle dispersion. The high uniform elongation, and hence high formability, of these steels results from the strain-induced martensitic transformation of retained austenite. This transformation increases significantly the hardening rate and therefore improves the ductility of the material in comparison to similar high strength steels, which do not present TRIP effect.

The key constituent of the TRIP steel microstructure is retained austenite, which is metastable at room temperature. Basic interest of the present thesis is the investigation of the stability of the retained austenite in low-alloy TRIP steels and how this stability influences transformation plasticity.

The present thesis develops a model, describing the kinetics of the evolution of martensite volume fraction during strain-induced transformation of dispersed austenite in low-alloy TRIP steels. The two distinct mechanisms responsible for the mechanically induced martensitic transformation are described in detail. The model takes into account the effects of several parameters influencing the kinetics of martensitic transformation .An effort is made to distinguish the individual effect of each one of the parameters influencing austenite stability. By understanding clearly the impact of each parameter, we can then move backwards and design the optimal heat treatment which results to the desirable mechanical characteristics for the material. A thorough understanding of the relation between microstructure and mechanical properties is essential in order to proceed to improvements of TRIP steels. The present work, therefore, aims at addressing the following research objectives:

- A mathematical model describing the kinetics of strain-induced transformation of retained austenite in low-alloy TRIP steels, which is in the form of particles into the microstructure. The model takes into account the influence of chemical composition, temperature, austenite particle size and stress triaxiality. The identification of the effect of each one of the microstructural parameters separately and their contribution on the martensitic transformation and the corresponding austenite stability is presented.

- Non linear curve fitting of the model in available experimental data, in order to predict the transformation behavior of low-alloy TRIP steels presenting retained austenite of different chemical stability in the form of dispersion.

- A reliable and accurate experimental procedure to investigate the microstructural characteristics of low-alloy TRIP steels. A correlation of the microstructure description to the macroscopic mechanical properties and specifically to the martensitic transformation has been examined.

- Experimental identification of the transformation kinetics of the retained austenite during deformation. In the experimental data exported non-linear curve fitting of the model described was applied. Evaluation of the results predicted by the model is presented.

- The strong stabilizing effect of austenite particle size refinement. Pre-strain tests were carried out in order to observe the evolution of mean austenite particle size during deformation. The influence of the austenitic grain size on the overall stress-strain behavior of low-alloy TRIP 700 steel is analyzed.

- The description of M_s^{σ} temperature model and how this model can be used in order to predict the carbon partitioning of the retained austenite.

- Simulation of the intercritical annealing with the use of computational softwares such as: Thermo-Calc and Dictra. The simulation can assist the design of the intercritical annealing in low-alloy TRIP steels.

All of these objectives could provide a good insight for further improvement of the performance of low-alloy TRIP steels, as well as for the optimization of the processing parameters.

1.2 Thesis outline

This thesis continues with the following chapters:

In Chapter 2 literature review of TRIP phenomenon is discussed. The reason why TRIP steels are so widely used in engineering applications is addressed. This chapter describes in detail the two distinct mechanisms, which can mechanically induce the martensitic transformation. General aspects of martensitic transformation as well as several parameters influencing austenite stability are discussed.
Chapter 3 describes the model applied in the present work in order to describe the kinetics of the evolution of martensite volume fraction during strain-induced transformation in low-alloy TRIP steels. The model has been fitted to available experimental data regarding the evolution of martensite as a function of plastic strain for several steels containing austenitic dispersions. The results concerning the fitting are discussed. The parameters influencing austenite stability and as a result the

transformation kinetics of the model are presented. Additionally, this chapter presents a description of the M_s^{σ} temperature model.

Chapter 4 describes the evolution of the austenite grain size during the strain-induced transformation. Here, the deformation and transformation of austenite grains obtained from uniaxial tensile tests are investigated with the combination of different methods. The model described in Chapter 3 was applied in the experimental data. Results concerning the stabilizing impact of the size of the retained austenite in the strain-induced transformation kinetics are presented.

Chapter 5 focuses on the modeling of intercritical annealing for two different low-alloy TRIP steels with the use of computational thermodynamic and kinetics software. The results obtained are discussed.

Finally, in chapter 6, the conclusions from the current research are presented and further suggestions for future work and development are proposed.

2 Literature review

2.1 Introduction

The new challenge for optimizing vehicle structures for weight is to develop steels with enhanced strength without compromising formability. TRIP steels are widely used in engineering applications due to their excellent combination of formability, high tensile strengths, weldability and good corrosion resistance.

Due to increasingly strict safety regulations and the need to reduce the fuel consumption, the car industry has become increasingly aware of the structural materials of better performance. The strength-elongation ratio of the austenitic stainless steels can be adjusted within a wide range by work hardening. Although, TRIP steels have a higher material cost than the plain carbon steel grades, their use can be cost effective if their good formability and high strength are reasonably well exploited in the part design and manufacturing process.

As the TRIP steels show a better strength/elongation ratio compared to almost any other metallic structural materials used in car body structures (Figure 1), they have become an attractive group of materials to be used in crash relevant structures. Components, which could be produced from these steel types, include side impact bars, unexposed chassis and wheel rims. These steels offer scope for the production of more economical, safe and environmentally friendly lightweight vehicles with potential for savings in raw materials, energy and reduction of harmful emissions.

For the last 20 years now, the steel industry corresponded to this demand by introducing new steel categories as the high strength low-alloy steels (HSLA), the interstitial free high strength steels (IF-HS) and the dual phase steels (DP-steels). However, the last years the investigation of TRIP steels has been started and as it can be seen from Figure 2, their mechanical properties are different from all the previous steel grades. TRIP steels offer very attractive combination of elongation and tensile strength. A comparison of different steel families can be made by the product $R_m \times A_{80}$ (R_m stands for tensile strength and A_{80} for total % elongation) which can be above 20.000 MPa × % for TRIP steels. The absolute elongation values can be as high as the values of the high-strength IF steels, which present the best formable high-strength steels developed so far. The tensile strength range of TRIP steels is 650 to 950 MPa and is much higher than today's tensile strength range of cold formable steels.

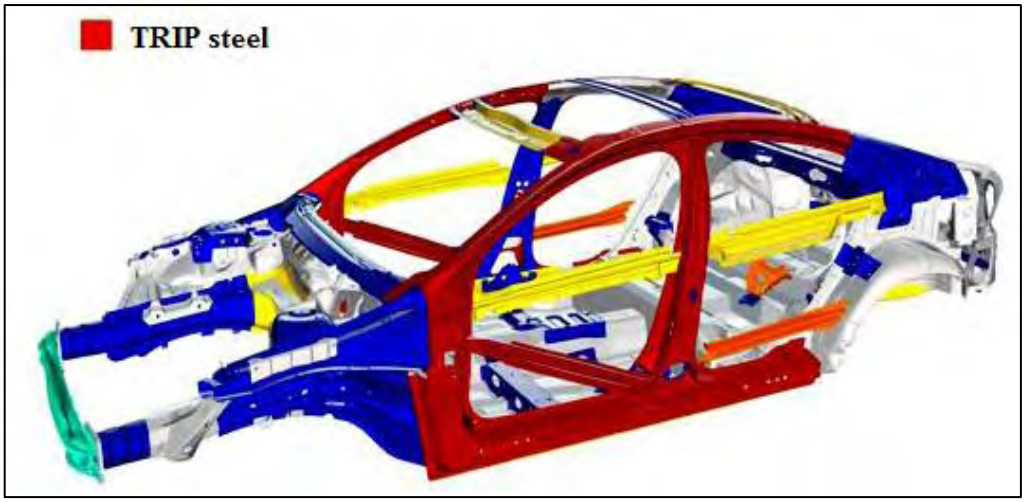

Figure 1: Car components manufactured from TRIP steels [1]

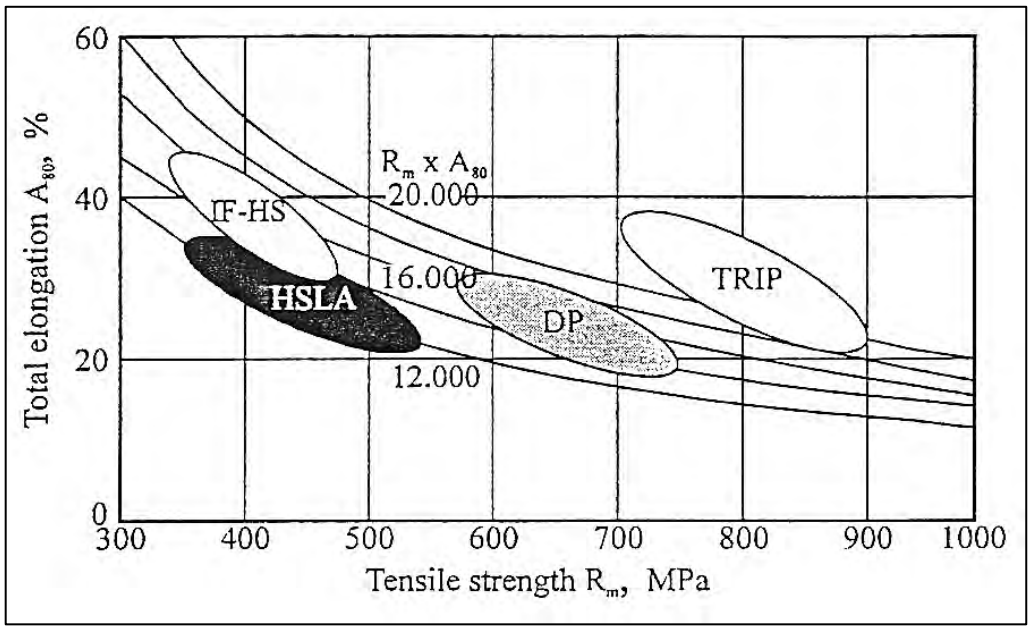

Figure 2: Total elongation and tensile strength of TRIP steels in comparison with conventional high strength steels [2]

The high formability in TRIP steels is attributed to the transformation-induced plasticity of retained austenite. The amount and stability of retained austenite are the key factors, which affect its transformation behavior during straining. The microstructure of low-alloy TRIP steels typically consists of ferrite, bainite and retained austenite. An electron microscopy picture of a typical TRIP microstructure is shown in Figure 3.

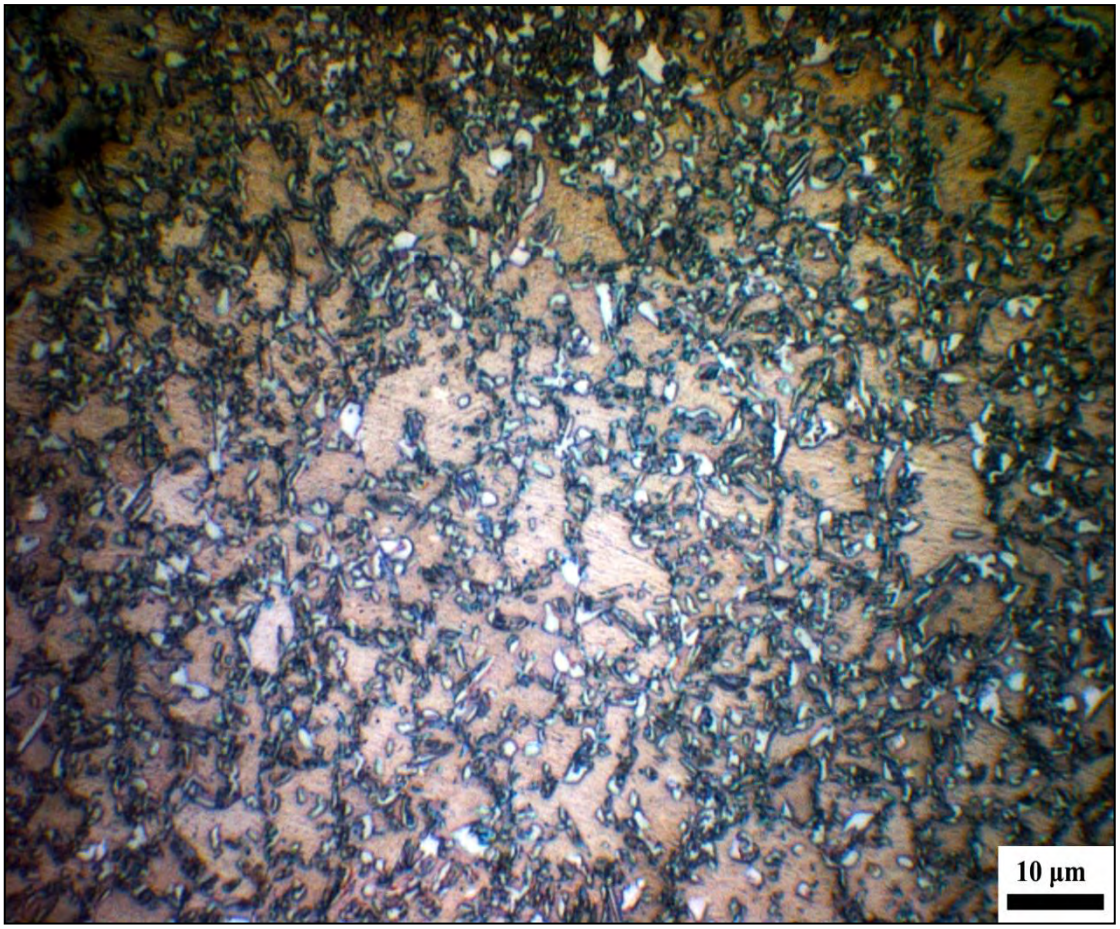

Figure 3: Microstructure of TRIP steel

The microstructural evolution and the mechanical behavior of TRIP steels are sensitive to chemical composition, temperature, austenite grain size and stress and strain state.

Ferrite has a body-centered cubic (BCC) lattice and it is the softest phase among the constituent phases. The size of ferrite grains in a typical TRIP steel are in the range of $5 - 10$ μm [3]. The microstructure of bainite consists of fine platelets of ferrite that form via a displacive (diffusionless) mechanism and cementite (Fe3C) that precipitates in-between and/or inside ferrite plates. In general, bainite is harder than intercritical ferrite due to its finer structure as well as the presence of carbide precipitations. The bainite in TRIP steels is generally referred to as "bainitic ferrite" and it is not exactly the same as the above explained typical bainite. The bainitic ferrite in TRIP steels is essentially carbide-free due to the presence of Al or Si, which restricts (or postpones) carbide precipitation. Austenite is normally stable at high temperatures and has a face-centered cubic (FCC) lattice. Carbon enrichment and the constraining effect from neighboring grains can stabilize austenite at room temperature. The strength of retained austenite in TRIP steels is generally higher than that of the ferritic constituents due to the strengthening effect of carbon. The unique mechanical properties of TRIP steels are mainly attributed to the presence of the metastable austenite phase in the room temperature microstructure. Upon application

of mechanical and thermal loads, the metastable retained austenite can transform into a harder martensitic phase, which would increase the effective strength of the material.

2.2 Heat treatment of TRIP steels

After cold rolling the steels undergo a two-step heat treatment shown in Figure 4, consisting of intercritical annealing followed by isothermal annealing at a lower temperature, to stabilize the retained austenite via the bainitic transformation.

At the first step, the specimen of steel is heated until a temperature of 700-900 ^{o}C where intercritical annealing takes place. The temperature and time (almost 3 minutes) of intercritical annealing are chosen in a way that a microstructure of 50% ferrite and 50% austenite to be formed. After intercritical annealing quenching is performed to an intermediate temperature above the martensite start temperature, which allows the bainite transformation to occur during isothermal holding. Bainite isothermal transformation takes place at temperatures 350-450 ^{o}C and times 200-600 seconds and leads to the transformation of a part of austenite to bainite. The amount of austenite transformed to bainite depends on the temperature and time of the bainite isothermal transformation. Therefore, after bainite isothermal transformation the steel obtains a microstructure of 50% ferrite, 35-45% bainite and 5-15% austenite. In this step, the remaining austenite is further enriched with carbon, which shifts the martensite start temperature below room temperature. Finally, the specimen of steel is quenched in room temperature without austenite transformed to martensite and the desirable microstructure of 50% ferrite, 35-45% bainite and 15-5% austenite remains.

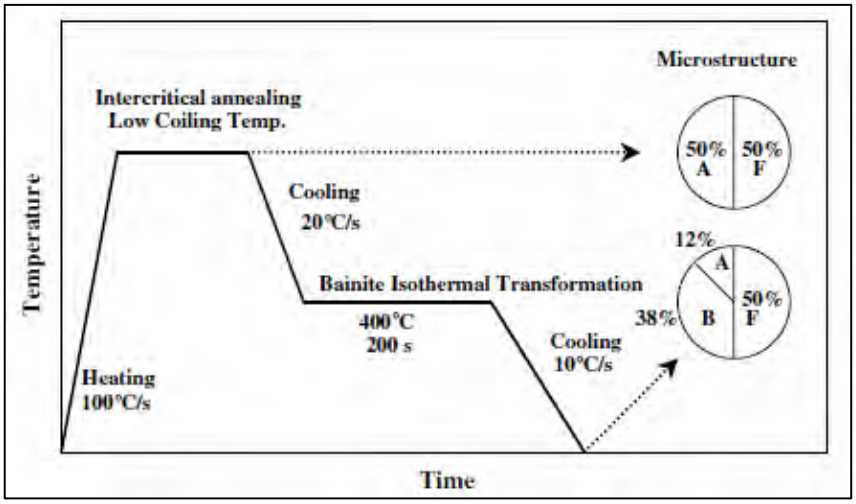

Figure 4: Schematic representation of the heat treatment performed for TRIP steels (A: austenite, B: bainite, F: ferrite) [4]

2.3 Mechanical performance

The reason why TRIP steels are so widely used is that they present excellent mechanical behavior. They present superior uniform elongation in comparison to other similar steels such as dual phase steels. TRIP steels yield greater elongation compared to dual phase steels and this property derives mainly to the strain-induced martensitic transformation of the retained austenite as it can be seen in Figure 5 bellow.

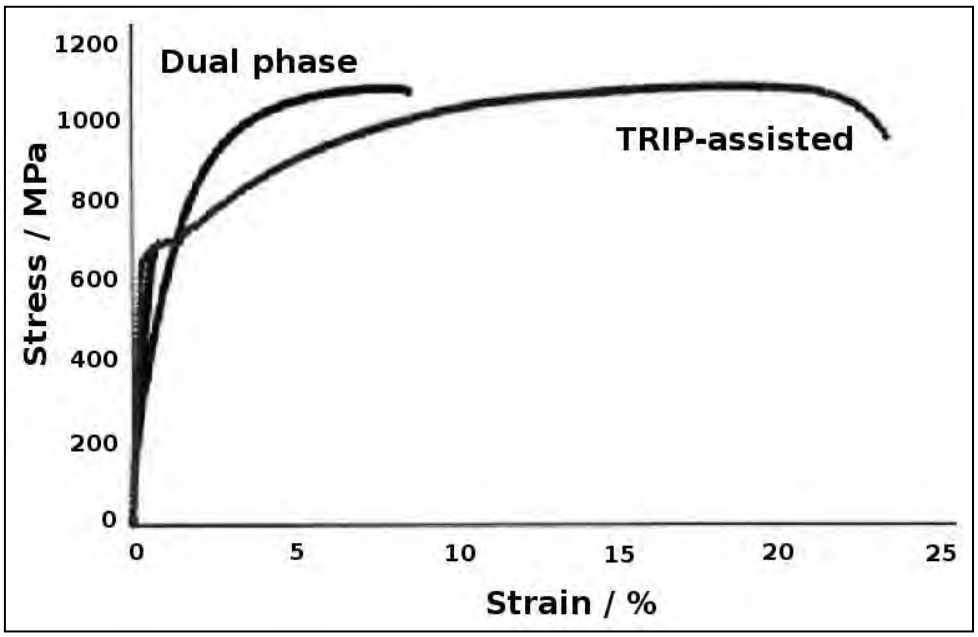

Figure 5: Superior elongation observed in a TRIP steel compared to a dual phase steel with similar strength level [5]

According to the work of Bhadeshia [6] the transformation strains themselves can contribute at most 2% to the observed elongation given the small fraction of austenite present in these materials. Moreover, the volume expansion accompanying the martensitic transformation leads to the generation of dislocations in the adjacent ferrite as seen in Figure 6, which freshly produced dislocations, can contribute in the deformation process [7]. The martensite formed during strain-induced transformation inherits the high carbon content of the austenite. The martensite produced during deformation does not impair the ductility.

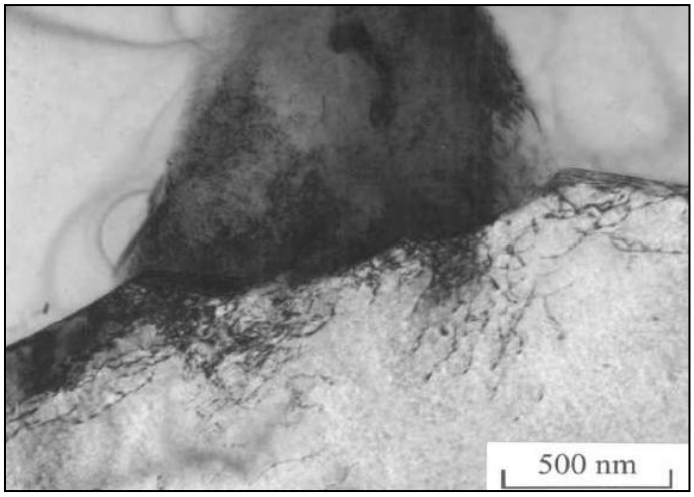

Figure 6: Dislocations generated in ferrite due to transformation of austenite during deformation [7]

TRIP steels exhibit excellent formability in comparison to several other steels with comparable strength. One of the main reasons, why these steels are so widely used in automotive products is their superior crash-worthiness. In a crash scenario, the strain rate may well exceed 250 s^{-1} and the prevailing state of stress and strain may be much more complex than iniaxial tension.
In Figure 7 bellow it is presented the superior crash-worthiness of TRIP steels in comparison to other types of steels.

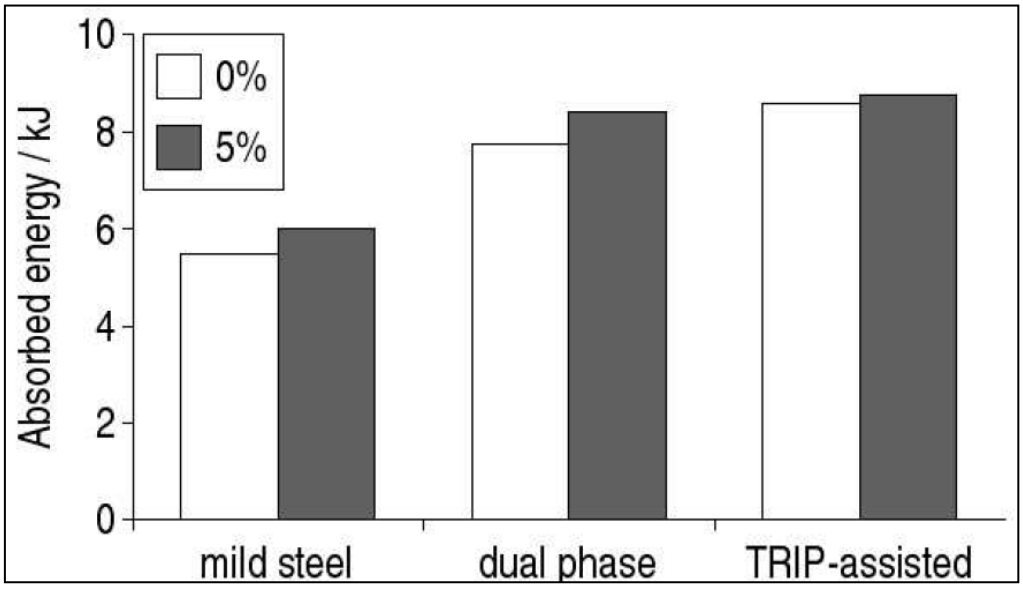

Figure 7: Schematic representation of the superior crash-worthiness of TRIP-assisted steels in comparison to other types of steels. The steels are tested with a prestrain of 0% and 5% in each case [8]

In the next section a description of martensitic transformation is presented, followed by a more specific discussion of the transformation plasticity phenomenon.

2.4 General aspects of martensitic transformation

One of the most important technological procedures is the hardening of the steel upon cooling. This strengthening is a result of structural change, which is called martensitic transformation. Rapid quenching of austenite to room temperature often results in the formation of martensite, in which the carbon, formerly in the solid solution in the austenite, remains in the exact same solution in the newly formed martenstitic phase. Martensite is of great importance in steels where it can confer an outstanding combination of strength and toughness. The stable grains need really low temperatures in order to transform, but the less stable austenite grains are prone to both a spontaneous transformation upon cooling and deforming-induced martensitic transformation.

Many materials other than steel are known to exhibit the same type of solid-state phase transformation, known as a martensitic transformation. Martensite occurs in, for example, nonferrous alloys, pure metals, ceramics, minerals, inorganic compounds, solidified gases and polymers.

Martenisic transformation can be considered to be a first-order solid-state structural change, which is:

a) displacive,
b) diffusionless and
c) dominated in kinetics and morphology by the strain energy arising from shear-like displacements.

This set of three characteristics is regarded as both necessary and sufficient to define a martensitic transformation.

Martensitic transformation is heterogeneous in nature and proceeds by the propagation of relatively sharp interfaces. The lack of diffusion creates a very precise orientation relationship between the parent austenite and the martensite product.

A martensitic phase transformation can be considered as the spontaneous plastic deformation of a crystalline solid in response to internal chemical forces. The phenomenogical theory was adopted in order to understand better and more precisely the martensitic transformation. According to this theory the transformation is accomplished by the Bain distortion and a shear deformation at the interface between austenite and martensite. The shear at the interface occurs by either slip or twinning. Figure 8 bellow presents a schematic representation of the martensitic transformation.

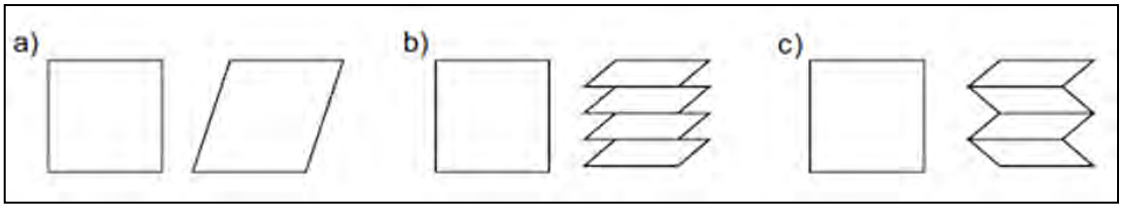

Figure 8: Schematic representation of the martensitic transformation. (a) the shape change predicted by Bain (b) shear at the interface between austenite and α' martensite (c) twinning at the interface of austenite and α' martensite [9]

The transformation produces a shear strain as well as a volume expansion, which can vary from 0 to 5 percent, depending upon the chemical composition of the alloy. The Bain distortion, which helps visualize the lattice correspondence between the parent and product phases is presented in Figure 9. As a consequence of Bain strain the correspondence related cell in the parent phase (indicated by bold lines) becomes a unit cell in martensite.

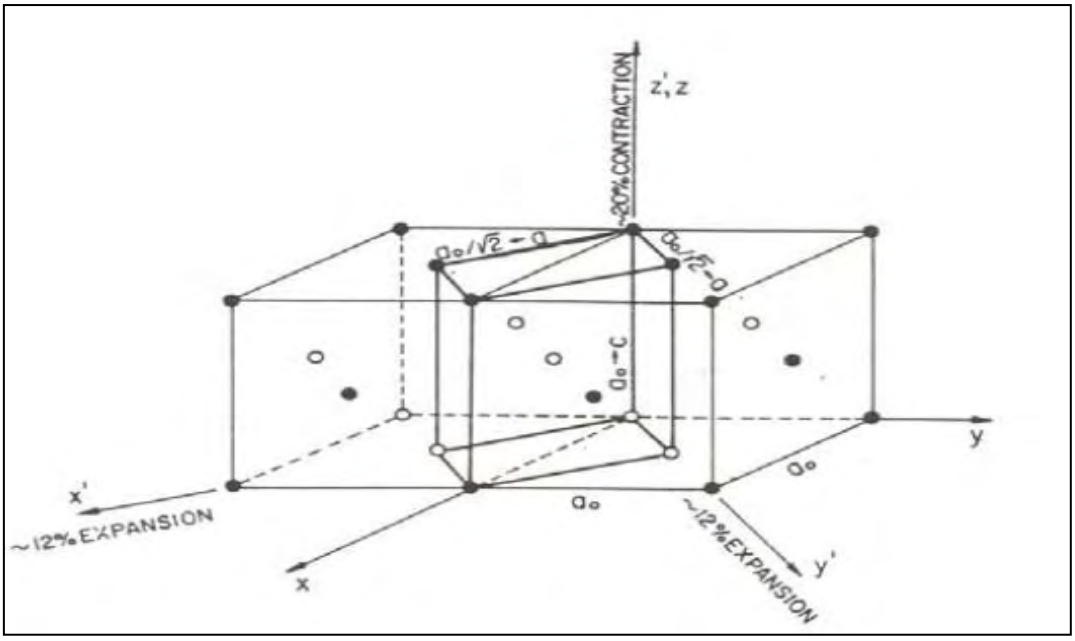

Figure 9: Lattice distortion and correspondence proposed by BAIN for the FCC→BCC (BCT) martensitic transformation in iron alloys [11]

The part of the lattice deformation which accomplishes the change in crystal structure, is a pure deformation, and is usually called the Bain distortion or Bain strain, the term originally adopted for the FCC→BCC (BCT) martensitic transformation in ferrous alloys.On the other hand, a shuffle is a coordinated shift of atoms within a unit cell, which may change the structure but, in itself, does not produce a homogenous lattice-distortive strain. Figure 10 illustrates, in simple form, the distinction between lattice-distortive and shuffle displacements. Even though displacive phase transformations may generally comprise various combinations of lattice deformations and shuffles, martensitic transformation is typically dominated by lattice deformations rather than by shuffles, although shuffles are not excluded.

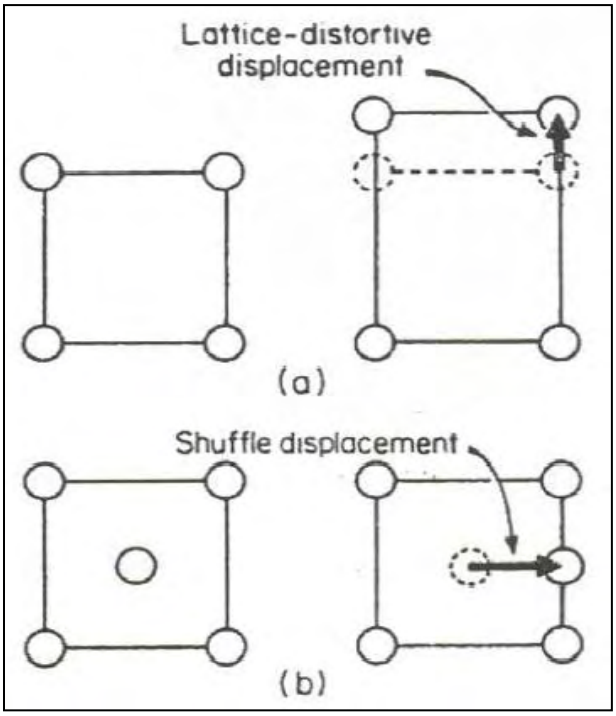

Figure 10: Schematic representation of homogeneous (a) lattice deformation and (b) shuffles [10]

2.5 Driving force for martensitic transformation

At any given temperature, there exists one preferential crystallographic structure corresponding to the lowest energy level. At relatively low temperatures the martensite phase has the thermodynamically preferred crystal structure, so that upon steel's quenching, the original austenite structure, stable at high temperatures, tends to transform into the more stable martensite. Figure 11 shows schematically the change in chemical free energies of martensite and austenite (parent phase) with temperature.

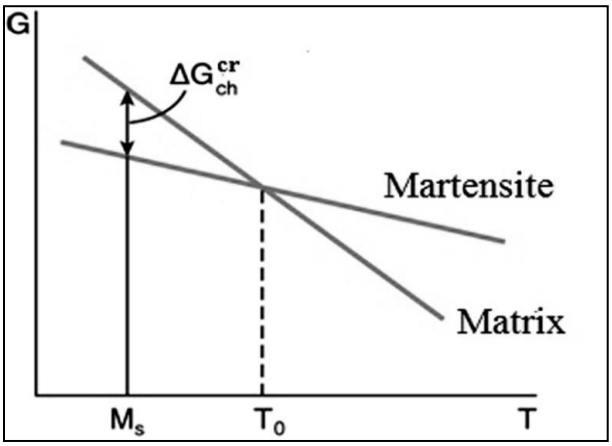

Figure 11: Schematic representation of free energy curves of the matrix and martensite phases as a function of temperature [11]

In T_o temperature the free energy of the two phases takes the same value, but as the temperature decreases, the difference of the free energy between the two phases enhances. The chemical driving force ΔG_{ch} is the difference between the free energy of BCC and FCC structures. At high temperatures the austenite has lower free energy, whereas at lower temperatures body-centered cubic (BCC) ferrite has lower free energy and is, therefore, the stable phase. In T_o temperature $\Delta G_{ch} = 0$, while for temperatures lower than T_o $\Delta G_{ch} < 0$. As we can observe the chemical driving force increases (becomes more negative) with a reduction in temperature. M_s is defined as the temperature, at which the chemical driving force takes a critical value ΔG_{ch}^{cr} needed to overcome the martensitic transformation energy. Spontaneous martensitic transformation takes place only if the difference between the chemical free energies of austenite and martensite reaches the critical value ΔG_{ch}^{cr}. The M_s temperature for the nominal composition of low-alloyed TRIP steel is about 350 ^{o}C. The M_s temperature for the austenite in TRIP steels is well below room temperature since the retained austenite has been enriched in carbon during the bainitic holding process. However, martensitic transformation can take place at temperatures higher than the M_s temperature, with the aid of mechanical driving force, as discussed in the following section.

When M_s is surpassed, the martensitic transformation continues upon further cooling and stops in M_f temperature.

2.6 Transformation plasticity

As denoted by the stress-temperature diagram of Figure 13 there are two modes of interaction of deformation with transformation termed: (a) stress-assisted transformation in which applied stress assists the operation of the same nucleation sites controlling transformation on cooling, and (b) strain-induced transformation controlled by the production of new nucleation sites with plastic strain. The stability of dispersed austenite against mechanically induced transformation is characterized by the M_s^{σ} temperature, while the stability of austenite against transformation on cooling is characterized by the M_s temperature. Due to the transformation dilation, this temperature is stress-state dependent.

Strain-induced martensitic transformation is of great importance for the mechanical behavior of austenitic stainless steels. The martensitic shape change itself contributes a mode of deformation, called TRansformation Induced Plasticity (TRIP), which can influence stress-strain behavior in important ways. This unique process allows for the design of materials which take advantage of the transformation itself, not simply the properties of transformation product. The notion of exploiting the properties of such a structural change is quite novel with respect to the classical view of the relationships between a material's structure and its properties.

TRIP steels are generally stable at room temperature. Without mechanical contribution in these steels the spontaneous martensite transformation starts at the M_S

temperature. As mentioned above the alloying elements could have a stabilizing or destabilizing impact on the austenite.

It is useful to distinguish between the roles of elastic stress and plastic strain in influencing the martensitic nucleation process. Martensitic transformation can also be triggered with the aid of external mechanical loading at higher temperatures. The applied stress generates a positive contribution to the chemical driving force for austenite to martsensite to transformation and thus the elastic deformation generates stress-assisted martensitic transformation at temperatures above M_s but below M_s^σ temperature. . In other words, the critical driving force for nucleating the sites that normally operate without any external stress at M_s can be attained at temperatures above M_s since the mechanical driving force makes up for the reduced chemical driving force at such higher temperatures. Stress-assisted transformation occurs bellow the yield strength of the austenite phase with the aid of the applied stress. This transformation is called stress-assisted (S.A.T.) because the existing nucleation sites are simply aided mechanically by the thermodynamic contribution of the applied stress.

Martensitic transformation can also occur above the M_s^σ temperatre and the transformation is assisted by the applied strain. Above M_s^σ significant plastic flow precedes the transformation, and an additional contribution to transformation can arise from the production of new and more potent nucleation sites by plastic deformation. This transformation is defined as strain-induced (S.I.T.). These nucleation sites are often grouped under the name shear-bands and the nucleation according to Olson and Cohen [12] occurs at the intersection of these shear-bands. In Figure 12 bellow it is presented the martensite volume fraction formed as a function of strain for the two distinct mechanisms.

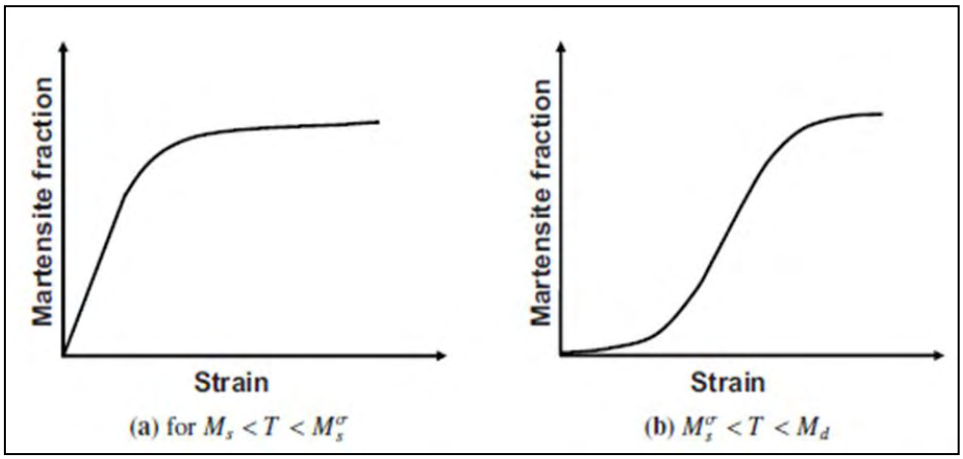

Figure 12: Schematic representation of (a) stress assisted and (b) strain-induced martensite volume fraction formed as a function of strain [13]

The three different martensitic transformation events of the deformation-induced martensitic transformation are plotted in Figure 13.

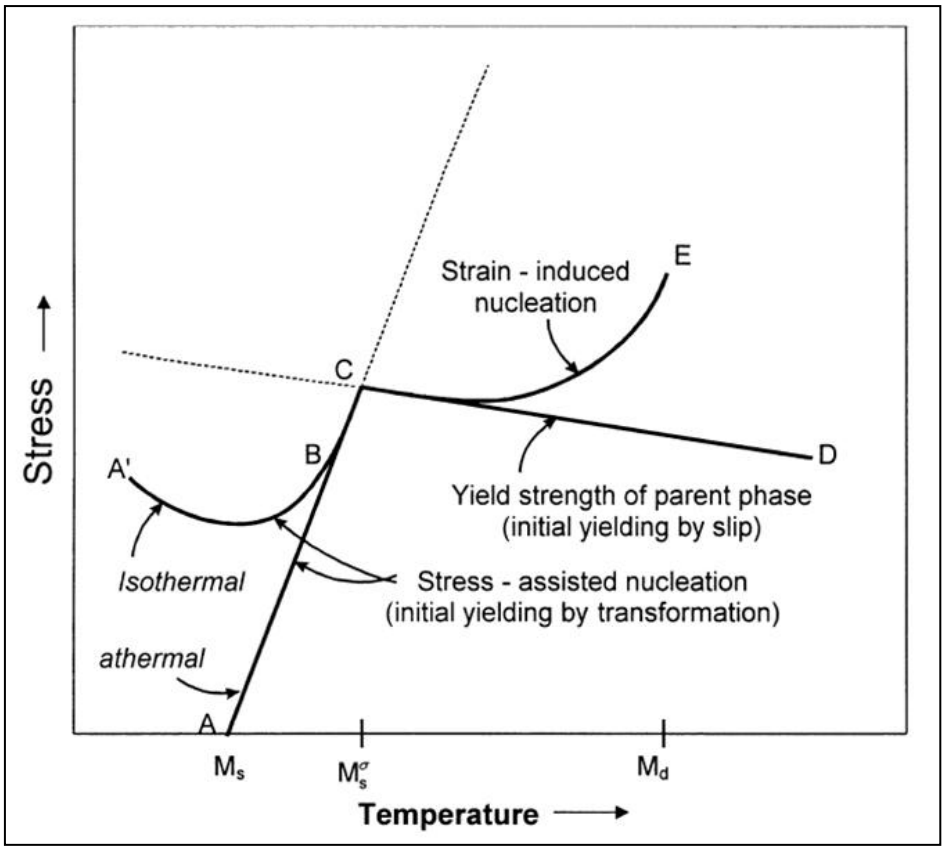

Figure 13: Schematic representation of stress assisted and strain-induced regimes of mechanically induced martensitic transformation [14]

Below the M_s (point A) temperature martensite will form spontaneously without any aid of stress. Deformation can stimulate the kinetics of solid-state phase transformations through both the thermodynamic effect of the applied stress and the production of new catalyzing defects by plastic strain. Between the M_s and M_s^σ martensite forms with the aid of applied stress. As the temperature raises the stress needed to initiate the transformation increases. Above M_s^σ (point C) the transformation is initiated after the applied stress reaches or even exceeds the yield strength of austenite and yielding occurs first by slip and then martensite can form at the new more potent nucleation sites newly generated by the slip. These new nucleation sites are created due to plastic deformation and this is the reason why this mechanism is defined as strain-induced transformation. The M_s^σ temperature defines an approximate boundary between the temperature regimes where separate modes of transformation dominate. Near the M_s^σ temperature both modes will operate. The plastic deformation of austenite could continue till fracture, which is point E in the figure presented above. This point also defines M_d temperature, which is the maximum temperature above which martensite transformation cannot be induced by deformation because the chemical driving force is so small that it is impossible to

nucleate martensite. With increasing temperature above M_s^σ the yield stress decreases and the stress necessary to initiate strain-induced transformation is close to the yield stress at temperatures just above M_s^σ , but it is significantly higher than the yield stress at higher temperatures. Due to the interaction between stress triaxiality and transformation volume change, the M_s^σ and M_d temperatures are stress-state dependent. For the case of austenite dispersions in Fe-C-Mn-Si alloys, the M_s^σ temperature depends on the following factors:

- Chemical composition of the austenite particles. Chemical composition (mainly carbon content) affects the chemical driving force of the martensitic transformation.
- Austenite particle size, which affects the probability of finding nucleation sites in the particle.
- Stress state. Stress triaxiality influences the transformation volume change of the retained austenite either by enhancing or by retarding the transformation kinetics, depending on the stress state.
- Strength of the matrix, which affects the mechanical driving force contribution to the total driving force for the martensitic transformation.

$$M_s^\sigma = f(x_{C,} x_{Mn,} V_P, \sigma_{y,} \sigma_h / \bar{\sigma})$$

The M_d temperature was found to be an inconvenient measure of the austenite stability since it is hard to measure; hence Angel [15] introduced the M_{d30} temperature. This is the temperature where 50% martensite will form at 30% true strain. Angel formulated the following empirical relation for the M_{d30} temperature:

$$M_{d30}=413-462(C+N)-9.2(Si)-8.1(Mn)-13.7(Cr)-9.5(Ni)-18.5(Mo) \quad (2.1)$$

According to Angel's research of the effect of temperature on strain-induced martensitic transformation during tensile loading, the amount of martensite formed decreases with an increase of temperature. Chemical driving force and stacking fault energy are temperature dependent parameters. As a result the formation of strain-induced α' martensite is affected by both of these parameters. An example of the temperature dependence of the strain-induced martensite during uniaxial tensile is presented below in Figure 14. This behavior presented in the following figure is attributed to the decrease of chemical driving force with increasing temperature. Although, the stacking fault energy is known to increase with increasing temperature, its role in the suppression of the α' martensite transformation has not been explicitly demonstrated in literature.

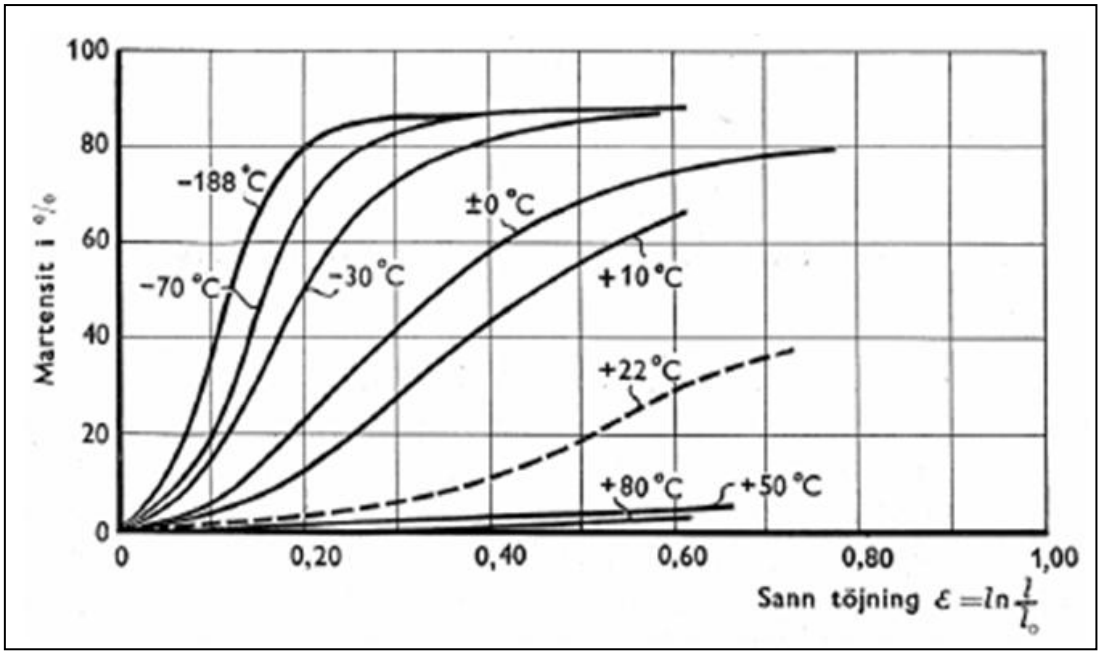

Figure 14: The transformation induced martensitic transformation in metastable austenitic stainless steels is enhaced by low temperatures [15]

The dominant martensitic phase formed in metastable austenitic stainless steels is α' martensite, which is body-centere tetragonal (bct). Due to the small amounts of interstitial carbon, a general approximation can be made that the α' martensite structure could be assumed to be close to body-centered cubic (bcc) structure.

2.7 Alloying elements in TRIP steels

The key factor in the selection of alloying elements is the improvement of the stability of retained austenite by using low-alloy concept. Below, it is addressed a brief report on the effect of common alloying elements in low-alloyed TRIP steels:

Carbon is the most effective austenite stabilizer and it improves the strength of austenite and martensite. Interstitial atoms, like carbon promote the FCC crystal structure and cause significant solid solution strengthening.

Apart from carbon other alloying elements are added in TRIP steels. Those elements ensure: a) the optimization of the volume fraction of retained austenite, b) the increase of the hardness of ferrite, c) the control of cementite precipitation, d) the increase in the hardenability by avoiding pearlite formation before bainite reaction.

The stacking fault energy of TRIP steels is low, typically about 0.20 J/m^2.There is a compositional dependence of stacking fault energy. Several researches have shown that the stacking fault energy of austenitic stainless steels tends to increase with increasing alloying.

Manganese and silicon are both austenite stabilizers. Silicon as known is a ferrite stabilizer but at the same time assists to retain carbon enriched austenite by suppressing cementite precipitation from austenite. Silicon strengthens ferrite by solid solution strengthening and this leads to an overall strengthening of the steel. Too

much manganese additions should be avoided because it promotes carbide formation. It is important also to note that the strength of the austenite and the presence of other phases in the vicinity of retained austenite play a crucial role at the $\gamma \rightarrow \alpha'$ transformation.

Aluminium inhibits cementite precipitation. This element is usually used to substitute silicon [16] but unlike silicon, aluminium does not strengthen ferrite and that's the reason why steels, in which silicon is replaced by aluminium may present lower hardness.

An alloying element which may be found in TRIP steels is phosphorous. Phosphorous is a ferrite stabilizer and has the same effects as silicon. Pickering [17] reported than an addition of only 0.1 wt% of phosphorous leads to an increase of about 75 Mpa in the ferrite strength. Table 1 shows the chemical composition of typical TRIP steels.

Table 1: Chemical composition of typical TRIP steels

C	Mn	Si	Al	P	Cu	Cr	Ni	Ti	V	B
0.18	1.33	1.67	0.13	0.008	-	0.026	0.021	0.014	-	-
0.29	1.40	1.50	-	-	-	-	-	-	-	-
0.18	1.50	0.25	0.44	0.015	-	-	-	-	-	-
0.20	1.4	0.5	0.7	0.04	-	-	-	-	-	-
0.14	1.51	1.49	-	-	0.51	-	-	-	-	-
0.15	1.51	1.52	-	-	0.51	0.39	-	-	-	-
0.15	1.50	1.53	-	-	0.51	-	0.41	-	-	-
0.15	1.52	1.55	-	-	0.50	0.39	0.41	-	-	-
0.20	1.80	1.00	-	0.03	-	-	-	-	0.11	0.003
0.18	1.4	0.8	-	-	-	-	-	0.1	-	-

Micro-alloying elements such as niobium, titanium and vanadium are occasionally used in small amounts in order to improve the mechanical properties by grain refinement and precipitation hardening. In general, micro-alloying elements impede the processes that need the movement of dislocations and/or grain boundaries.

2.8 Factors affecting austenite stability

In this section a brief discussion about the main parameters, which determine the austenite stability is held.

2.8.1 Proportion of phases

TRIP steels consist of ferrite, bainitic ferrite, and retained austenite with or without traces of martensite. As reported by Choi et al. [18], a high volume fraction of retained austenite improves elongation as well as the ultimate tensile strength of the steel. C content in retained austenite increases with bainite transformation time but converges to a certain point. This carbon enrichement leads to the reduction of Ms in

values lower than the room temperature. The effect of bainite transformation on the C enrichment in the retained austenite is depicted in Figure 15.

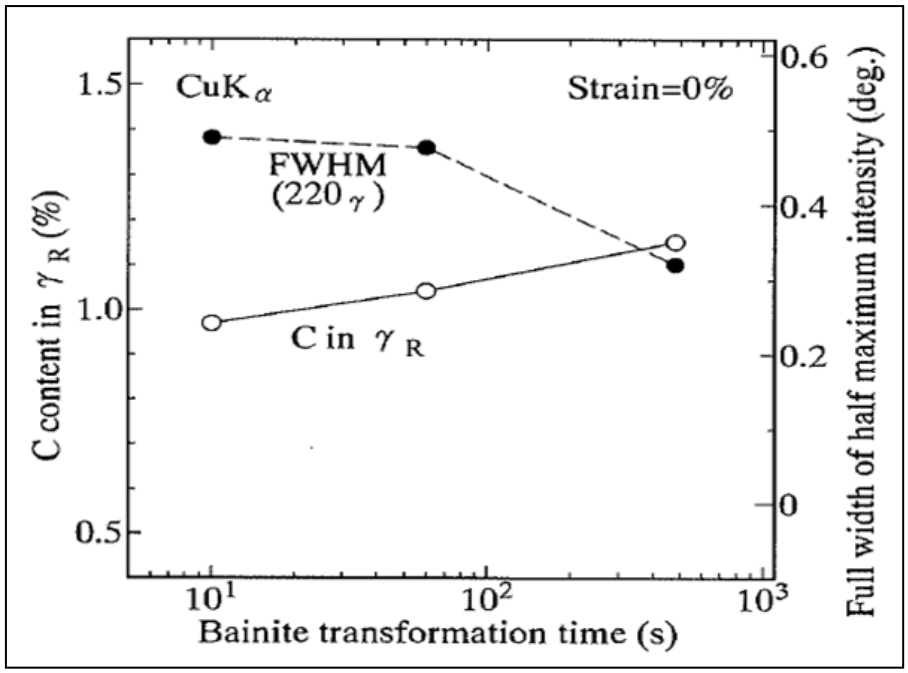

Figure 15: Effect of bainite transformation time on C content in retained austenite [19]

It should be noted that high retained austenite volume fraction or high ferrite fraction during intercritical annealing implies less bainite, leading to a reduction in strength.

2.8.2 Stability of retained austenite

2.8.2.1 Chemical stability

The stability of the retained austenite should be such that it transforms progressively during deformation. Austenite should transform progressively during deformation, so that damage can be accommodated to all stages of deformation. Carbon enrichment in retained austenite is of great importance. As known carbon content has a strong stabilizing effect by lowering the chemical driving force for martensitic transformation. The higher the C content, the higher the stability of the retained austenite. Whereas C, Mn, and Si depress the M_S temperature of retained austenite, Al increases the M_S temperature. It should be mentioned that the retained austenite after isothermal bainite transformation is not homogenously enriched with carbon. Two types of retained austenite can be considered. The retained austenite can be located within the ferrite matrix or in the vicinity of hard phases such as bainite or martensite. These two types of retained austenite present different morphologies and carbon concentrations, which influence the stability. Austenite particles in the vicinity of bainite are richer in carbon. Austenite particles with lower carbon content transform

first during martnesitic transformation. As the plastic strain increases the more stable austenitic particles transform (Figure 16).

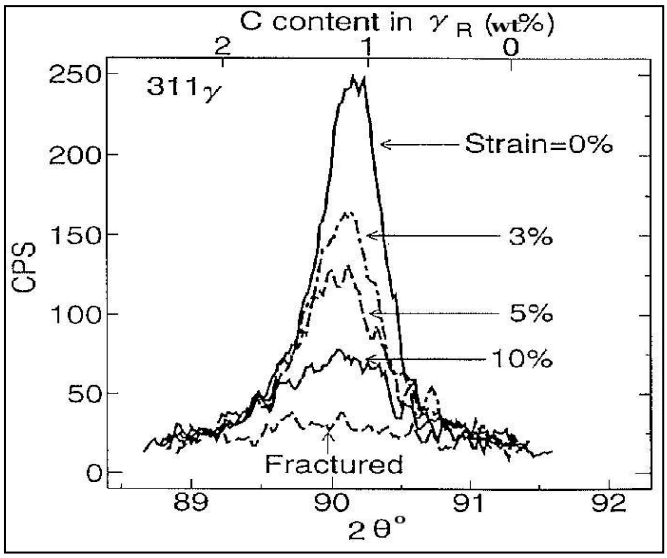

Figure 16: Effect of carbon content and plastic strain in the transformation of retained austenite [19]

2.8.2.2 Grain size

Apart from carbon content, another stabilizing factor of great importance is the austenite particle size. A reduction of the size of the retained austenite is a crucial stabilization factor. According to Wang et al.[20] the grain size of retained austenite should be in the range of 0.01 to 1 μm to ensure the TRIP effect. Larger retained austenite particles are unstable and transform quickly to martensite at small strains. On the other hand, 0.01 μm particles are too stable to undergo the strain-induced transformation. The smaller the austenite particle size is, the lower is the probability of presence of substructures such as stacking faults or other defects in the particle, which serve as nucleation sites for the martensitic transformation. In case of heterogeneous nucleation (i.e. at grain or phase boundaries) the probability of nucleation of martensite in an austenite grain is proportional to the surface area and hence the size of the grain. The droplet experiments of Turnbull [21] have shown that the nucleation frequency per droplet is proportional to the droplet surface area. Thus, subdividing the system into smaller droplets could cause a shortage of nuclei for the most of the droplets. It is a rational assumption to say that the smaller austenite grains are stabilized due to the lack of sufficient nuclei. An important reason why a decrease of the grain size will generate less strain-induced martensitic transformation is that the grain boundaries serve as effective obstacles for the growth of martensite laths.

A second way through which grain size influences the transformation kinetics is the interfacial energy. The interfacial energy of martensite is directly related to the thickness and length of martensite plates, or indirectly to the initial austenite size since the growth of martensite plates stops at grain boundaries.

The strain-induced transformation kinetics depends also from the orientation of the austenite particles. Some particles present favorable orientation to the stress applied in the material.

2.8.2.3 Mechanical stability

The strength of the austenite and the presence of other phases in the vicinity of retained austenite play an important role in the $\gamma \longrightarrow \alpha'$ transformation. Less transformation occurs when the surrounding matrix is stronger. An increase in the hardness of ferrite will have as a consequence the delay of the transfer of the applied stress to the austenite and hence the onset of TRIP phenomenon.

In general any increase in the hardness of the surrounding matrix phase can be beneficial for the mechanical properties.

At the design of TRIP steels it should be noted that any increment of matrix strength may not always be beneficial. Sakuma et al. [22] showed that increasing carbon content from 0.1 to 0.4 wt% increases the volume fraction as well as the stability of the retained austenite ,which leads to a reduce in the ferrite content, thereby increasing strength with an associated loss in ductility. As a result from this any advantage associated with TRIP steels is removed.

2.8.2.4 Temperature

The austenite stability is temperature dependent. Higher temperatures stabilize the austenite by both the reduction of the chemical driving force and the increase in intrinsic–fault energy. The strength and elongation of the individual phases are very likely to depend on the temperature.

2.8.2.5 Strain rate and stress state

The stress and the strain rate are two additional factors which influence the strain-induced martensitic transformation.

Most investigations carried out to clarify the effect of strain rate on the strain-induced transformation have indicated that the transformation is suppressed with increasing strain rate [23]. This was explained in terms of adiabatic heating, which decreases the chemical driving force of the transformation according to several studies. On the other hand, it has been found that high strain rate ($10^3 s^{-1}$) promoted shear band formation in AISI 304 steel compared to the low strain rate($10^{-3} s^{-1}$).

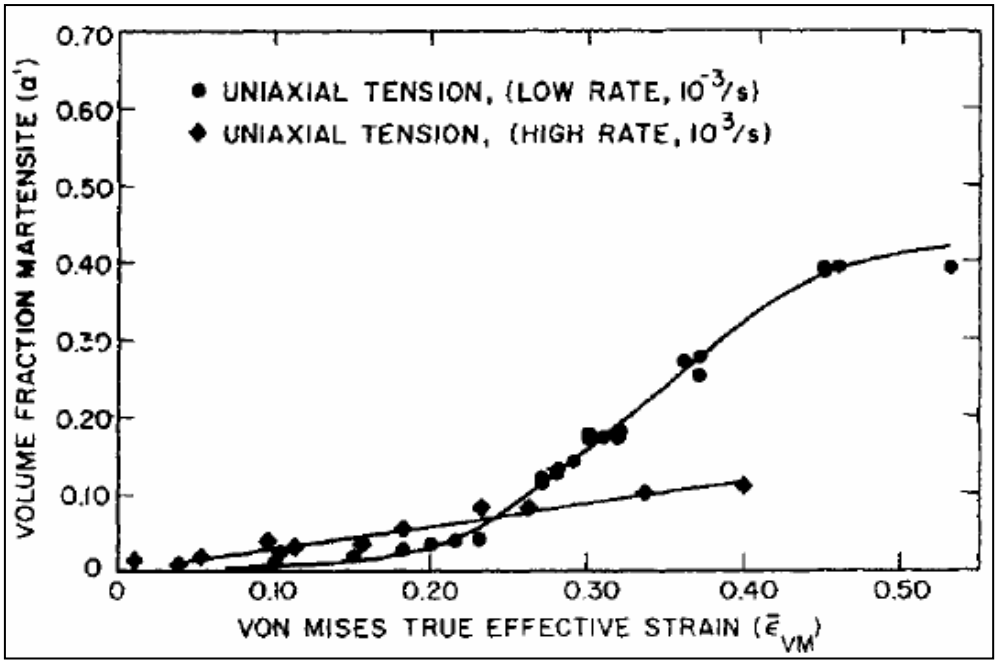

Figure 17: Effect of strain rate on the formation of strain-induced α'-martensite in AISI 304 austenitic stainless steel examined in uniaxial tension [24]

This led to an increase in the number of shear band intersections and higher volume fraction of α'-martensite at the early stages of tensile deformation as it can be seen in Figure 17. However, at strains higher than 0.25 the volume fraction of α'-martensite was suppressed at the high strain rate. This was attributed to a decrease in the chemical driving force of the transformation due to adiabatic heating.

High strain rate tensile testing is referred as dynamic mechanical testing. The volume fraction size, morphology and distribution of retained austenite have all been shown to affect the dynamic mechanical properties. Strain rate is believed to promote formation of shear-bands, which aid the strain-induced martensitic transformation due to the formation of more nucleation sites. Figure 18 depicts the effect of strain rate on the flow curve at different test temperatures.

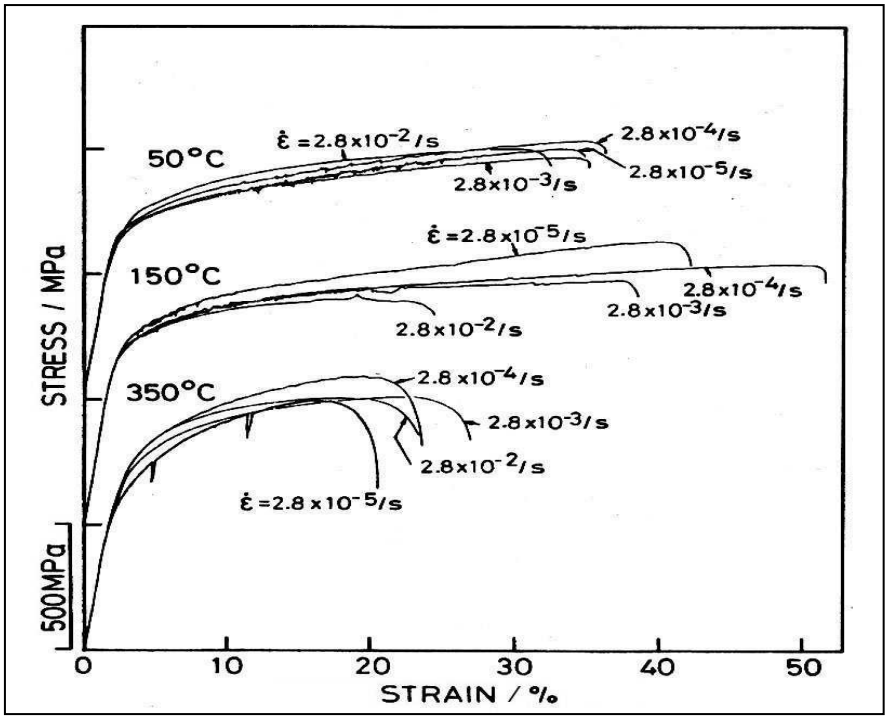

Figure 18: Effect of strain rate on the flow curve at different test temperatures [25]

The martensitic transformation is sensitive to the stress state. For example, hydrostatic stresses have been shown to suppress the transformation, as it is associated with an increase in volume. Patel and Cohen [26] have found that biaxial stress produces more matrensite than uniaxial stress or compression.

Unlike uniaxial tension or compression, strain-induced martensitic transformation is always known to be suppressed by the hydrostatic pressure. Hence, the stability of the retained austenite can be enhanced by applying hydrostatic pressure during tensile test, resulting higher uniform elongation. That's important because retained austenite in such a case would not be fully transformed during forming, thereby allowing the TRIP effect to be utilized for crash-worthiness.

To summarize the strain-induced transformation of retained austenite has been considered to be the major influencing factor of the mechanical performance of the steel. A moderately stable austenite appears to be the key to optimize ductility. A progressively austenite transforming is desirable during strain-induced transformation. The kinetics of the strain-induced transformation and how each of the above mentioned factors influences the transformation is the subject of this thesis.

2.9 Effect of temperature and strain rate on plastic deformation of single – phase face-centered cubic (FCC) metals

2.9.1 Effect of temperature and strain rate on flow stress

Temperature and strain rate influence flow stress of a crystalline material due to the thermal activation of dislocation motion. The flow stress σ consists of two components:

$$\sigma = \sigma^* + \sigma_E \tag{2.2}$$

σ^*: thermal component

σ_E: athermal component

The athermal component originates from long-range forces caused by, e.g. other dislocations. These long-range forces cause barriers, which are too high to be surpassed by thermal activation. Thus, it is considered that the athermal component is temperature dependent only through the temperature dependence of the elastic modulus, which is indicated by the subscript E.

The thermal component σ^* is significant when the dislocations are overcoming short-range obstacles. As the temperature increases, so does the thermal activation. Consequently, the thermal component of the flow stress decreases.

The strain rate affects the thermal component of the flow stress. The reason is that with increasing strain rate the probability of thermal activation decreases. Therefore, the thermal component of the flow stress increases with increasing strain rate. This behavior is referred as positive strain rate sensitivity. On the other hand, during high speed deformation the adiabatic heating increases the thermal activation and may cause decrease at the thermal component of the flow stress.

In FCC metals the thermal component of the flow stress is small. This means that these metals exhibit a rather small temperature dependence of the yield strength. However, the work-hardening rate of the FCC metals is largely affected by the stacking fault energy. As the temperature decreases the same happens to the stacking fault energy. Consequently, the work-hardening rate of FCC metals may increase with decreasing temperature.

2.9.2 Effect of temperature and strain rate on flow ductility

According to Considére's criterion the onset of the plastic instability, corresponding to uniform elongation is described by the following Equation:

$$\sigma = \frac{d\sigma}{d\varepsilon} \tag{2.3}$$

σ: flow stress

$\frac{d\sigma}{d\varepsilon}$: work-hardening rate

As mentioned again in the previous section, the work hardening rate of FCC metals increases with decreasing temperature, while the yield strength stays relatively unaffected by the temperature. On the other hand, strain rate affects both the yield strength and the temperature due to adiabatic heating. The uniform elongation of FCC metals is affected both by temperature and strain rate. The uniform elongation increases with decreasing temperature.
Besides the uniform elongation, also the post-uniform elongation is affected by the temperature and strain rate. Adiabatic heating softens the material. The influence of adiabatic heating on the softening of the material is more intense in the neck area where the local strain is higher.

2.10 Modeling of the mechanical constitutive behavior

A constitutive model for TRIP steels should predict the rate of martensitic formation and how the evolution of martensite affects the stress-strain curve. There are several parameters, which should be taken into consideration by the model. Several modeling efforts have been undertaken in the past mainly focused on homogeneous austenitic steels.
One of the first attempts was made by Olson and Azrin [27]. They proposed a model that makes use of the "rule of mixtures" relation in order to relate the flow stress of TRIP steels to the deformation induced martensite content:

$$\sigma = \sigma_A + f\Delta\sigma \tag{2.4}$$

σ_A: is the austenite flow stress
$\Delta\sigma$: is the strength difference between austenite and martensite

In Figure 19 the dashed σ-ε curves are the experimental data, which were addressed in the same study by Olson and Azrin. The dotted lines σ_M and σ_A labeled represent the flow properties of stable austenite and martensite, respectively. The transformation curves observed at temperatures above and below M_s^σ and their associated σ-ε curves are denoted by the solid curves in Figure 19 (a) and (b) respectively.

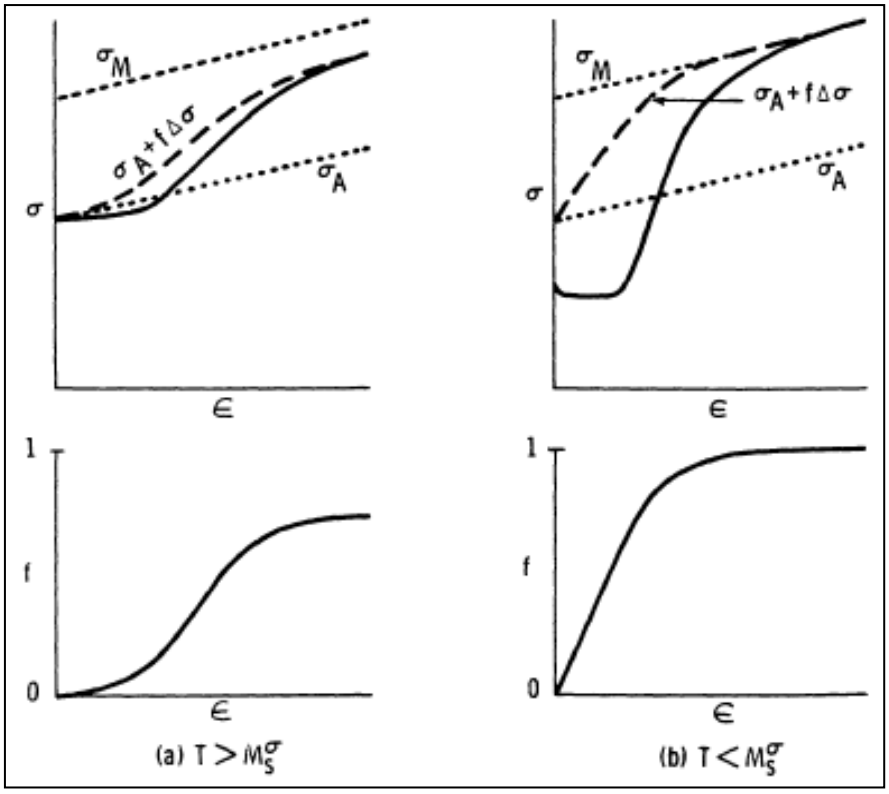

Figure 19: Comparison of the results obtained by equation 2.4 with the experimental data. (a) Behavior of material above M_s^σ, (b) behavior of material bellow M_s^σ[28]

As Figure 19 suggests, the curve measured above M_s^σ are in qualitative agreement with the rule of mixtures. On the other hand, the corresponding curve for temperature below M_s^σ differs significantly because of the "dynamic softening" effect, which takes place due to the simultaneous transformation of the austenite into martensite, during deformation.

Narutani et al. [29] based on the rule of mixture, which was previously described and after experimental measurements proposed the "Strain Corrected Rule of Mixtures, SCRM". This rule predicts the flow behavior σ_s of metastable austenite from the strain-induced transformation kinetics and the flow properties of the two separate phases.

$$\sigma_s = [1 - f] * \sigma_\gamma * (\varepsilon - \alpha f) + f * \sigma'_\alpha(\varepsilon - \alpha f) \quad (2.5)$$

where σ_α' and σ_γ are the flow stresses of austenite and marteniste respectively. The strain is denoted by ε and α is considered a parameter, which takes the value of 0.12. The volume fraction of martensite forming is denoted by f.

The following expression was adopted to describe the flow stress of the transformed material:

$$\sigma = \sigma_s - \Delta\sigma_d \quad (2.6)$$

The calculated flow behavior σ_s, allows us to calcutale the dynamic softening effect $\Delta\sigma_d$. Narutani found out that the "dynamic softening" $\Delta\sigma_d$ is proportional of the $\frac{df}{d\varepsilon}$ and is given by the following expression:

$$\Delta\sigma_d = \beta \frac{df}{d\varepsilon}\sigma_s \tag{2.7}$$

Where β, is a parameter and takes the value of $5.2 * 10^{-2}$.By the combination of equations (2.5), (2.6) and (2.7) derives the following expression:

$$\sigma = \left\{[1-f] * \sigma_\gamma(\varepsilon - \alpha f) + f * \sigma_\alpha^{'}(\varepsilon - \alpha f)\right\} * [1 - \beta \frac{df}{d\varepsilon}] \tag{2.8}$$

The functional form used in this model yields reasonable agreement with experimental data from uniaxial tension tests, as shown in Figure 20.

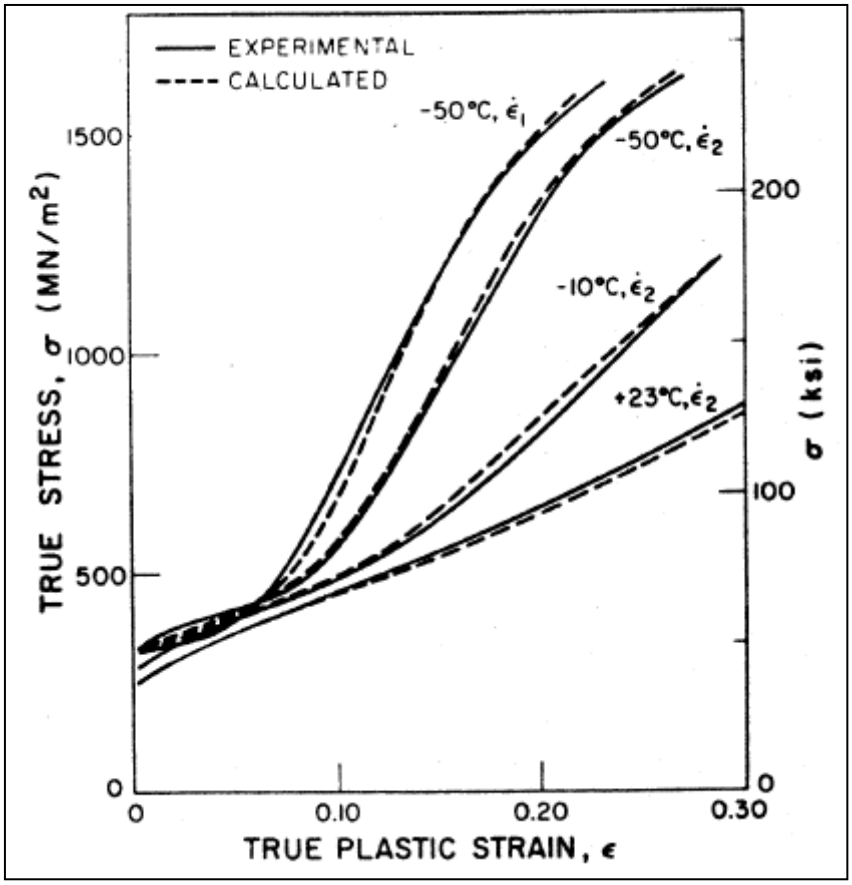

Figure 20: Comparison of experimental and calculated stress strain curves for 14Ni-7Cr stainless steel studied by Naturani, et al. [29]

In the following chapter, a brief review of several models used to describe the kinetics of strain-induced martensitic transformation is presented.

2.11 Conclusions

In this chapter a literature review of the TRIP phenomenon and it's applications on the automotive industry were presented. A review on several factors affecting austenite stability was investigated. In the following chapter a model describing the kinetics of strain-induced transformation of dispersed austenite in low-alloy TRIP steels is presented.

3 Model describing the kinetics of strain-induced transformation of dispersed austenite in low-alloy TRIP steels

3.1 Introduction

In the previous chapter a brief description of the martensite transformation and of the factors influencing the austenite stability has been presented. The austenite stability is as important as the volume fraction of the retained austenite in the TRIP steel. In this chapter a model describing the kinetics of the evolution of martensite volume fraction during the strain-induced transformation of dispersed austenite in low-alloy TRIP steels has been developed. The model is based on the modification of the nucleation site potency distribution by the applied stress and plastic strain for the description of the stress-assisted and strain-induced transformation regimes respectively. The model is fitted to available experimental data regarding the evolution of martensite as a function of plastic strain for several steels containing austenitic dispersions. The influence of several parameters on the expression used to describe the kinetics of the transformation is presented. Besides chemical composition of retained austenite and temperature, the model takes into account the effects of austenite particle size and stress triaxiality. Austenite particle size refinement has a strong stabilizing influence by retarding the strain-induced transformation kinetics. Stress triaxiality becomes important in stabilized austenite dispersions (either chemically stabilized or by size refinement) by enhancing the kinetics of the strain-induced transformation. The kinetic model can be used for the development of a constitutive model describing the mechanical behavior of TRIP steels.

A description of the M_s^{σ} temperature as a characterization of the retained austenite stability is being discussed. As mentioned in the previous chapter M_s^{σ} temperature depends on several factors, which influence austenite stability.

The M_s^{σ} model [14] was implemented in the steel presented in a previous work of Haidemenopoulos et al. [30], in order to calculate the carbon content of the retained austenite of the steel presented in this paper.

Chemical composition, austenite particle size, neighboring phases, and stress-triaxiality are the most important factors influencing the stability of retained austenite and the strain-induced transformation kinetics [31-36]. These factors are interrelated and it is difficult to separate each individual effect. In an effort to gain a deeper understanding on the effects of these factors, several models have been developed for the kinetics of strain-induced transformation of austenite in TRIP steels. These models have been reviewed by Samek et al. [37] and they are presented in Figure 21.

Equation for $V_{\alpha'}$	Reference
$V_{\alpha'} = \dfrac{V_\gamma^0}{1 + \dfrac{1}{e^k \varepsilon^p}}$	Ludwigson–Berger–Angel
$V_{\alpha'} = \dfrac{V_\gamma^0}{1 + \dfrac{p}{k_p \varepsilon^p V_\gamma^0}}$	Burke–Matsumura–Tsuchida
$V_{\alpha'} = V_\gamma^0(1 - \exp(-k_s\varepsilon))$	Sugimoto
$V_{\alpha'} = V_\gamma^0(1 - \exp(-(k_s - \beta_h P_h)\varepsilon))$	Pychmintsev
$V_{\alpha'} = V_\gamma^0\left(1 - \exp\left[-\beta(1 - \exp(-\alpha\varepsilon))^n\right]\right)$	Olson–Cohen
$V_{\alpha'} = V_\gamma^0 A \varepsilon^{1/2}$	Gerberich
$V_{\alpha'} = V_\gamma^0\left(1 - \exp\left(-k_G\varepsilon^c\right)\right)$	Guimarães

Figure 21: Models for the strain-induced martensitic transformation kinetics [37]

The model by Angel [15] and Ludwigson et al. [38] is empirical and takes into account autocatalytic effects, i.e., the acceleration of transformation by the transformation-induced generation of new martensitic nuclei. The model by Matsumura et al. [39], which was based on the work of Burke [40] and modified by Tsuchida et al. [41], takes into account the stability of austenite and autocatalytic effects. In the model proposed by Sugimoto et al. [42] the rate of transformation is proportional to the fraction of untransformed austenite and austenite stability. The model by Olson et al. [43] was the first to take into account the physical mechanisms of martensitic nucleation induced by plastic strain. In that model, shear band intersections were considered as the potential nucleation sites for the transformation. The rate of shear band formation is influenced by composition and temperature through the stacking fault energy. All models described above were developed for homogeneous austenitic alloys and do not take into account that, in low-alloy multiphase TRIP steels, the austenite phase is dispersed in the form of particles in the microstructure. Therefore, the effect of austenite particle size on transformation kinetics is not considered in the aforementioned models. Only recently Zhang et al. [44] investigated the effect of particle size through a modification of the Burke-Matsumura-Tsuchida model [39-41]; however, it was not possible to differentiate between the effects of particle size and carbon partitioning in the austenite. There are also experimental data showing that particle size and stress triaxiality have important influence on strain-induced transformation and associated mechanical behavior [45, 46].

The aim of this work is to develop a kinetic model for the description of the fraction of martensite formed as a function of plastic strain in steels, where the austenite is present in the form of a dispersion of particles. The model is able to predict the effects of austenite particle size, chemical composition of austenite particles, temperature and

stress-state triaxiality on the strain-induced transformation kinetics. In section 3.2 a literature review of the basic elements of martensite nucleation theory and the potency distribution of nucleation sites is presented. The new model is then described in sections 3.3-3.5.

3.2 Model description

3.2.1 Martensitic nucleation and potency distribution of nucleation sites

The model is developed for steel containing retained austenite in the form of dispersed particles of average volume V_p per particle. Martensitic transformation can be mechanically-induced in these dispersed austenite particles by two distinct mechanisms: stress-assisted and strain-induced nucleation [47] as described in the previous chapter. In the stress-assisted regime, martensite nucleates on pre-existing nucleation sites. Those are the same sites which operate during the traditional transformation on cooling. In the strain-induced regime, new and more potent nucleation sites are created by plastic deformation of the austenitic phase. As the steel is stressed and deformed plastically, retained austenite will transform to martensite by the simultaneous operation of both mechanisms. The stress-assisted mechanism prevails at stresses lower than the yield-strength of austenite, whereas the strain-induced mechanism prevails after the yield-strength has been surpassed. The volume fraction of martensite forming as a result of the mechanically-induced transformation is denoted by f. This is the relative volume fraction with respect to the initial volume fraction of austenite and takes values between 0 and 1.

The model is based on the Olson-Cohen theory of heterogeneous martensitic nucleation [48-50]. According to this theory, the formation of a martensitic nucleus takes place by the dissociation of an existing defect, which serves as a nucleation site for the transformation. Dissociation of such a defect creates a fault structure or martensitic embryo, the growth of which is determined by the energy change accompanying the dissociation. The energy per unit area of an embryo with a thickness of n crystal planes is denoted by $\gamma_f(n)$ and is given by

$$\gamma_f(n) = n\rho\left(\Delta G_{ch} + E_{str} + W_f\right) + 2\gamma_s \tag{3.1}$$

where ΔG_{ch} is the chemical driving force for martensitic transformation (energy per mole), γ_s is the fault/matrix interfacial energy, ρ is the density of atoms in the fault plane (moles per unit area), E_{str} is the elastic strain energy associated with distortions in the fault interface plane (energy per mole), and W_f is the frictional work of interfacial motion (energy per mole), which occurs during the dissociation process. Spontaneous martensitic nucleation occurs when $\gamma_f(n) \le 0$. In this case, the dissociation is barrierless and occurs at a critical value of the driving force, i.e., when $\gamma_f = 0$. The change of the energy per unit area is presented in Figure 22.

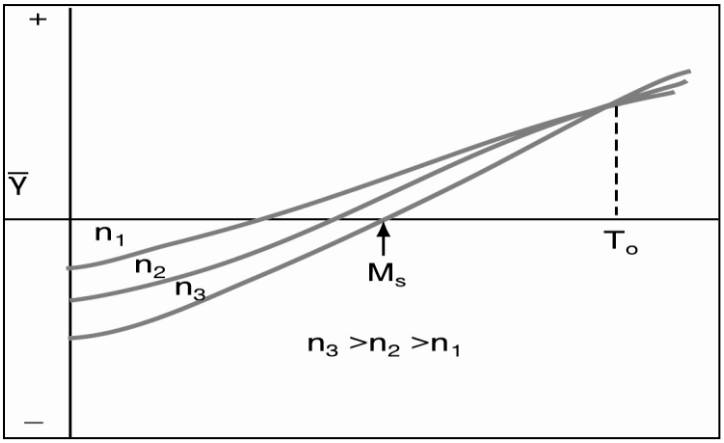

Figure 22: Change of the energy per unit area for three different thicknesses of n crystal planes (n1, n2, n3) [11]

Based on the above, the *potency* of a nucleation site can be defined by the thickness n (in number of crystal planes) of the nucleus that can be produced from the defect by barrierless dissociation. The critical value n^* for nucleation follows from Equation (3.1) as:

$$n^* = -\frac{2\gamma_s}{\rho\left(\Delta G_{ch} + E_{str} + W_f\right)} \tag{3.2}$$

The critical n^* for martensitic nucleation is temperature-dependent through the term ΔG_{ch}. Later it will be shown that it could also be stress-dependent, through the addition of a stress-dependent mechanical driving force ΔG_σ in the denominator of (3.2). The critical value n^* also depends on the chemical composition of the austenite through the compositional dependence of ΔG_{ch} and W_f.

Let N_v^0 be the total number of nucleation sites of all potencies per unit austenite volume and
N_v the number of sites of sufficient potency to nucleate martensite (operational sites) per unit austenite volume. Cohen and Olson [51] derived the cumulative defect-potency distribution dN_v from the Cech and Turnbull small-particle experiments in Fe–30%Ni alloys [21] as:

$$dN_v = dN_v^0 \, e^{-a n^*} \tag{3.3}$$

where *a* is a shape factor.

The model developed in this work is based on a modification of the potency distribution of equation (3.3); the modification is based on Kuroda's [52] suggestion that the overall potency distribution is the sum of the stress-modified and strain-

modified distributions of nucleation sites: $dN_v = dN_v^{\sigma} + dN_v^{\varepsilon}$. This accounts for the effects of stress σ and plastic strain ε on the evolution of the number of operational sites N_v in a uniaxial tension test. The modification of the potency distribution by stress and strain is described in sections 3.3 and 3.4 respectively, while the overall potency distribution is described in section 3.5.

3.3 Potency distribution for stress-assisted transformation

Application of a uniaxial stress σ that causes elastic strains only can trigger martensitic nucleation through a mechanical contribution $\Delta G_{\sigma}(\sigma)$ to the chemical driving force ΔG_{ch}:

$$n^*(\sigma) = -\frac{2\gamma_s}{\rho\left[\Delta G_{ch} + \Delta G_{\sigma}(\sigma) + E_{str} + W_f\right]}. \tag{3.4}$$

The potency distribution of Equation (3.3) becomes:

$$dN_v^{\sigma}(\sigma) = dN_v^{\sigma 0}\, e^{-a_{\sigma} n^*(\sigma)} \tag{3.5}$$

where a_{σ} is the shape factor in the stress-modified distribution.

If we make the assumption that the variation of ΔG_{σ} with σ is insignificant, then n^* is constant to first approximation and the last equation can be integrated to yield:

$$N_v^{\sigma} = N_v^{\sigma 0} \exp\left(-a_{\sigma} n^*\right) \tag{3.6}$$

3.4 Potency distribution for strain-induced transformation

Plastic strain in the austenite phase generates new nucleation sites and the factor dN_v^o in equation (3.3) depends on plastic strain. Let N be the maximum number of sites per unit austenite volume and N_v^o the total number of nucleation sites of all potencies per unit austenite volume. In a uniaxial tension test an increment of plastic strain dε causes a change $dN_v^{\varepsilon o}$, which is proportional to the number of available nucleation sites $N - N_v^o$ it also assumed that $dN_v^{\varepsilon o}$, is proportional to the value of plastic strain ε raised to a power, say m-1, i.e., we write

$$dN_v^{\varepsilon o} = \left(N - N_v^{\varepsilon o}\right)\alpha \varepsilon^{m-1} d\varepsilon \tag{3.7}$$

where α is a proportionality constant. Then

$$dN_v^{\varepsilon} = dN_v^{\varepsilon 0} \exp\left[-a_{\varepsilon} n^*(\sigma)\right], \qquad n^*(\sigma) = -\frac{2\gamma_s}{\rho\left[\Delta G_{ch} + \Delta G_{\sigma}(\sigma) + E_{str} + W_f\right]}, \tag{3.8}$$

where α_ε is the shape factor in the strain-modified distribution. Equation (3.7) can be integrated to yield

$$N_v^{\varepsilon 0}(\varepsilon) = N\left[1 - \exp\left(-k\,\varepsilon^n\right)\right], \qquad k = \frac{\alpha}{n}, \tag{3.9}$$

where the initial condition $N_v^{\varepsilon 0}(0) = 0$ has been used.

Again, if we make the assumption that the variation of dG_σ with σ is insignificant, then n^* is constant to first approximation and equation (3.8a) can be integrated to yield

$$N_v^{\varepsilon}(\varepsilon) = N_v^{\varepsilon 0}(\varepsilon)\exp\left(-a_\varepsilon\, n^*\right) \tag{3.10}$$

where $N_v^{\varepsilon 0}(\varepsilon)$ is defined by (3.9) above.

3.5 Overall Potency distribution and transformation fraction

Let V^a the austenite volume, V^m the martensite volume, and $V = V^a + V^m$ the total volume, so that the volume fraction of martensite is $f = V^m/V$. If N_v changes to $N_v + dN_v$, the martensite volume created per unit austenite volume is $v_p\, dN_v$, where V_P is the average volume of the austenite particles (here we assume that the martensite volume equals the austenite volume; a correction that accounts for volume change is possible). The total change in martensite volume dV^m due to dN_v is

$$dV^m = \left(v_p\, dN_v\right)V^a = \left(V - V^m\right)v_p\, dN_v \tag{3.11}$$

If we divide the last equation by the total volume *V*, we find that

$$\frac{dV^m}{V} = \left(1 - \frac{V^m}{V}\right)v_p\, dN_v \qquad \text{or} \qquad df = (1-f)\,v_p\, dN_v, \tag{3.12}$$

which is integrated to yield

$$f(N_v) = 1 - \exp\left(-v_p\, N_v\right) \qquad \text{with} \qquad N_v = N_v^\sigma + N_v^\varepsilon, \tag{3.13}$$

where it was taken into account that *f* vanishes for $N_v = 0$.

If we now make the assumption that the variation of ΔG_σ with σ is insignificant, then Equations (3.6) and (3.10) can be used for the evaluation of N_v^σ and N_v^ε; in that

case the above expression (3.13a) for the martensite volume fraction f can be written in the form

$$f(\varepsilon) = 1 - \exp\left[-v_p\, N_v(\varepsilon)\right], \tag{3.14}$$

where

$$N_v(\varepsilon) = N_v^{\sigma} + N_v^{\varepsilon}(\varepsilon), \tag{3.15}$$

$$N_v^{\sigma} = N_v^{\sigma 0} \exp\left(-a_{\sigma}\, n^*\right), \tag{3.16}$$

$$N_v^{\varepsilon}(\varepsilon) = N_v^{\varepsilon 0}(\varepsilon) \exp\left(-a_{\varepsilon}\, n^*\right), \qquad N_v^{\varepsilon 0}(\varepsilon) = N\left[1 - \exp\left(-k\,\varepsilon^m\right)\right]. \tag{3.17}$$

When the plastic strain ε vanishes, f takes on the stress-assisted portion of the transformation f_{SA}. According to Equation (3.14) we have that

$$f_{SA} \equiv f(0) = 1 - \exp\left(-v_p\, N_v^{\sigma}\right) \tag{3.18}$$

It is interesting to note that the amount of transformation depends on the size of the austenite particles through v_p in (3.14) and (3.18). In fact, the volume fraction f increases with the particle size v_p.

3.6 Fitting the model to available experimental data

3.6.1 Experimental steels

The result described by equation (3.14) was fitted to available experimental data by Samek et al. [37] and Itami et al. [19]. The chemical composition of the steels used from these works is shown in Table 2.

Table 2: Chemical composition (in mass%) of the steels considered in this study

Steels	C	Mn	Si	Al	P	Reference
Steel 1	0.24	1.61	1.45	0.03	0.006	[37]
Steel 2	0.25	1.70	0.55	0.69	0.007	[37]
Steel 3	0.19	1.68	0.48	0.84	0.066	[37]
Steel 4	0.14	1.66	1.94	0.025	0.008	[19]

Steels 1 and 4 are typical CMnSi steels, Steel 2 is a CMnSiAl steel with partial replacement of Si with Al, and Steel 3 is a CMnSiAlP steel with partial replacement of Si with Al and P. In all steels under consideration the TRIP microstructures were obtained by a two-step heat treatment consisting of intercritical annealing followed by holding at the bainitic isothermal transformation temperature. The resulted microstructures in all cases consisted of ferrite, bainite and retained austenite. Steels

1, 2 and 3 have received identical heat treatment. Steel 4 has three variants corresponding to three holding times (10, 60 and 480 sec) at the bainite transformation temperature of 400°C. These variants are listed as Steel 4/10, Steel 4/60 and Steel 4/480 respectively. The transformation fraction f was determined as a function of plastic strain ε by measuring the saturation magnetization interrupted tensile testing. In Steels 1, 2 and 3 the measurements were performed for temperatures in the range of 10 to 100 °C whereas in Steel 4 the measurements were performed at room temperature.
Details on retained austenite volume fraction and particle size as well as chemical composition of austenite are given in [31] and [45].
In order to apply the model to the steels of Table 2, various components entering the equations (3.15)-(3.17) have to be calculated as described in the following.

3.6.2 Chemical driving force

The chemical driving force ΔG_{ch} for martensitic transformation of austenite particles is a function of chemical composition (carbon and manganese in the austenite) and temperature. The chemical driving force for martensitic transformation is defined as

$$\Delta G_{ch} = G(\text{bcc}) - G(\text{fcc}) \tag{3.19}$$

where $G(\text{bcc})$ and $G(\text{fcc})$ are the free energies of bcc and fcc phases of the same composition. These free energies were calculated with the Thermo-Calc software system by employing the TCFE6 database [53]. The results for steels 1, 2 and 3 are given as a function of temperature as follows:

Steel 1: $$\Delta G_{ch}(T) = -5071.56 + 7.12T \quad (\text{in J/mol}) \tag{3.20}$$

Steel 2: $$\Delta G_{ch}(T) = -4755.31 + 6.95T \quad (\text{in J/mol}) \tag{3.21}$$

Steel 3: $$\Delta G_{ch}(T) = -4470.02 + 6.79T \quad (\text{in J/mol}) \tag{3.22}$$

where T is temperature in K.

The driving force term described by Equations (3.20)-(3.22) is plotted as a function of temperature in Figure 23.

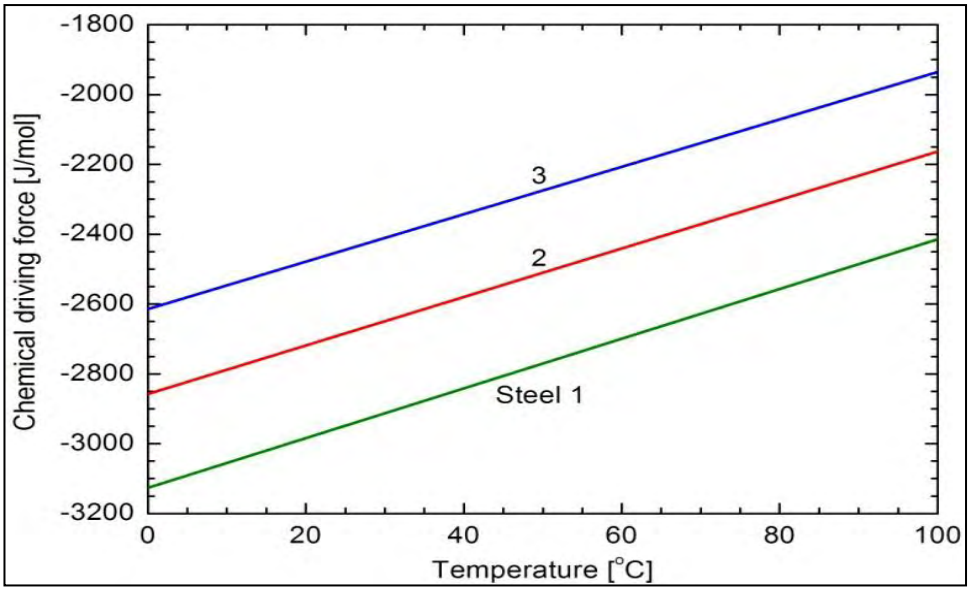

Figure 23: Variation of chemical driving force with temperature for Steels 1, 2 and 3

It can be deduced that, regarding chemical stabilization, the retained austenite in Steel 1 has the lowest stability while the retained austenite in Steel 3 has the highest stability. The retained austenite in Steel 2 possesses an intermediate stability between the other two steels. These observations are in accordance with the carbon content of retained austenite as determined in [37]. For Steel 4 the ΔG_{ch} term was calculated at 20°C, since the fraction martensite vs strain data were obtained at room temperature. The calculations were carried out for the three variants and the results are -2546, -2341 and -2091 J/mol for the 4/10, 4/60 and 4/480 variants respectively.

3.6.3 Mechanical driving force

The mechanical driving force contribution ΔG_σ is proportional to the applied stress σ:

$$\Delta G_\sigma = \sigma \frac{\partial \Delta G}{\partial \sigma} \tag{3.23}$$

and is given as a function of the stress-state by Patel and Cohen [26] as

$$\frac{\partial \Delta G}{\partial \sigma} = -0.715 - 0.3206 \frac{\sigma_h}{\bar{\sigma}} \quad (\text{in } \frac{\text{J}}{\text{mol MPa}}), \tag{3.24}$$

where $\sigma_h = \sigma_{kk}/3$ is the hydrostatic stress and $\bar{\sigma}$ is the von Misses equivalent stress. The ratio $\sigma_h / \bar{\sigma}$ is known as the "triaxiality" of the stress state. In uniaxial tension, $\frac{\sigma_h}{\bar{\sigma}} = 1/3$ and the mechanical driving force contribution from Equation (3.24) is -0.822 J/(mol MPa). In considering stress effects on the potency distribution of Equation (3.3), two limiting cases are considered. A fully-biased distribution, which is

based on the assumption by Patel and Cohen [26] that the operative nucleation sites have an optimum orientation for maximum interaction with the applied stress. In this case the ΔG_σ term is given by Equations (3.23) and (3.24) and is used in Equation (3.8b) for the calculation of n^*. Second, it is considered the opposite extreme of a fully-random distribution, which is based on the assumption by Olson et al. [54] that the nucleation sites are randomly oriented. In this case, ΔG_σ is approximately one third (1/3) of that predicted by the fully-biased distribution. Therefore, the ΔG_σ term is replaced by $\Delta G_\sigma / 3$ in Equation (3.4), which describes the potency distribution in the stress-assisted transformation regime. The value of stress in Equation (3.23) was taken equal to the yield strength of retained austenite. A value of 550 MPa was adopted from the work of Samek et al. [37] for steels 1, 2 and 3, while the values 382, 382 and 527 MPa were adopted for steel variants 4/10, 4/60 and 4/480 respectively from the work of Itami *et al*. [19].

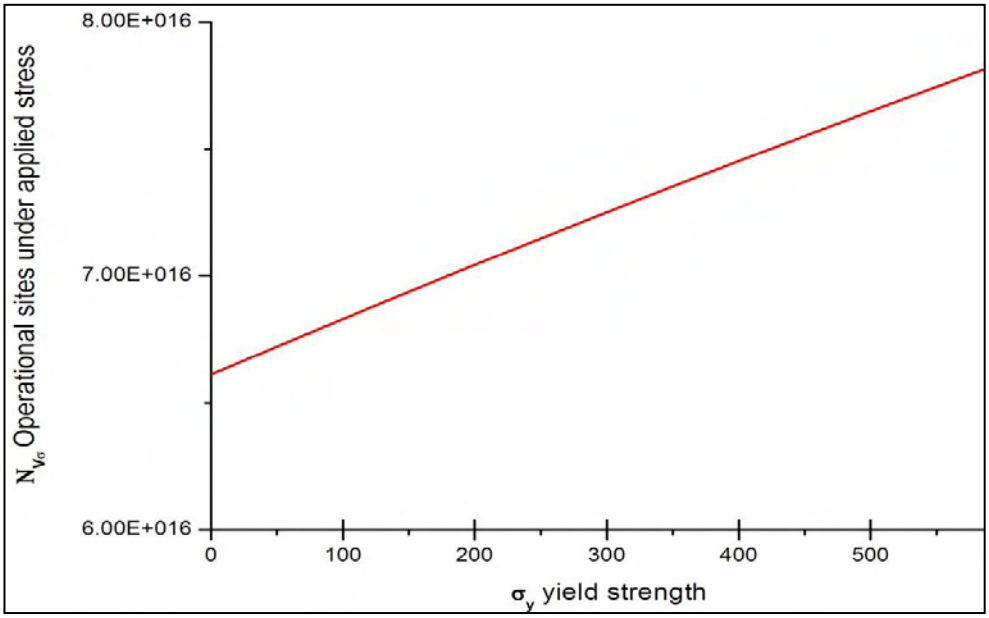

Figure 24: Variation of operational sites under applied stress with yield strength for Steel 1 at 20°C

The value of the yield strength depends mainly from the C but also from the Mn content of the retained austenite. The mechanical driving force, while it favors the martenstitic transformation, has not as strong contribution in the energy equilibrium of the martensitic transformation as the chemical driving force. However, the effect of the mechanical driving force on the kinetics of the martenistic transformation is enhanced at really stable austenite particles. In Figure 24 we can observe how the yield strength affects the number of operational sites, which trigger martensitic nucleation during stress-assisted transformation in Steel 1. The value of N_v^σ follows a linear increase with the yield strength.

3.6.4 Frictional work of interfacial motion

The frictional work of interfacial motion during martensitic nucleation W_f is a function of chemical composition of retained austenite. Frictional work is taken equal to the critical driving force at the M_S temperature.Two ways have been followed in order to develop an expression of W_f. The first way is to assume a linear increase of W_f with C and Mn content:

$$W_f = 1169 + 8777 X_C + 2246 X_{Mn} + 19900 X_C X_{Mn} \tag{3.25}$$

The second way takes into account the treatment of Labusch [55], where the solution hardening effect is proportional to the 2/3 power of the alloying elements and adopting the data of Kuroda [52] for Fe-C-Mn alloys, we obtain a 2/3 power-law expression. This 2/3 power-law expression was adopted for the present work. According to Labusch, the critical shear stress to move a dislocation through a random array of obstacles in the glide plane is proportional to the 2/3 power of the concentration of alloying element and is given by the following expression:

$$W_f = 1.893 \times 10^3 X_{Mn}^{2/3} + 1.310 \times 10^4 X_C^{2/3} \quad (\text{in J/mol}) \tag{3.26}$$

where X_{Mn} and X_C are the mole fractions of Mn and C in the austenite.

It is interesting to obtain the contribution of each one of these two alloying elements in the total frictional work (Figure 25).

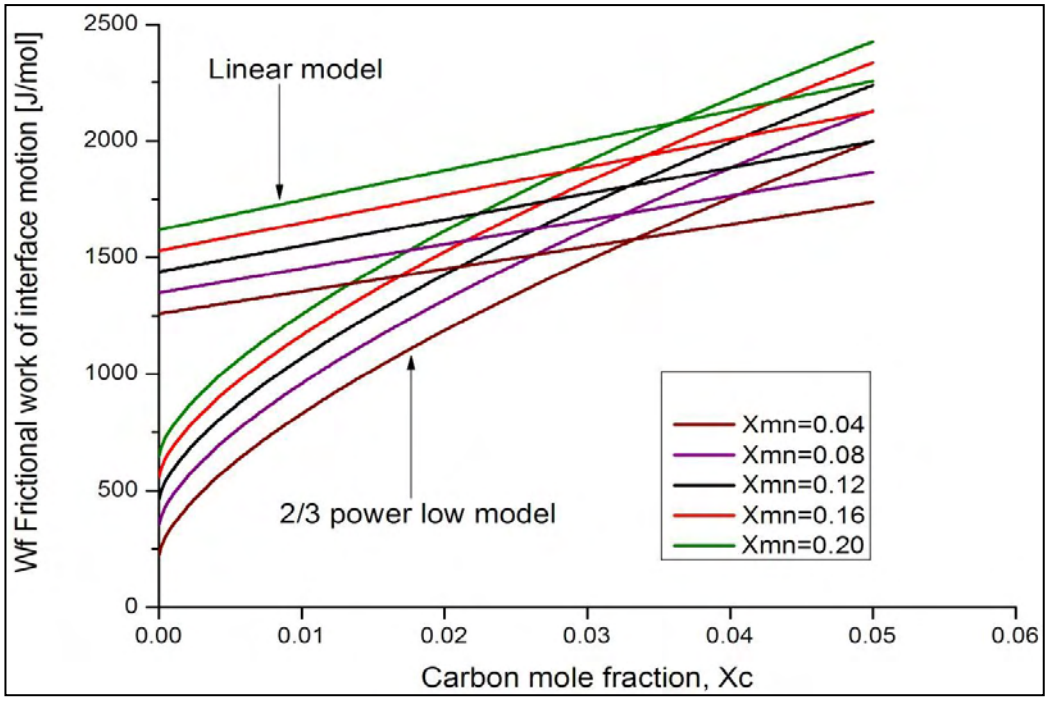

Figure 25: Frictional work of interfacial motion as a function of mole fraction of C and Mn in austenite. The two families of curves correspond to the linear and the 2/3 power-law approximation respectively

The frictional work of interfacial motion W_f has the highest preventing contribution in the energy equilibrium of the martensitic transformation. The effect of the alloying elements of C and Mn in the frictional work is evident. An increase in the contents of those elements leads to an increase in the frictional work W_f. This results to the total energy equilibrium of the martensitic transformation by retarding or even preventing the transformation at high carbon contents. An increase in the content of those elements hinders transformation kinetics not only by increasing the value of W_f but at the same time by decreasing the contribution of chemical driving force as discussed in previous section. It is also interesting to note that compared to Mn, C is a much more stabilizing factor concerning retained austenite. At low carbon contents, the discrepancy between the linear and the 2/3 power-law model is large approaching almost 1000 J/mol.

3.6.5 Shape parameters and other constants

For the Fe-30%Ni small particle experiments of Cech and Turnbull [21], the shape parameter of the potency distribution of equation (3.3) has been evaluated by Olson and Cohen [51] as $a = 0.866$. For the less stable retained austenite in the low-alloy Fe-Mn-C steels considered in this work, the shape parameter for the pre-existing nucleation sites should have a much lower value. The value of $a_\sigma = 0.1$ was used in Equation (3.5) for the stress-modified distribution. Based on the assumption that the nucleation sites created by plastic strain are more potent than the pre-existing sites, a

lower value of $a_\varepsilon = 0.03$ was adopted for the strain-modified potency distribution in Equation (3.8a). The values of the remaining parameters were taken from [14, 56] as follows: $E_{str} = 500$ J/mol, $\gamma_s = 0.15$ J/m^2, $\rho = 3\times10^{-5}$ mol/m^2, $k = 46$ and $n = 3.45$. The average volume of austenite particles was taken equal to $v_p = \frac{4}{3}\pi R^3 = 4.18\times10^{-18}$ m^3 considering a mean radius of 1 μm as suggested by the measurements of austenite particle size by TEM in [37]. The values of the various parameters used in this work are summarized in Table 3.

Table 3 Values of various parameters used in the model describing the kinetics of evolution of martensite during strain-induced transformation

Parameter	Value	Parameter	Value
a_σ	0.1	ρ	3×10^{-5} mol/m^2
a_ε	0.03	k	46
E_{str}	500 J/mol	m	3.45
γ_s	0.15 J/m^2	v_p	4.18×10^{-18} m^3

3.6.6 Fitting parameters

Non-linear curve fitting was performed with fitting parameters the pre-existing nucleation sites $N_v^{\sigma 0}$ and the maximum sites that can be produced by plastic deformation N per unit volume. It should be noted that the fitting parameters for all temperatures and steel compositions considered are quite stable and of the order of 1.5-4x10^{17}m^{-3} for $N_v^{\sigma 0}$ and 1.9-5x10^{19}m^{-3} for *N*. The value of the $N_v^{\sigma 0}$ parameter is consistent with the value of 2x10^{17}m^{-3} reported in [52] for Cu-Fe alloys and the value of 10^{16}m^{-3} reported in [57] for ceramic systems.

3.6.7 Effect of austenite composition

The effect of chemical stabilization of retained austenite, arising mainly from carbon partitioning, is shown in Figure 26, where the fraction martensite, from Equation (3.14), is plotted against plastic strain and compared against experimental data from interrupted tensile testing. Figures 26a-c correspond to testing temperatures 10, 20 and 65^{o}C for Steels 1, 2 and 3 of Table 2. Figure 26d corresponds to 20^{o}C for the three variants of Steel 4 (variants 4/10, 4/60, 4/480).

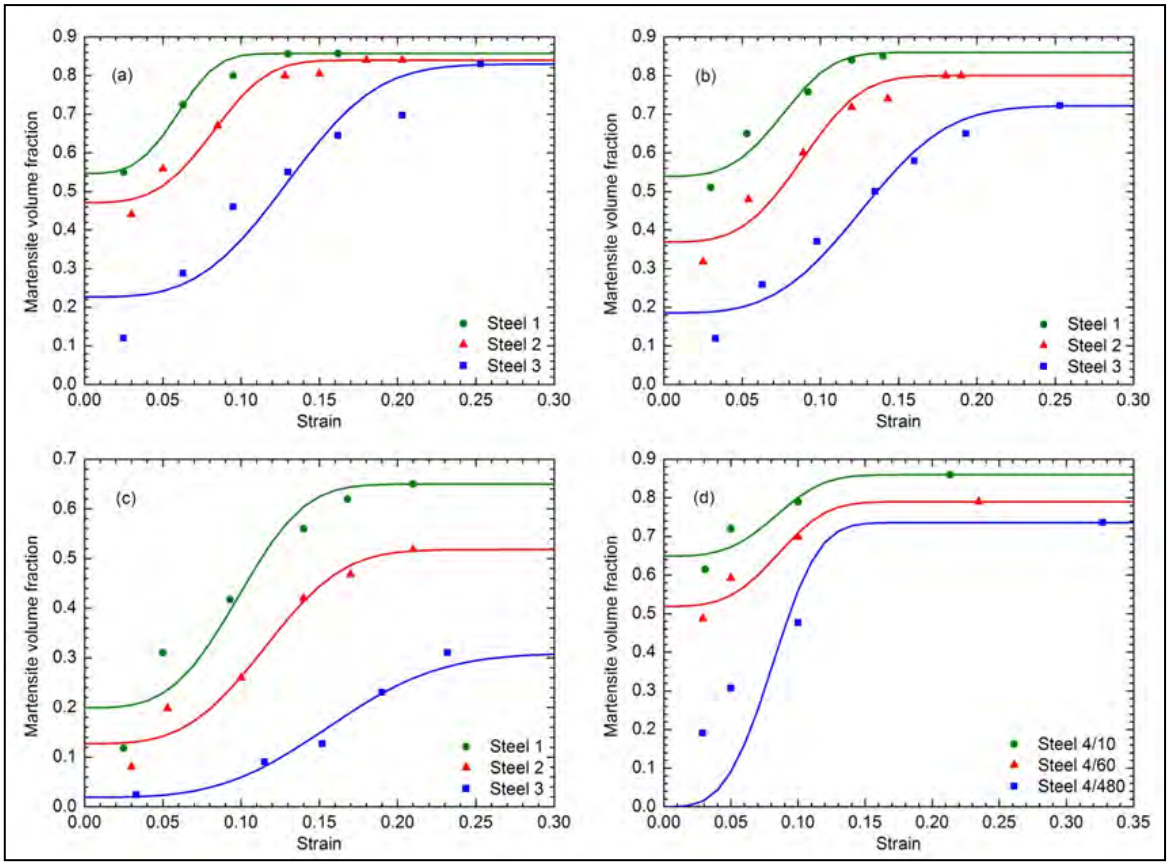

Figure 26: Variation of martensite volume fraction with axial strain. Comparison of model and experimental data: (a) 10°C, (b) 20°C, (c) 65°C for Steels 1, 2, 3 and (d) 20°C for Steels 4/ 10, 4/60, 4/480

The model predicts well the sigmoidal shape of the strain-induced transformation, i.e., initially the rate of transformation increases with strain, reaches a fairly constant rate $df/d\varepsilon$ and then the rate decreases at higher strains as saturation is approached. Regarding Steels 1, 2 and 3, the model predicts higher transformation fractions for Steel 1, lower for Steel 3 and intermediate fractions for Steel 2 at the three temperatures and for the strain range considered, reflecting the effect of chemical stabilization of retained austenite, in accordance with the discussion of Figure 23. The same holds for the three variants of Steel 4 in Figure 26d, where in Steel 4/10 the retained austenite possesses the lowest stability, in Steel 4/480 the highest and in Steel 4/60 an intermediate stability, in accordance with the chemical driving force calculations presented in the previous section.

In Figures 26a-d, the value f at zero plastic strain $(\varepsilon = 0)$ is the aforementioned stress-assisted portion of the transformation f_{SA} and agrees well with the experimental data. In the stress-assisted case, the transformation is exclusively triggered by the pre-existing nucleation sites. The value of f_{SA} increases as the chemical stability of retained austenite decreases.

Other important aspects are the constant transformation rate $df/d\varepsilon$ and the saturation level at high strains. The rate $df/d\varepsilon$ and the saturation level follow the

chemical stabilization of retained austenite, i.e., $df/d\varepsilon$ increases as the chemical stability of retained austenite decreases. The difference between the saturation levels of Steels 1, 2 and 3 are high at 65°C and almost diminish at 10°C. It is important to note, that the saturation level does not reach the value of 1 (complete transformation) for the transformation temperatures considered.

3.6.8 Effect of temperature

The effect of temperature on the kinetics of strain-induced transformation is shown in Figure 27 for Steels 1, 2 and 3. The transformation fraction increases with decreasing temperature due to the increase of the chemical driving force ΔG_{ch} for martensitic transformation. The rate $df/d\varepsilon$ and the saturation level also increase with decreasing temperature due to the temperature dependence of the driving force.

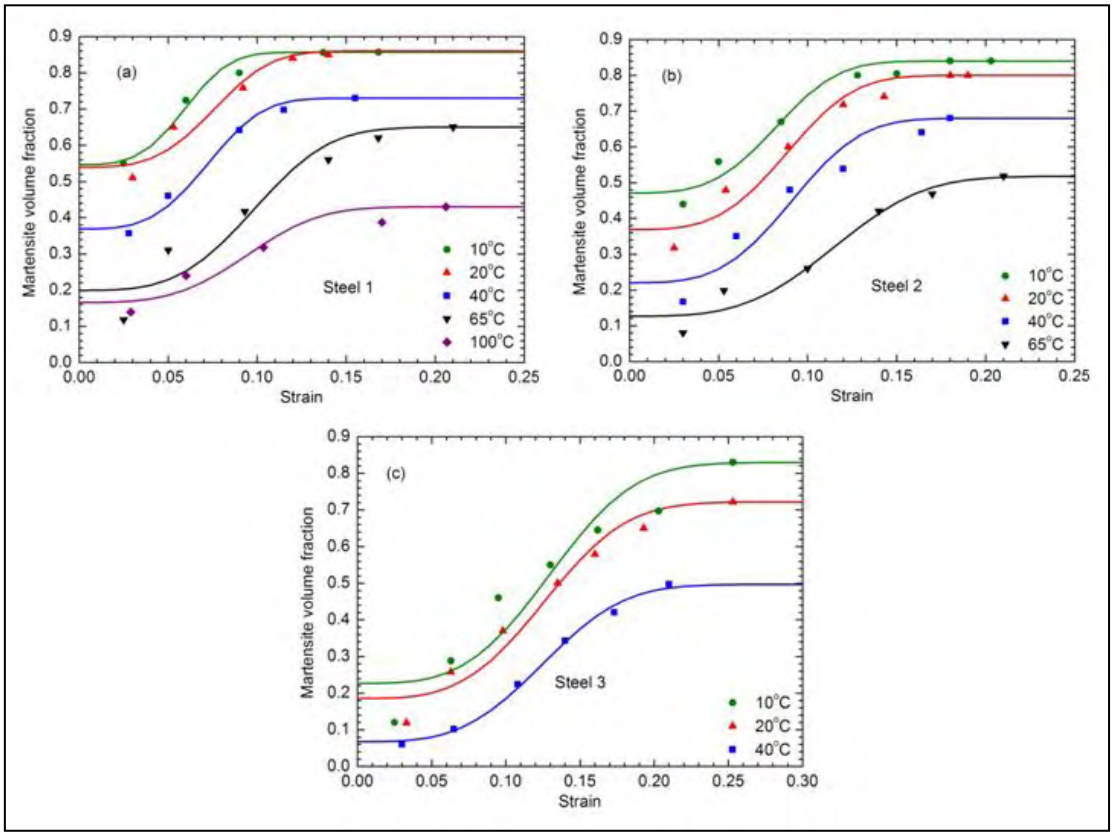

Figure 27: Variation of martensite volume fraction with axial strain. Comparison of model with experimental data for (a) Steel 1 (b) Steel 2 and (c) Steel 3

As mentioned in section 3.2.1 the critical n^* for martensitic nucleation is temperature-dependent through the term ΔG_{ch}. In Figure 28 it can be seen how temperature affects the critical nucleation thickness for Steels 1, 2 and 3. With decreasing temperature less potent nucleation sites (sites of low number of n crystal planes) are activated to produce transformation. Always at the same temperature, strain-induced transformation triggers nucleation sites of lower potency compared to stress assisted

transformation. This is due to the optimal orientation of the nucleation sites to the applied stress in strain-induced mechanism.

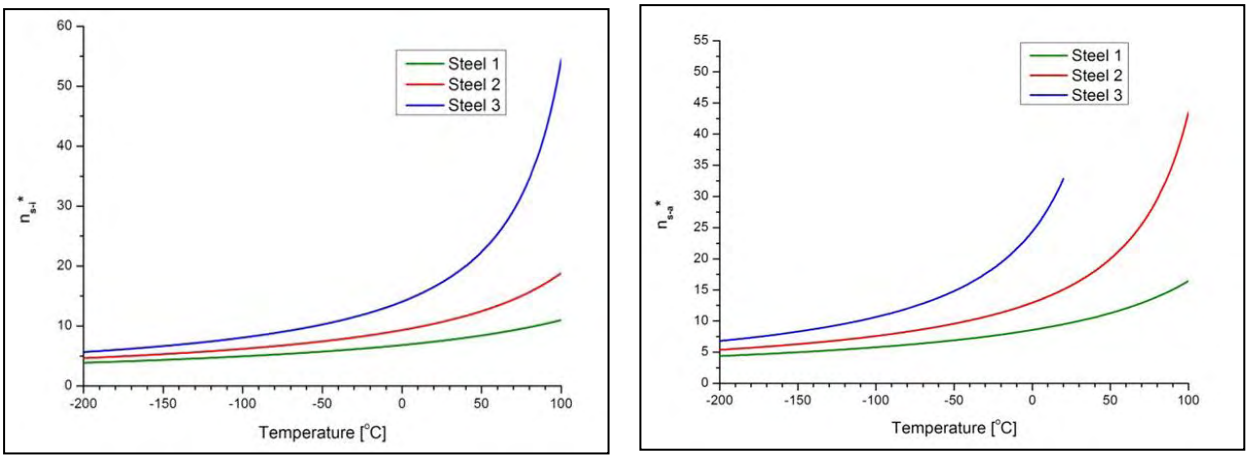

Figure 28: Variation of critical value of n* for martensitic transformation with temperature for Steels 1, 2 and 3

At low temperatures the discrepancy between the critical thicknesses n^* of the two distinct mechanisms is low. However, as the temperature increases the thicknesses needed to trigger stress-assisted transformation increase with higher rate compared to strain-induced transformation. It is interesting to note that at temperatures a little bit higher than room temperature the more stable Steel 3 cannot practically trigger stress assisted transformation, because of the significant decrease in the chemical driving force. The model predicts that stress assisted transformation can occur for Steel 3 until approximately 75^{o}C but the critical thickness needed is in the range of thousands. The lower the n^* value is the higher is the contribution of each transformation mechanism in the total transformation kinetics as it can be seen by Equations (3.6 and 3.10). These observations resulting from the model about the potency distribution of the nucleation sites are in accordance with the experimental data as determined in [37].

3.7 Implications of the model

The model presented above predicts the evolution of martensite during strain-induced transformation taking into account the effects of the chemical composition of austenite, temperature, average size of austenite particles and stress triaxiality. In this section the effect of temperature on the stress assisted portion of the transformation is discussed together with the effects of austenite particle size and stress triaxiality.

3.7.1 Stress-assisted transformation

It was shown in the previous section that both the transformation fraction and the transformation rate increase with decreasing temperature. The same holds for the stress-assisted portion of transformation f_{SA}, which is plotted against temperature in

Figure 29. It is clear that the lower the temperature, the higher the contribution of stress-assisted transformation relative to the strain-induced transformation.

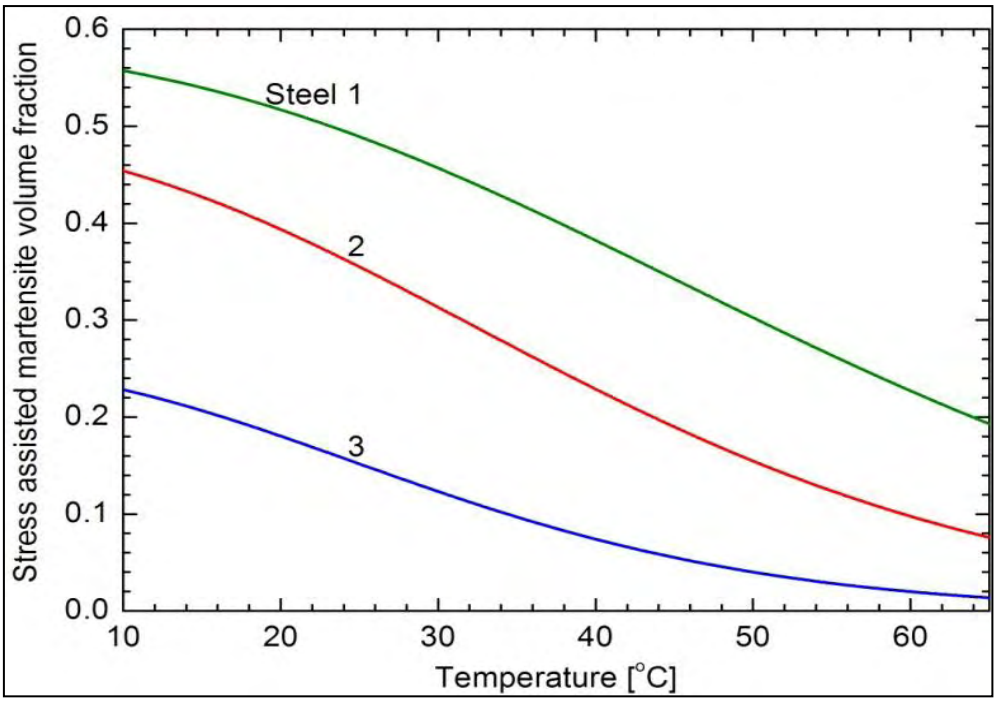

Figure 29: The fraction martensite formed through stress-assisted transformation (f_{SA}) as a function of testing temperature for Steels 1, 2 and 3

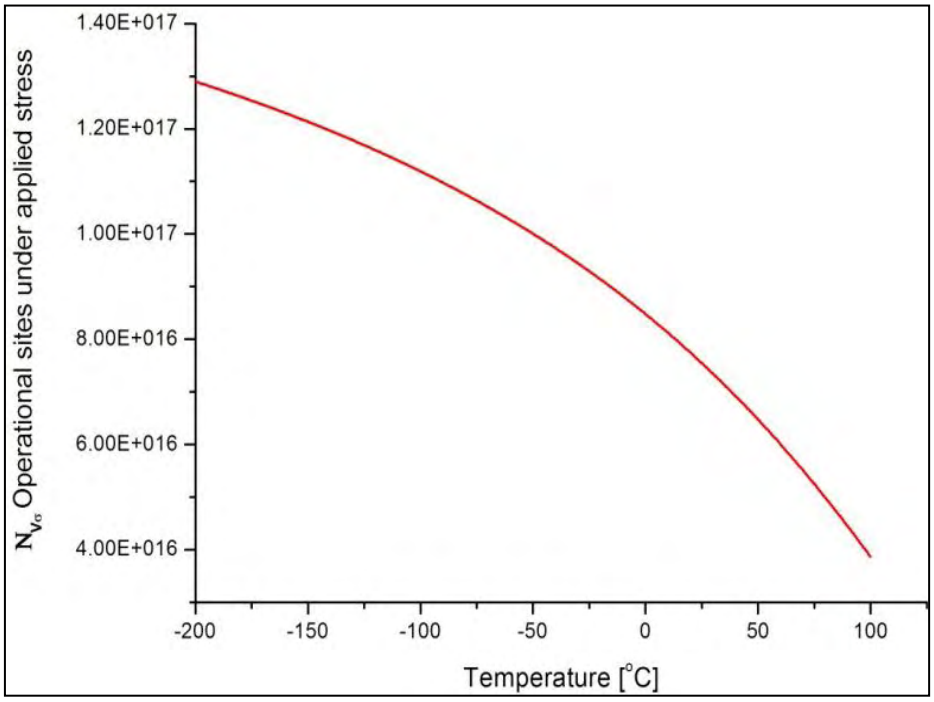

Figure 30: Variation of operational sites under applied stress with temperature for Steel 1

As we observe from Equation (3.6) the operational sites under applied stress (the sites that produce transformation during stress-assisted transformation) increase with decreasing temperature. In Figure 30 we can observe the increasing trend of the operational sites N_v^{σ} with decreasing temperature for Steel 1. The stress-assisted portion of the transformation f_{SA} , depends directly from the operational sites N_v^{σ} value from Equation (3.18).

3.7.2 Effect of austenite particle size

In order to investigate the effect of the austenite particle size, the model was applied to an austenite-containing steel for the following conditions: carbon content of retained austenite 0.8 mass%, tensile testing temperature 20°C, $N_v^{\sigma 0}$ =2x10^{17}m^{-3}and N=2x10^{19}m^{-3}. According to Equation (3.14), the particles size affects the transformation through v_p , the average volume of the austenite particles. The austenite particles are assumed to be spherical with radius R , so that $v_p = \frac{4}{3}\pi R^3$. The results are shown in Figure 31 where the transformation fraction is plotted as a function of plastic strain for spherical austenite particles with 0.1-1.0 μm average radius.

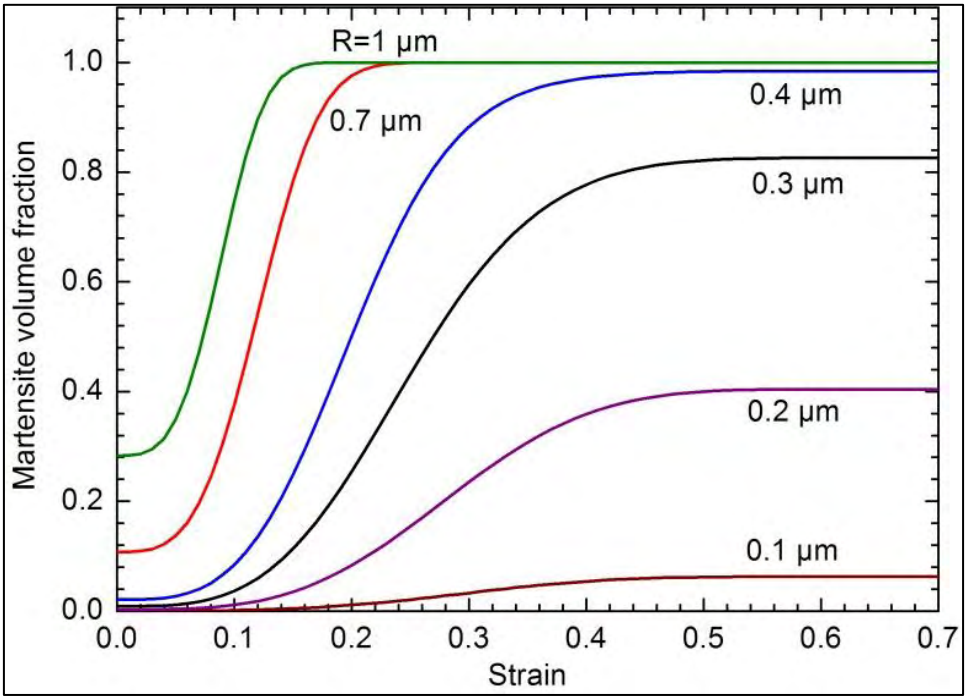

Figure 31: Effect of particle size on the curve for a steel with 0.8 mass% C (T=20°C). R is the radius of the spherical austenite particles

The stabilizing effect of austenite particle size refinement is evident. For example at ε=0.2, while the transformation in the steel containing 1μm - sized particles has been completed, the transformation for the steel with 0.1 μm-sized austenite particles has

barely started. In addition the transformation rate $df/d\varepsilon$ increases with the size of the austenite particles and the transformation is completed (f=1) only for steels containing large particles.

3.7.3 Effect of stress triaxiality

Stress triaxiality (stress state) influences the transformation kinetics through the interaction with the transformation dilatation. The effect is complex and to a first approximation can be taken into account through the mechanical driving force contribution, as described by Equations (3.23) and (3.24). In order to investigate the effect of stress triaxiality, the model was applied to a steel containing dispersed austenite of higher carbon content (1 mass%), which reduces the chemical driving force ΔG_{ch} for martensitic transformation. This leads to an increased relative contribution of the mechanical driving force ΔG_{σ} to the total driving force and emphasizes the effect of stress triaxiality. The temperature was set to 20°C and two cases regarding the average austenite particle size were considered: 1 and 0.3μm radius. The same $N_v^{\sigma 0}$ and N values as in the case of section 3.7.2 were adopted. The results are shown in Figure 32, where the transformation fraction is plotted as a function of plastic strain for three values of the triaxiality factor $\frac{\sigma_h}{\bar{\sigma}}$: -1/3 corresponding to uniaxial compression, 1/3 corresponding to uniaxial tension, and 3, which is a relatively high triaxiality factor representing a stress state ahead of a plastically deforming plane-strain mode-I crack tip.

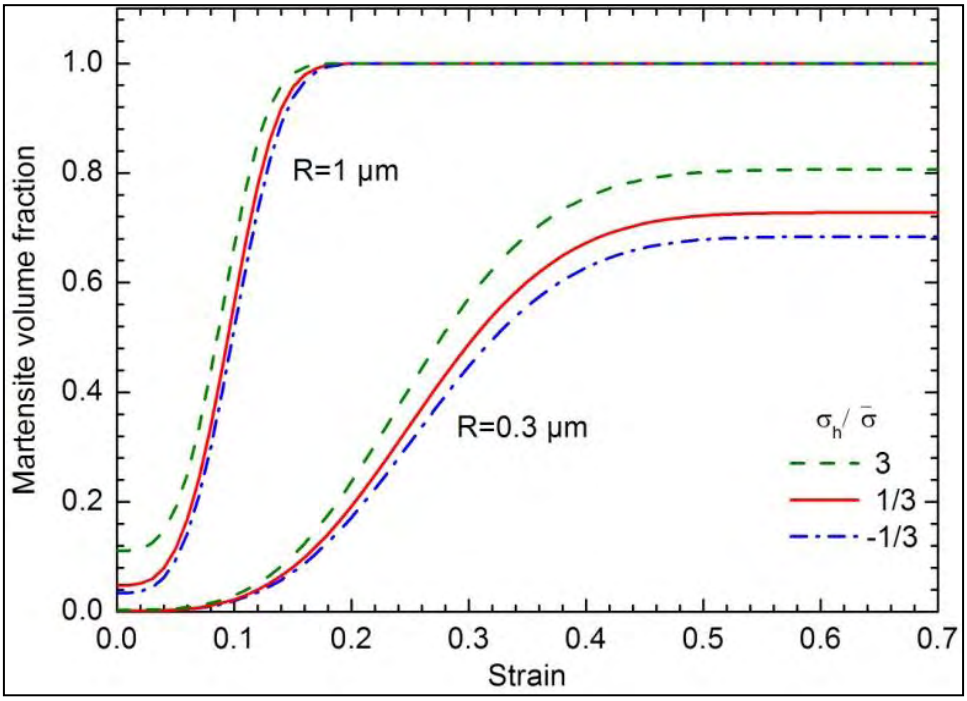

Figure 32: Effect of stress triaxiality on the curve for a steel with 1 mass% C (T=20°C, R=1μm and R=0.3μm)

Relative to the case of uniaxial tension, uniaxial compression results in a lower transformation fraction, while the high-triaxiality crack-tip stress state results in a higher fraction of transformation. The effect of stress triaxiality changes with the average austenite particle size. In the less stable 1μm particle dispersion, stress triaxiality affects the stress-assisted transformation and the strain-induced transformation at low strains, while in the more stable 0.3μm particle dispersion the stress triaxiality effect is stronger at higher plastic strains. Judging from Figure 32, the stress triaxiality effect is not as strong as the particle size effect of Figure 31, however, as stated above, it could become important in austenitic dispersions with high chemical stability.

3.8 Effect of various parameters used in this model

In the model described several parameters have been used. The values of these parameters influence the kinetics of the transformation and they have been adopted through literature review and specifically from the work of Kuroda [52]. For instance as mentioned before in this chapter the values of the shape parameters have changed in comparison to Kuroda's study. In this section several diagrams are presented showing the effect of those parameters. Steel 1 of Samek's work was adopted in order to investigate the effect of those parameters and the conditions: tensile testing temperature 20°C, $N_v^{\sigma 0}$ =2x10^{17}m^{-3}and N=2x10^{19}m^{-3} were used to proceed to the calculations.

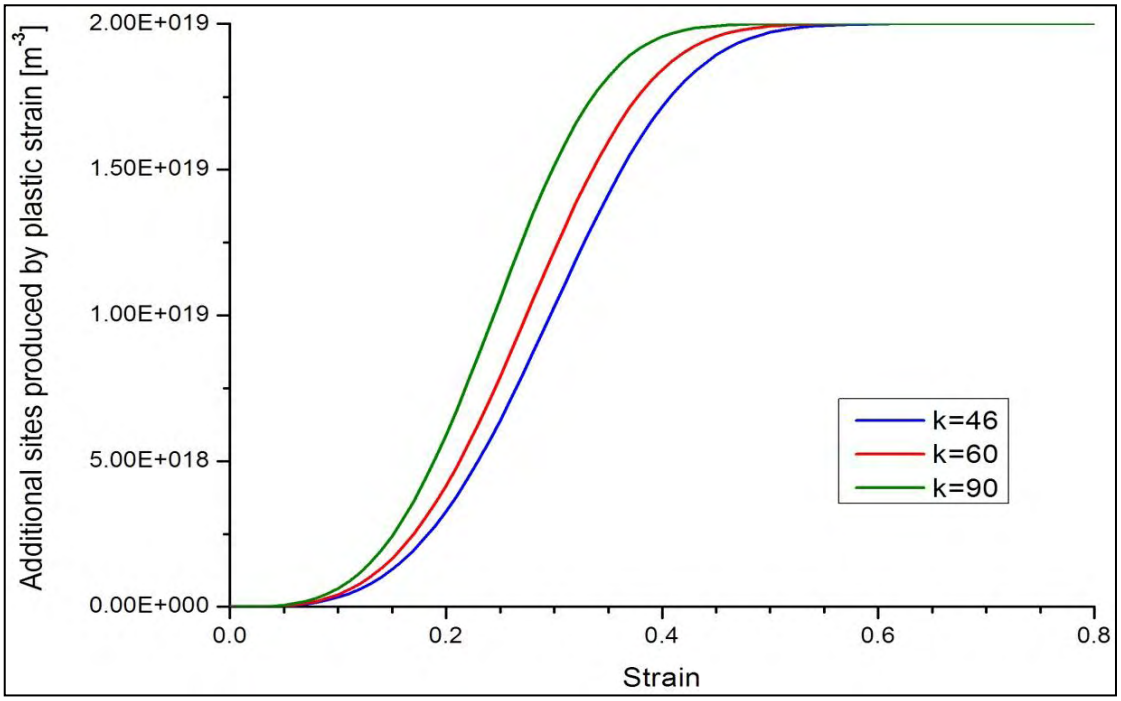

Figure 33: Variation of additional sites produced by plastic strain with axial strain for Steel 1 for three different values of the parameter k

According to Equation (3.9) the additional sites produced by plastic strain change when the value of k changes. The results are shown in Figure 33 where the additional sites produced by plastic strain $N_v^{\varepsilon 0}$ are plotted as a function of plastic strain. It is evident that as the value of k increases so does the number of $N_v^{\varepsilon 0}$ parameter. However, for the values of k under consideration it can be seen that the order of the additional sites produced stays quite stable.

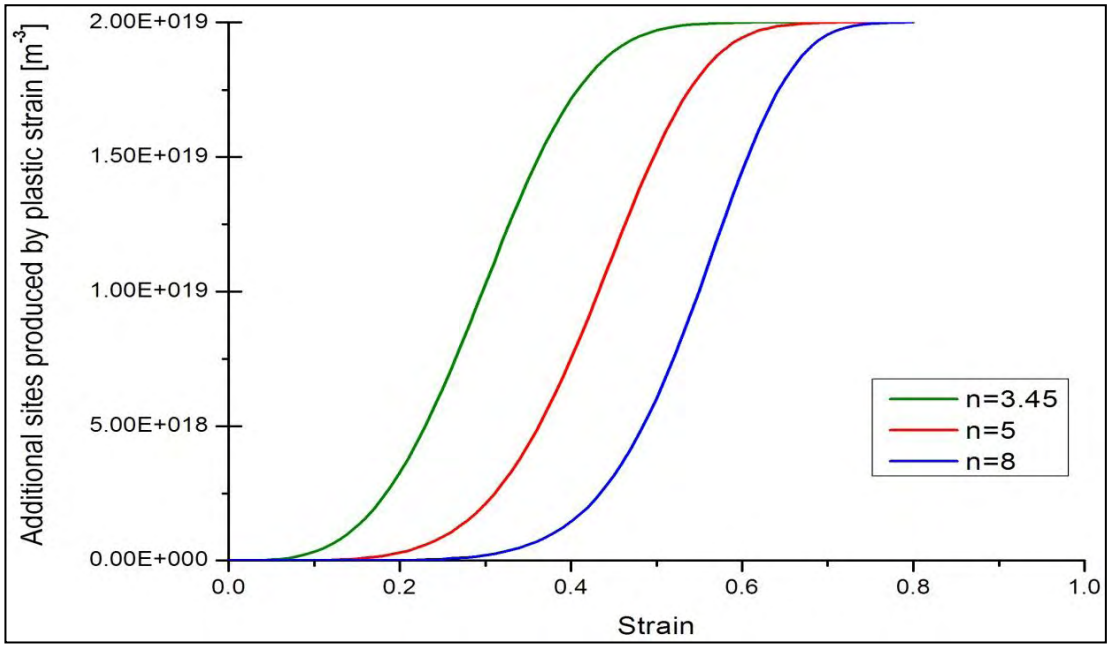

Figure 34: Variation of additional sites produced by plastic strain with axial strain for Steel 1 for three different values of the parameter n

Figure 34 presents the variation of additional sites produced by plastic strain with axial strain for Steel 1 under consideration for different values of the n parameter. An increase of the n value of Equation (3.9) leads to a decrease in the number of $N_v^{\varepsilon 0}$ value and consequently to a decrease of the strain-induced portion of the total transformation. At the same strain (i.e. $\varepsilon = 0.2$), while additional sites by plastic strain have been produced for the $n = 3.45$ value, for the two other n values the strain-induced transformation has barely or not even started.

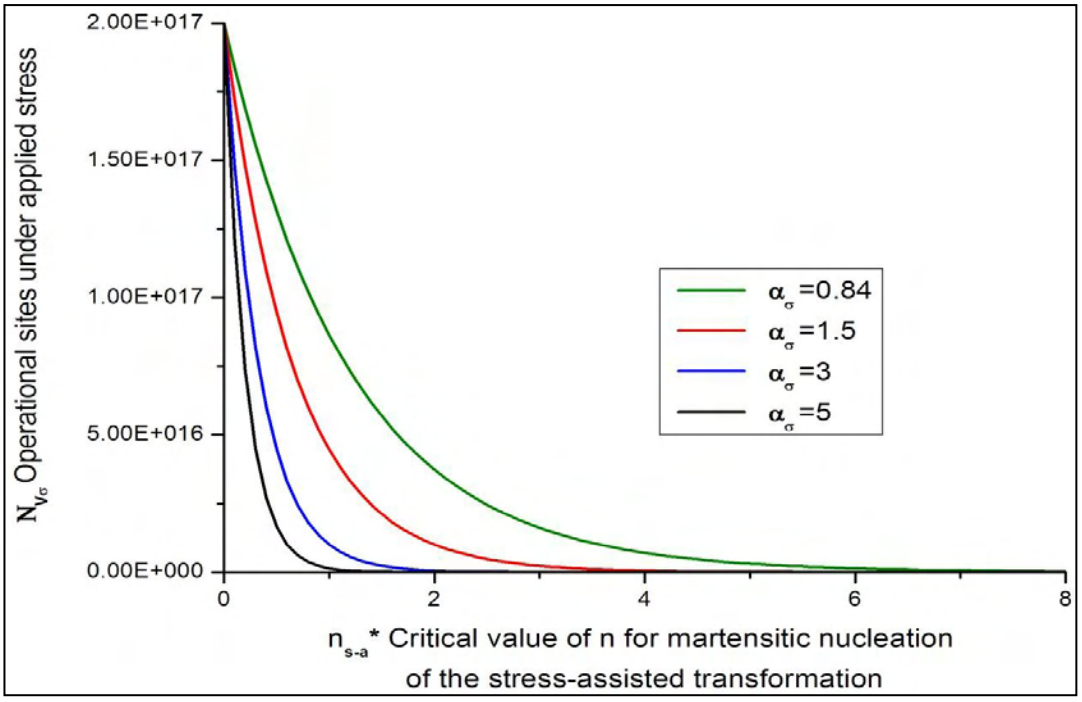

Figure 35: Variation of operational sites under applied stress with critical value of for stress-assisted martensitic transformation for Steel 1

Equation (3.16) shows that the operational sites under applied stress, which trigger stress-assisted transformation, depend from the critical thickness of the nucleation sites. As the critical thickness for stress-assisted transformation decreases less potent nucleation sites transform leading to an increase in the value of the operational sites. In Figure 35 we observe that for a given critical thickness as the shape parameter of the stress-assisted transformation a_σ increases the number of operational sites decreases. Even with the initial shape parameter of $a_\sigma = 0.84$, which was adopted in Kuroda's [52] work as obtained in Figure 35, in order stress-assisted transformation to be triggered in the less stable Steel 1, sites of really low potency need to be activated. Through this observation it can be better understood why a diminished value of $a_\sigma = 0.1$ was adopted in the present work. According to the model, by adopting a shape parameter a_σ in the range of 1.5-5 a dissociation of a defect with critical value of n^*_{s-a} greater than approximately 6 crystal planes is impossible to happen.

In Figure 36 below it can be seen how the new shape parameter affects the value of the operational sites N_v^σ.

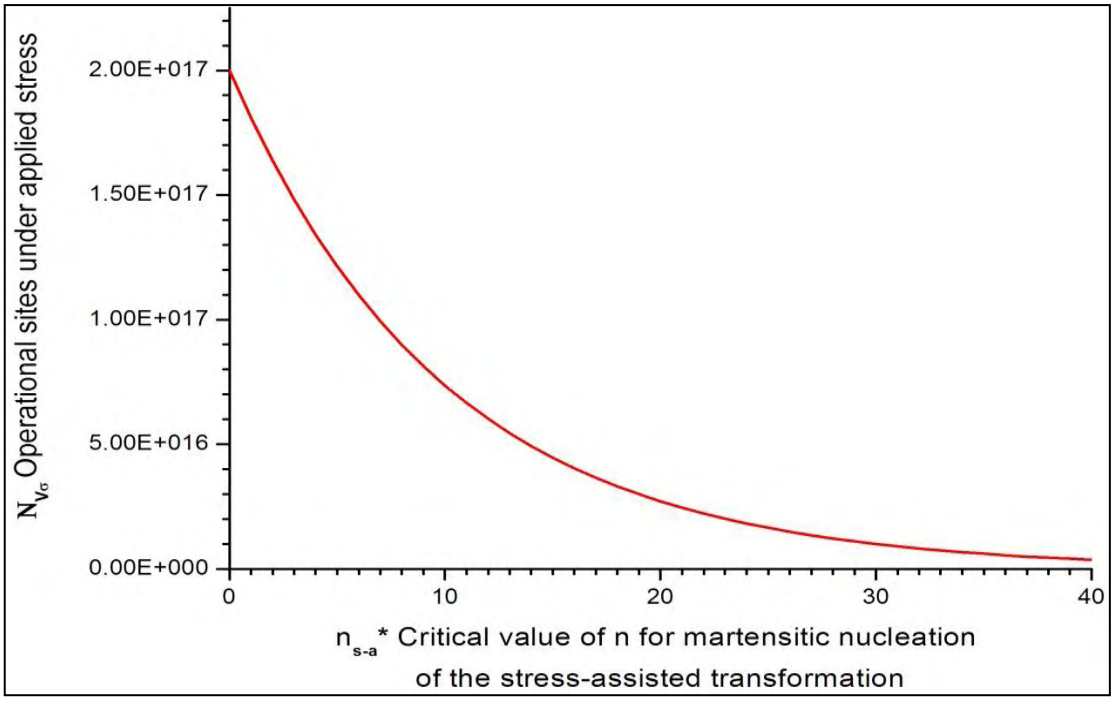

Figure 36: Variation of operational sites under applied stress with critical value of for stress-assisted martensitic transformation for Steel 1

3.9 Implementation of the M_s^{σ} model for the calculation of the carbon content in the retained austenite

The model of the M_s^{σ} temperature [14], which was described in the previous chapter, is based on the Olson and Cohen [48-50] theory. In a previous work of Haidemenopoulos et al. [30], high cycle fatigue tests were carried out to determine the S-N fatigue curve of TRIP steel 700. The austenite stability of this steel was measured by implementing a special technique for determination of M_s^{σ} temperature.

The M_s^{σ} temperature was measured using the Single Specimen-Temperature Variable-Tensile technique (SS-TV-TT). The accuracy of the method increases with the amount of retained austenite in the microstructure. After having measured the M_s^{σ} temperature, calculation of the carbon content of the retained austenite by applying the M_s^{σ} model, which is described in the following section, follows.

3.9.1 Calculation of the M_s^{σ} temperature

The transformation stress $\sigma = \sigma_{\tau}$, at which the martensite nucleation is triggered, can be found by combination of Equations (3.4), (3.6), (3.23), (3.13a) :

$$\sigma_t = \frac{1}{\frac{\partial \Delta G}{\partial \sigma}} * \left[\frac{2\alpha_{\sigma}\gamma_s}{\rho \ln\left[-\frac{\ln(1-f)}{N_v^{\sigma 0} V_p} \right]} - \Delta G_{ch} - W_f - E_{str} \right] \qquad (3.27)$$

The M_s^{σ} temperature can be found by setting the transformation stress equal to the yield strength ($\sigma_\tau = \sigma_y$) in Equation (3.27) and solve for the temperature. The temperature is hidden into ΔG_{ch} term.

Implementing a linear curve fitting in available experimental data the following expression for ΔG_{ch} is given:

$$\Delta G^{ch} = -7381.6 + 69447 x_C + 19296 x_{Mn} - 38776 x_C x_{Mn} + 6.7821 T - 33.45 x_C T \quad (3.28)$$

The M_s^{σ} temperature can be obtained if we insert the expressions for the chemical driving force Equation (3.28), mechanical driving force Equation (3.24) and frictional work, Equations (3.25)-(3.26) into the expression for the transformation stress, Equation (3.27), and solve for the temperature. The resulting expressions are the following:

for the linear W_f model, Equation (3.25) :

$$M_s^{\sigma} = (6.7891 - 33.45 x_C)^{-1} * (A + 5712.6 - 78224 x_C - 21542 x_{Mn} + 18876 x_C x_{Mn} + \sigma_y \left(0.715 + 0.3206 \sigma_h / \bar{\sigma}\right)) \quad (3.29)$$

for the 2/3 power law W_f model, Equation (3.26) :

$$M_s^{\sigma} = (6.7891 - 33.45 x_C)^{-1} * (A + 6881.6 - 69447 x_C - 19296 x_{Mn} + 38776 x_C x_{Mn} - 1893 x_{Mn}^{\frac{2}{3}} - 13100 x_C^{\frac{2}{3}} + \sigma_y \left(0.715 + 0.3206 \sigma_h / \bar{\sigma}\right)) \quad (3.30)$$

where A is given by the following expression:

$$A = \frac{2 \alpha_\sigma \gamma_s}{\rho \ln\left[-\frac{\ln(1-f)}{N_v^{\sigma 0} V_p}\right]} \quad (3.31)$$

The values of the various parameters used in the M_s^{σ} model are summarized in Table 4.

Table 4: Values of various parameters used in the M_s^{σ} model

Parameter	Value	Parameter	Value
a_σ	0.866	ρ	3×10^{-5} mol/m^2
$N_v^{\sigma 0}$	2×10^{17} m^{-3}	E_{str}	500 J/mol
γ_s	0.15 J/m^2	f	0.01

The austenite particle volume v_p has been assumed to be spherical. A mean radius of 3 μm was adopted in the calculations based on the measurements of the work of Haidemenopoulos et al. [30] for the TRIP steel under consideration.

3.9.2 Material and heat treatment

The chemical composition (in mass%) of the investigated TRIP steel is presented in the following table:

Table 5: Chemical composition (in mass%) of the steel under consideration

Steel	C	Al	Mn	Si	P	Reference
TRIP 700	0.2	1.33	1.8	0.04	0.016	[30]

Following cold rolling the material was subjected to a specific heat treatment in order to produce a microstructure with dispersed austenite content at room temperature. Two different annealing procedures were carried out, resulting to two different initial austenite volume fractions and stabilities. Heat treatment (A) included itercritical annealing at 890 ^{o}C for 60 s, to obtain a ferrite-austenite structure , cooling at 50K/s to 400 ^{o}C and holding for 420 s to enable the isothermal transformation of austenite to bainite. Heat treatment (B) included intercritical annealing by holding at 890 ^{o}C for 60 s, cooling at 50K/s to 460 ^{o}C and holding for 120 s. The heat treatment schedules are presented in Figure 37.

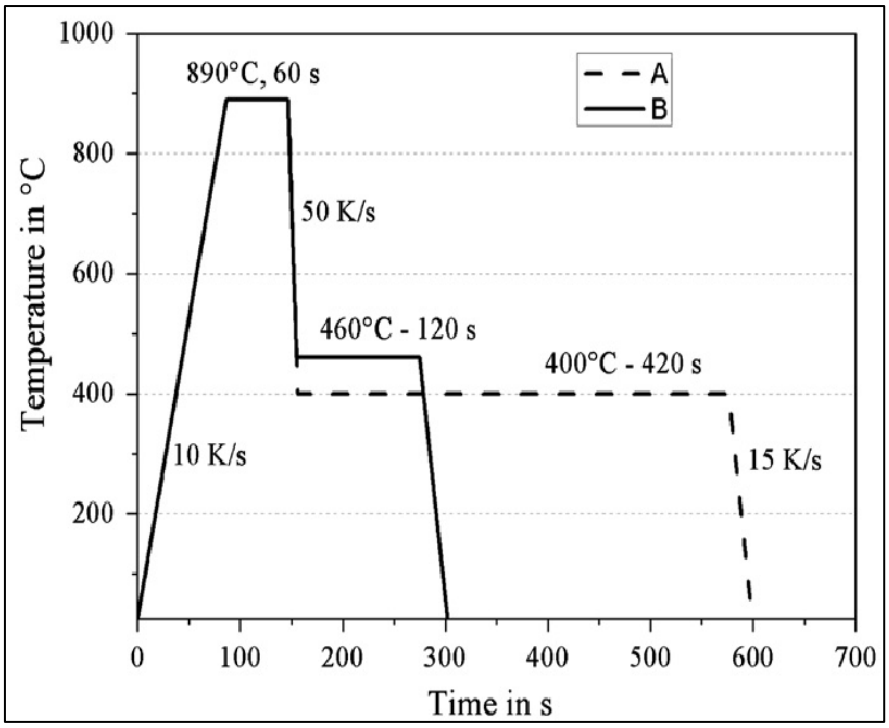

Figure 37: Representation of heat treatment A and B for TRIP steel 700 [30]

The carbon enrichment of austenite from bainite during bainitic transformation leads to the stabilization of the retained austenite. In addition, material (A) is more stable than material (B), because of the more efficient carbon partitioning from bainite to austenite, during isothermal holding at the bainite transformation temperature and therefore, carbon enrichment of retained austenite. The different austenite stability leads to different yield stresses for the two materials.

3.9.3 Calculation of the carbon content of the retained austenite

The values of the M_s^{σ} temperature were measured through the experimental procedure (SS-TV-TT) as mentioned before. However, there is not any information concerning the carbon content of the retained austenite. Scope of this section is to observe the prediction of the M_s^{σ} model concerning the carbon content of the retained austenite, after implementing the measured M_s^{σ} temperature values of the two materials into the model. This information is very useful, because without any experimental procedure an estimation of the retained austenite carbon content can be made. In order to proceed to calculations it should be mentioned that the Mn content, which is needed in Equations (3.29)-(3.30) was taken equal to the initial Mn content of the TRIP 700 steel under consideration.
The properties of the TRIP steel 700 are shown in Table 6.

Table 6: Tensile properties of TRIP 700 (A) and (B) materials

TRIP 700	RA(%)	M_s^{σ} (°C)	σ_{y02}(MPa)
A	11.2	-15	538
B	14.3	-5	482

The results, which were given by Equations (3.29)-(3.30) about the C content of the retained austenite are presented in the Table 7.

Table 7: Chemical composition (in mass%) of the retained austenite of Steel (A) and (B) for the linear and the 2/3 power low M_s^{σ} model

TRIP 700	Linear model	2/3 power law model
A	0.943	0.910
B	0.910	0.883

From the results presented in Table 7 we can come to the following conclusions:

- There is a strong chemical stabilization effect associated with C mainly enrichment of the austenite particles. A small increase in the carbon content of the retained austenite results to a significant drop of the M_s^{σ} temperature. In this case the M_s^{σ} temperature decreases by 10°C for an 3.62% and 3.05%

increase in the carbon content of the retained austenite according to linear and 2/3 power law model respectively. As the austenite stability decreases the M_s^{σ} increases.

- The discrepancy between the linear and the 2/3 power law M_s^{σ} models is significant, when we have to choose the model, which we want to adopt to estimate the chemical composition of the carbon, because of the aforementioned stabilizing effect of the carbon.
- Knowing the M_s^{σ} temperature Equations (3.29) or (3.30) can be used to calculate the carbon partitioning in the retained austenite.
- M_s^{σ} temperature defines an approximate boundary between the temperature regimes where separate modes of transformation dominate.

4 Evolution of the austenite grain size during the strain-induced transformation

4.1 Introduction

One of the key factors, which can influence metal sheet mechanical properties during material multi-step deformation process, is pre-strain. In this study it is investigated the influence of the strain factor in the transformation-induced plasticity of the steel. The plastic deformation accompanying the pre-strain tests leads to an increase in the number of nucleation sites. The nucleation site probability derives not only by the stress triaxiality, temperature and plastic strain, but also by pre-strain to simulate the transformation-induced plasticity characteristic for TRIP steel. As the strain increases the shear-band intersections increase and new more potent nucleation sites are created. The excellent mechanical properties of TRIP steels derive from the transformation of the retained austenite during plastic strain deformation, which deduces a localized increasing of the strain-hardening coefficient during deformation process of TRIP steels and delays the onset of necking and ultimately leads to a higher uniform and total elongation. Pre-strain tests were applied to clarify the deformation behavior of uniaxial tension of the TRIP steel in five different pre-strains. In each strain the pre-strain test was implemented twice in order to verify the credibility of the results delivered. As the strain increases the fraction of the retained austenite decreases. The main reason why this experiment took place was to show that the mean size of the retained austenite decreases as the strain increases. This rational assumption is concluded from the fact that the larger the grain size of the retained austenite is, the higher is the probability a nucleation site of great potency to be found. It has been experimentally observed in studies of fully austenitic alloys and multiphase TRIP steels that the resistance to martensitic transformation increases as the grain size of the austenite decreases (Leal and Guimaraes [58] and Jeong et al. [59]). Gonzáles et al.[60] studied the effect of austenite grain size on the strain-induced α'- martensite transformation in AISI 304 steel. The transformation was found to be enhanced by large grain size. The grain size of the retained austenite to some extent can be controlled through a suitably chosen thermal processing route [61]. Consequently, in order to optimize the mechanical characteristics of TRIP steels, it is relevant to understand in detail the effect of the austenitic grain size on the onset and evolution of the martensitic transformation, which is the main objective of the present chapter.

Various models have been proposed for transformation-induced plasticity but only a few of them address the issue of grain size effects. Adopting a geometrically linear framework, Reisner et al. [62] studied the transformation rate in a Cu–Fe and a low-alloyed TRIP steel, although grain size effects were only included for the Cu–Fe alloy. They predicted that the number of alternating bands of martensitic twins increases with increasing grain size. Based on a modification of a model proposed by Olson and Cohen [43] and applying the Hall–Petch relation for the austenitic phase, Iwamoto and Tsuta [63] studied the influence of grain size on the mechanical response of an austenitic stainless steel. Their phenomenological model, which does

not explicitly take into account the crystallography of the transformation systems, predicts an increase in effective tensile strength for an increase in austenitic grain size. This result is ascribed to the formation of less martensite for smaller grain sizes. Also based on a modification of the Olson-Cohen model, Perlade et al. [64] proposed a one-dimensional constitutive formulation for low-alloyed TRIP steels. The effective strength resulting from stress-assisted and strain-induced transformations was found to be sensitive to the austenitic grain size.

Through this experimental procedure it is interesting to note how the strain percentage influences the rate of the retained austenite grain size reduction.

Following cold rolling the material was subjected to a specific heat treatment in order to produce the final microstructure. In this microstructure austenite is found in the form of dispersion. After the pre-strain experiment followed measurement of the fraction as well as of the size of the retained austenite. Through this procedure useful results regarding the impact of the size of the retained austenite in the martensitic transformation can be exported. The methods used to determine the size and the fraction of retained austenite after the pre-strain test are examined in this chapter.

4.2 Material

The steel under consideration in this study is the continually annealed TRIP 700 with initial volume fraction of retained austenite 15.8% and 1.5 mm thickness. This steel is widely used and belongs to the advanced high strength steels (AHSS). It presents high yield strength and consists of ferrite, bainite and metastable retained austenite. The strain hardening, which results from the TRIP phenomenon, is the reason why this material is widely used for critical structural body parts of automotive industry.

The material under study was given to us by Voestalpine company. The chemical composition of the material is presented in the table below.

Table 8: Chemical composition in (%) weight of the steel

Material	C	Al	Mn	Si	P
TRIP 700	0.202	1.07	1.99	0.348	0.009

From this material twelve different specimens have been cut according to ASTM standards from a flat sheet at 0^{o}degrees rolling direction. The tensile geometry is presented in Figure 38. Mechanical testing was carried out by means of uniaxial tensile tests towards the rolling direction at different deformations. The objectives of the tensile tests were to study the effect of the austenitic particle size on the kinetics of the transformation.

The evaluation of transformation plasticity strain is a very difficult task, especially in the case of tensile loading. In the transformation plasticity test, a charge is applied to the specimen just before the beginning of the transformation. This charge is maintained constant during the transformation.

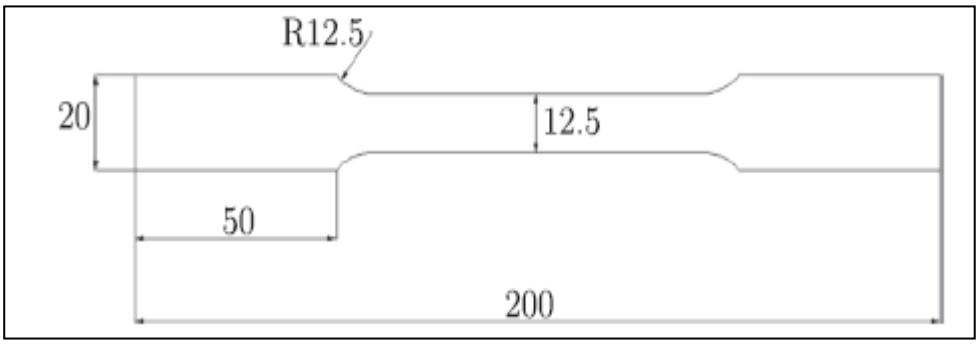

Figure 38: Tensile specimen geometry

Extensometer 25 mm was used in the longitudinal direction of the specimens (Figure 39).

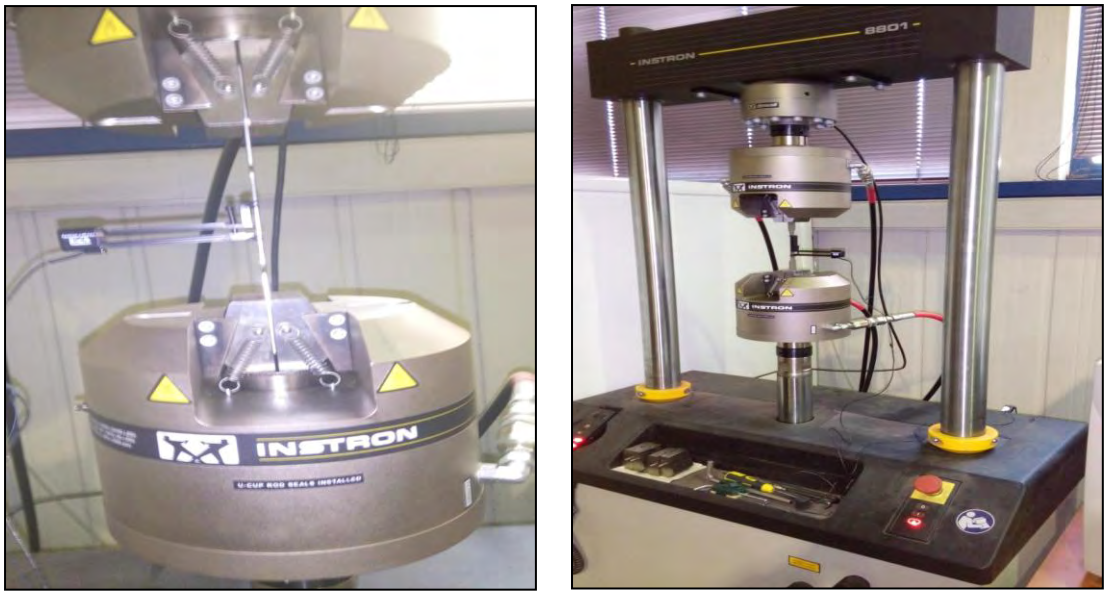

Figure 39: Demonstration of pre-strain test experiment

The mechanical properties of the material were determined by uniaxial tensile tests and they are collated to the microstructure of the steel. Those tests were carried in order to analyze the transformation of retained austenite into martensite during deformation. The first two specimens were pre-strained till fracture and from the data exported from the tensile testing machine the following diagram of Figure 40 is presented.

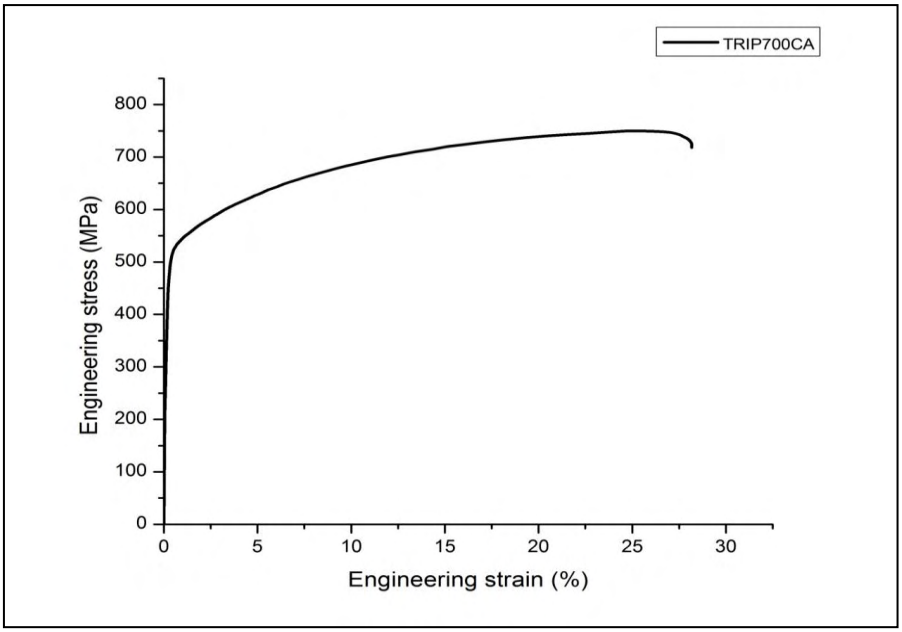

Figure 40: Engineering stress-strain curve in TRIP 700 steel

Table 9: Tensile properties of TRIP steel 700

Material	σy_{02}	σ_{uts}	ε_g	$\varepsilon_{failure}$
TRIP 700	474	731	23.3	29.9

Table 9 shows the tensile properties of TRIP steel 700. Pre-strain tests were performed twice at each strain at: 4, 8, 12, 18 and 22 % plastic strain.

4.3 Optical microscopy and etching technique

The optical microscopy was adopted as another method to investigate the microstructure and specifically the austenitic particle reduction during the deformation. From the tensile test specimens, samples parallel to the tensile axis were cut by the cutting machine. Digital micrographs were taken from each sample at arbitrary locations. Purpose of this procedure is the examination of the morphology of the steel and the average austenite particle size.

From the microscopy various grain sizes were obtained but it was difficult to distinguish the austenitic matrix. Attempts have been made with Scanning Electron Microscopy to distinguish the austenitic from the marentisitic matrix.

The metallographic preparation of TRIP steel specimens is performed in a standard fashion. In order to reveal the microstructure, an appropriate etchant is required which attacks various phases to different extent, producing a surface relief. After literature review and trials and errors it was found that better results are obtained by a two-stage etching using nital and 10% Na2S2O5 solution [65]. The ten different samples were grinded with 220, 500, 800, 1000 silicon carbide paper grade followed by polishing with 1 mm diamond past. Upon grinding and polishing, the specimens were etched with 3% nital (HNO3) for 5 seconds to reveal grain boundaries. The Nital etching is used for visualizing grain boundaries. This etchant is a 3 % solution of HNO3 in

ethanol. For the next step one minute etching 10% solution of Na2S2O5 (sodiumbisulfide etching) is used to reveal separately martensite, austenite and carbide containing phases. In this step, in addition to height differentiation of phases, the hardened phases (bainite or martensite) are colored.
These two etches reveal:

- Ferrite: It appears brown(grain).
- Bainite: Appears dark blue.
- Austenite: The austenite stays white but the island boundaries are etched.
- Martensite: It has the same color with austenite.

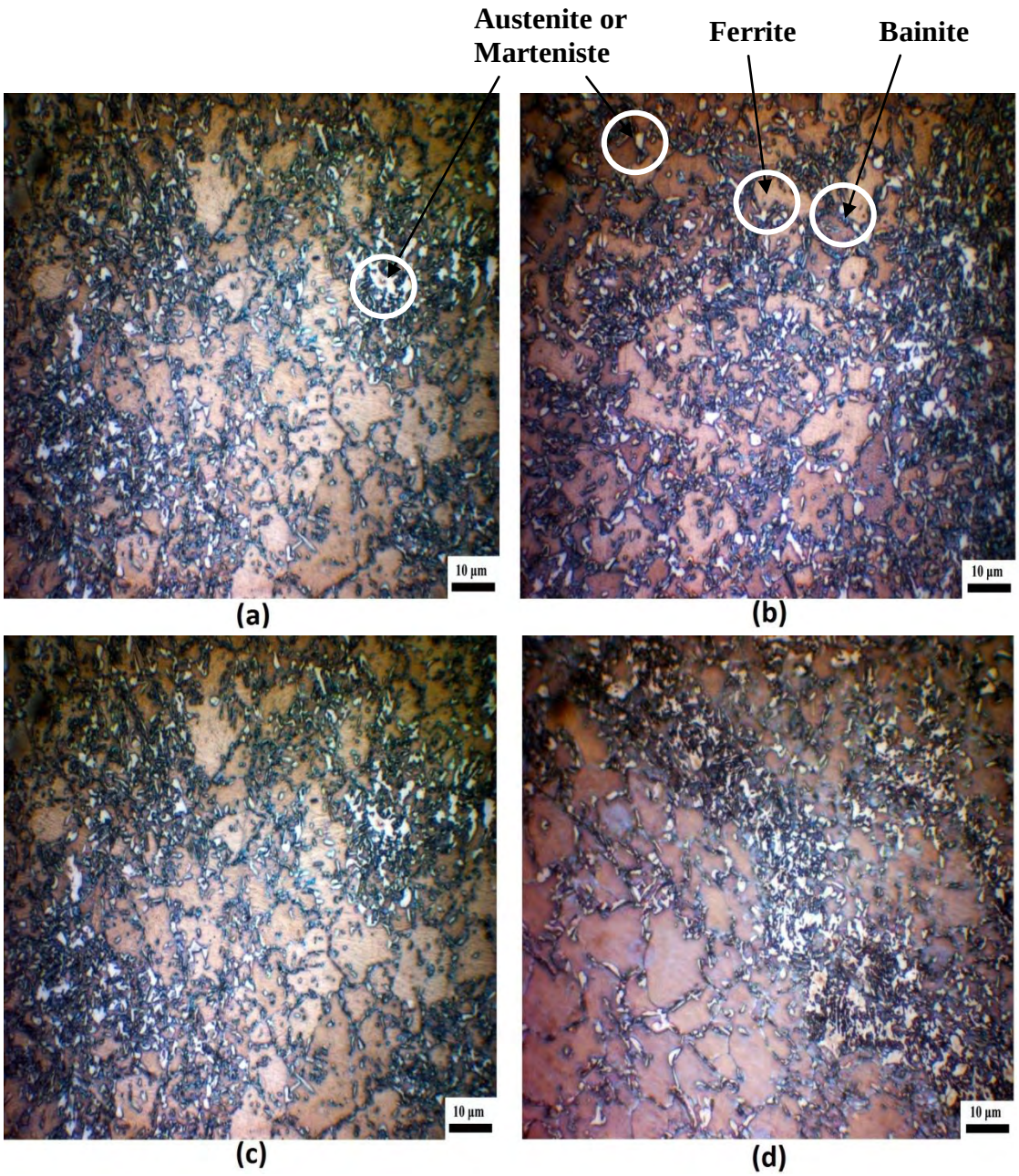

Figure 41: Microstructure of TRIP 700 steel (a) in untransformed material (15.8% RA) (b) after 4% deformation (13.7% RA) (c) after 8% deformation (12.1% RA) (d) after 12% deformation (7.1% RA)

Upon the selective etching produces, a light microscope with polarizing prism can be used as well. Figure 41 shows that different phases appear in different colors, which aids the identification of microstructure.

4.4 Magnetic method and volume fraction results

Determining the exact fraction of retained austenite is crucial in order to understand the impact not only of the retained austenite size on the kinetics of the transformation but also of the trend of M_s^{σ} temperature.

The magnetic method was adopted for the determination of retained austenite. Magnetization measurements have intrinsic advantages compared to other methods because they are accurate and probe the bulk of the material. This procedure took place in Linz Austria by Voestalpine company using saturation magnetization measurements. This method is based on the basic principle that ferrite (α'-Fe) is ferromagnetic while austenite (γ-Fe) is paramagnetic. The difference in saturation magnetization of specimens with and without austenite is related to the volume fraction of non-ferromagnetic retained austenite. Ferrite, martensite and cementite are ferromagnetic at temperatures below the Curie temperature while the austenite is paramagnetic. At first the exact volume of each specimen was measured. This was important because the following measurements were carried out based on the volume of the specimen. A quantitative determination of the volume fraction of the existing phases and especially of the retained austenite is essential for the evaluation of the TRIP steel properties. The size of the specimens was 14 x 3.5mm.

Before the measurement each specimen is inserted in a core of soft iron, where there is an inductive coil and a measuring coil. If the vacancy of the core and the permeability of the iron are large enough, we can assume that the magnetic lines, which come out from the edges of the specimen are entirely closed by the core. Thus, the magnetic field of the bar has the same value, assuming the coil and the bar had infinite length.

The specimen is magnetized till corrosion and it is afterwards rapidly exported from the core. Meanwhile, the local maximum U_a of the voltage is measured and through this measurement the magnetic induction B_m can be calculated. The retained austenite is given by the following equation:

$$\text{Retained austenite } \gamma_r\,[\%] = (B_s - B_m) * 100 / B_s \tag{4.1}$$

$$B_s = 2.158 - 0.15 * [\%C] - 0.048 * [\%Si] - 0.024 * [\%Mn] \tag{4.2}$$

B_s is the saturation of the specimen without austenite and B_m is the saturation after the measurement.

This method has the advantage of measuring the entire volume of the specimen. On the other hand the disadvantage is that there is no accurate method for the calculation of B_s without any error. That's the reason why the absolute value of this measurement

hides an error, which while comparing the measurements does not create any problem.
The volume fraction of the retained austenite, which was measured by the magnetic method as a function of the deformation is presented in Table 10.

Table 10: Measurments of retained austenite (RA) prior and after pre-strain test

Sample #	Deformation	Initial volume fraction (%)RA	Volume fraction (%)RA after test	% transformation of retained austenite
1_1	4%	15.8	13.0	17.72
1_2	4%	15.8	12.6	20.25
1_3	8%	15.8	10.3	34.81
1_4	8%	15.8	10.5	33.54
1_5	12%	15.8	8.6	45.56
1_6	12%	15.8	9.5	39.87
1_7	18%	15.8	6.7	57.59
1_8	18%	15.8	6.9	56.32
1_9	22%	15.8	5.2	67.08
1_10	22%	15.8	5.5	65.18

The stabilizing effect of the size of the retained austenite in the martensitic transformation is evident. This can be deduced from Table 10. Strain-induced transformation is affected by the austenite particle size. At the beginning of the strain-induced transformation at low strains the transformation rate is high whereas as the strain increases, the rate of the strain-induced transformation decreases. At higher strains the larger grains of austenite transform fully into martensite and as the transformation continues the more stable smaller austenitic particles suppress the kinetics of the transformation mechanism.

4.5 Determination method of the fraction of retained austenite

As it was mentioned again in previous chapter our model predicts that the austenite particle refinement has a strong stabilizing influence by retarding the strain-induced transformation kinetics. In order to validate this assumption ten pre-strained specimens (1_1-1_10) were sent in Cyprus University of Technology, in the Department of Mechanical Engineering where magnetic force microscopy (MFM) was implemented by Prof. G. Constantinides. The purpose of this research was to resolve the evolution of the morphological characteristics of the TRIP steel's microstructure as a function of the applied stress/strain. Exploiting the magnetic characteristics of the ferrite and bainite phases in contrast to the paramagnetic nature of the retained austenite useful results were extracted.
Magnetic force microscopy (MFM) has been in use ever since the principles of scanning probe microscopy have been presented. The feedback mechanism in this type of imaging is the magnetic interaction between a magnetic probe and magnetic

domains that might be present in a materials' microstructure. This type of interaction can be exploited for imaging purposes in which ferromagnetic and paramagnetic domains can be separated with high spatial resolution ([66]-[68]).
AC-MFM mode records the space distribution of the phase shift of a vibrating magnetic cantilever caused through the magnetic interaction with the surface. The nature of the interaction depends on the distance between the tip and the surface – one therefore needs to ensure that this is accounted, which in practice is taken into account by means of a 'two-pass method'. In the first pass the topography of the specimen is determined in 'semi-contact' mode. During the second pass the cantilever raster-scans at a fixed (predetermined) distance from the sample surface and the magnetic interactions during this constant-height flight are determined. The tip-sample separation is kept at a distance of 50-100nm in order to eliminate any Van der Waals' forces and probe only the long-range magnetic force. For every scan the height-image and the magnetic image are collected.
In the AC MFM during second pass the cantilever resonance oscillations are used to detect the magnetic force data (just as in the non-contact or semicontact modes). In AC MFM the microscope detects the force derivative: the force gradient in the point dipole approximation can be written in the form:

$$F' = n \, \mathrm{grad}(n F), \; F = (m \, \mathrm{grad}) H \qquad (4.3)$$

where n is unit vector normal to the cantilever plane. It is seen that AC MFM signal is proportional to the stray field second derivative.
In this study MFM has been used to isolate the paramagnetic phases from the microstructure and quantify their size and volumetric proportions, as a function of the pre-stressing of the material. An Ntegra-Prima, NT-MDT instrument has been used. A silicon cantilever with magnetic cobalt-chromium coating (and additional anti-corrosive layers) has been used in this study.

4.6 Results extracted by the MFM

Figure 42 presents a typical result of an AC-MFM image of TRIP steel. The deformation profile is shown in a 2-d (Figure 42(a)) and 3-d (Figure 42(c)) mode. It is evident that in the deformation mode only topographical characteristics are visible, which relate to the roughness resulted from the polishing procedure during the preparation of the specimens. It is impressive to see that the magnetic signal (2-d Figure 42(b), 3-d Figure 42(d)) reveals a completely new structure not evident in the deformation profile. This magnetic image is the result of the magnetic interaction between the magnetically coated silicon tip and the ferromagnetic phases that are present in the microstructure. Magnetic oscillations can be attributed to a series of factors including crystal orientation, crystal anisotropy, etc. Dark zones (close to zero-interaction) can be interpreted as areas where paramagnetic phases are present. It should be noted however that the selection of the level below of which is interpreted as zero interaction is a rather arbitrary process. Once a threshold level is defined one

can proceed with a grain analysis where the number of grains, mean grain size and volumetric proportions of the grains can be calculated. The image processing has been performed using the open source SPM software Gwyddion.

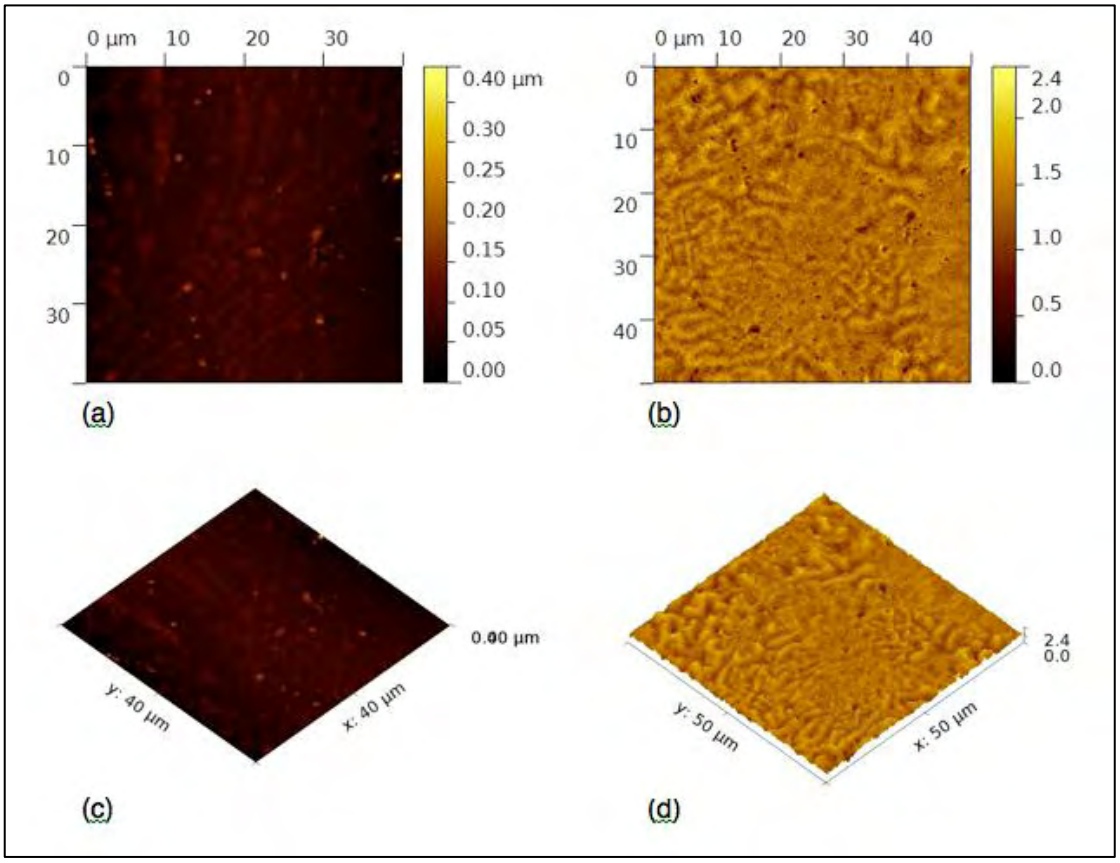

Figure 42: Deflection (a,c) and Magnetic (b,d) image of a TRIP steel (ε=4%). 2-d (a,b) and 3-d (c,d) visualizations

MFM images for all pre-strained TRIP specimens are shown in Figure 43 and the results of grain analysis are presented in Table 11. Dark zones in the MFM images are areas of low magnetic interactions whereas green and red areas correspond to ferromagnetic domains. The only paramagnetic phase in TRIP steels is the retained austenite; therefore the grain analysis gives access to retained austenite characteristics: volume fractions, mean RA size, number of RA grains. It is evident that as the deformation of the specimen increases the volume fraction of retained austenite decreases with an associated reduction in the mean grain size as it can be seen in Figure 44.

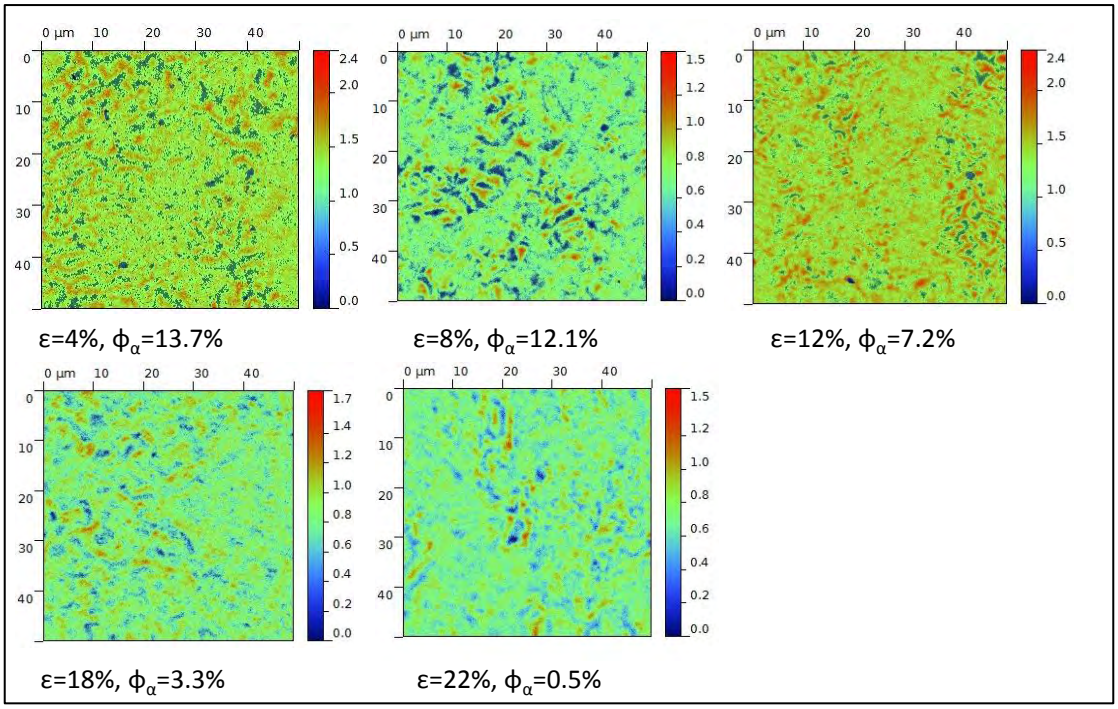

Figure 43: Deflection (a,c) and Magnetic (b,d) image of a TRIP steel (ε=4%). 2-d (a,b) and 3-d (c,d) visualizations

Table 11: Results from image grains analysis using the threshold method

Strain, ε [%]	Volume Fraction of RA [%]	Mean Grain Size [nm]
0	15.8	340
4	13.7	305
8	12.1	135
12	7.1	134
18	3.3	116
22	0.5	112

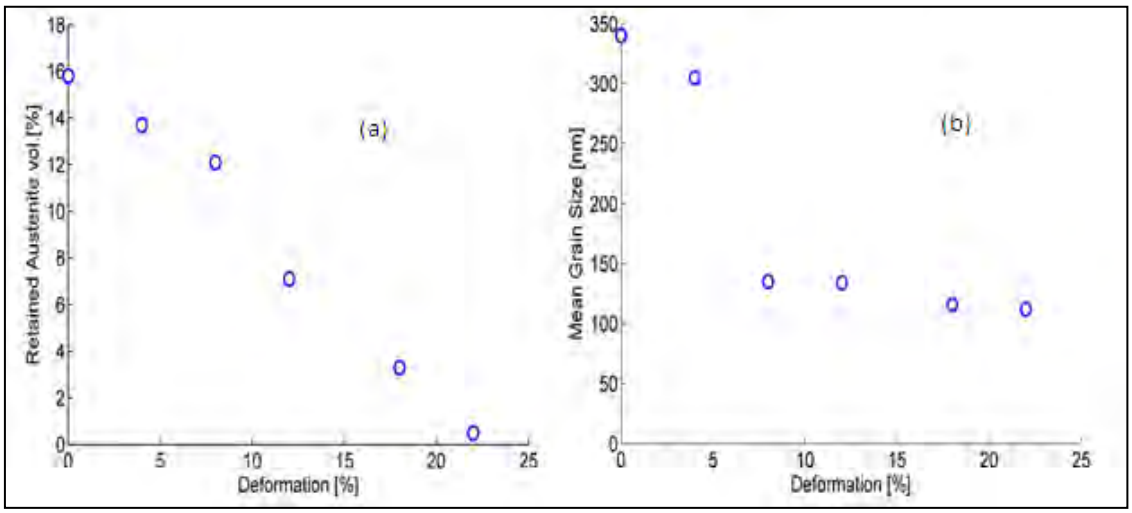

Figure 44: Evolution of retained austenite volume fraction (a) and mean grain size (b) as a function of specimen deformation

The volume fraction of the strain-induced martensite formed can be detected through the previous diagram. It is reasonable to say that the austenitic particle size influences considerably the kinetics of the transformation, especially at low strains where as it can be seen from 0 to 4% deformation the transformation rate is quite rapid (almost 20% transformed austenite) in comparison to further strain values. At the beginning of the transformation the larger austenitic particles, which are more likely to offer more potent nucleation sites transform and as the size of the mean austenitic particle size reduces so does the transformation rate.

The model describing the kinetics of strain-induced transformation of dispersed austenite, which was presented in the previous chapter, was applied in the experimental data of Figure 44a. In Figure 45 Equation (3.14) has been fitted to the available experimental data and the martensite volume fraction is plotted against plastic strain.

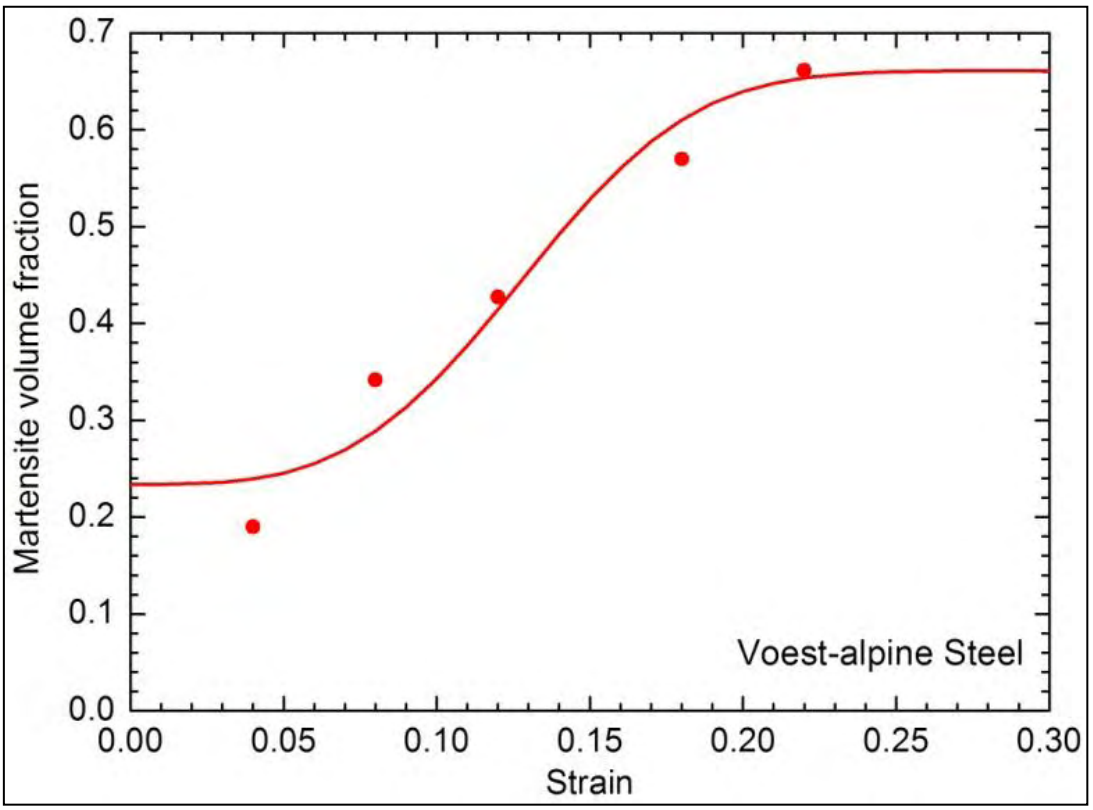

Figure 45: Variation of martensite volume fraction f with axial strain ε. Comparison of model and experimental data at 25°C for TRIP Steel 700

The average austenite particle size was set equal to the initial mean radius (R=340 nm) , which was measured at 0% deformation. The model predicts well the sigmoidal shape of the strain-induced transformation. The saturation level does not reach the value of 1.The pre-existing nucleation sites $N_v^{\sigma o}$ and the maximum sites that can be produced by plastic deformation were found by the above non-linear curve fitting and are $3.031 \times 10^{17} m^{-3}$ and $5.88 \times 10^{18} m^{-3}$ respectively. The results of the fitting parameters

come in accordance with the fitting parameter values, which were presented in the previous chapter.

4.7 Results

The tensile tests have shown us that the stability of the austenite increases as the grain size decreases. Austenite stability influences the unaxial performance of the material. The rate of the transformation in strain-induced martensite in tensile straining depends on the austenitic grain size. The mean grain size from 340 nm at the untransformed TRIP steel decreased after the deformation to 112 nm at 22% deformation.

Consequently, the effective strength is initially higher for smaller grains. In addition, the martensite transformation is partially suppressed as the grain size decreases. The transformation is more homogeneous for smaller grains and consequently, the effective transformation strain is larger. Apart from the austenitic grain size the austenitic grain orientation influences the transformation (whether it is favorable to the applied stress or not).

At strains greater than 18 % the stabilizing effect of the particle size becomes more evident. The larger the particle size is the lower the strain needed to transform it. Large austenitic particle size favors the martensitic transformation at small applied plastic strains. An efficient way to produce a TRIP steel with great work-hardening is to produce a microstructure of finer distribution and small medium austenitic particle size.

Mean austenite particle size affects both the stress-assisted and the strain-induced portion of the total martensitic transformation. During the early stages of deformation, mainly the larger grains deform, whereas smaller grains deform at later stages. The larger the mean austenite particle size is, the higher is the contribution, especially of the strain-induced portion on the transformation. This trend indicates that the size as well as the carbon concentration (important stabilizing factor) play an important role in the stress and strain partitioning between the phases and also between different austenite grains resulting on the kinetics of the martensitic transformation.

5 Modeling of intercritical annealing

5.1 Introduction

Industrial processing of TRIP steels involves various stages of heat-treating, such as Intercritical Annealing and Bainitic Isothermal Treatment, in order to produce a dispersion of retained austenite particles and bainite in a ferritic matrix as mentioned again in Chapter 2. Retained austenite then transforms to martensite during forming processes undergone by the steel. In the present chapter a coupled thermodynamic / kinetic calculation of austenite formation during intercritical annealing of low-alloy TRIP steels is presented. Two low-alloy TRIP steels were investigated. The first of them represents a typical composition of the low-alloy TRIP steels, while the other one contains aluminum as alloying element.

After cold rolling the steels undergo a two-step heat treatment shown in Figure 46, consisting of intercritical annealing followed by isothermal annealing at a lower temperature, to stabilize the retained austenite via the bainitic transformation. Much attention has been paid to the second step, i.e. isothermal annealing, since it was realized that bainite transformation temperature and annealing time affect the amount and stability of retained austenite [69].

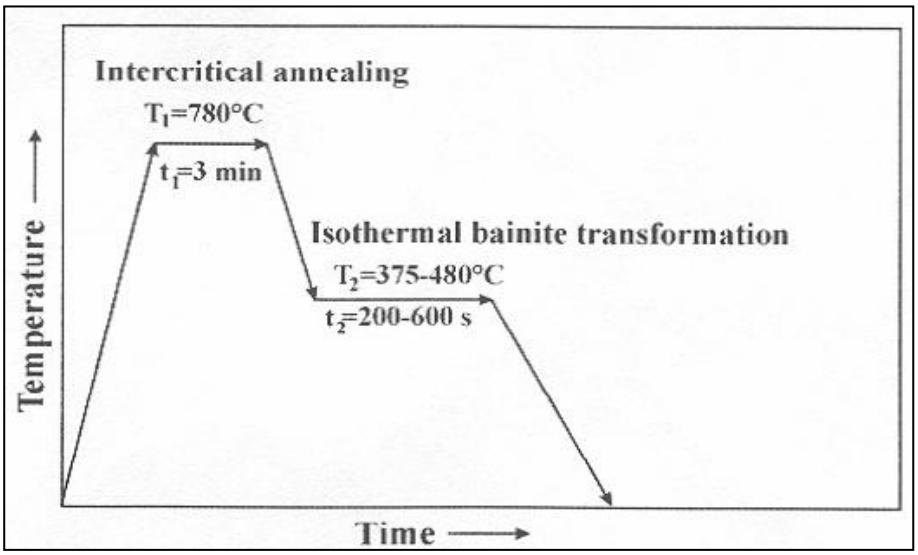

Figure 46: Schematic representation of the two stage heat treatment typically applied in TRIP steels [69]

The first step has received much less attention and in most investigations intercritical annealing is performed at a temperature necessary to produce 50% ferrite and 50% austenite. Usually this temperature is established either experimentally or directly read off the Fe-C phase diagram. It is very important, however, to consider phase transformations which occur upon heating, because the microstructural state after intercritical annealing, i.e. volume fraction, chemical composition and homogeneity of austenite, has a great influence on the kinetics of bainite transformation during the

isothermal annealing step and, thus, on the stability of retained austenite, resulting on the kinetics of the martensitic transformation.

In recent years, computational alloy thermodynamics and kinetics have enabled the simulation of the microstructural evolution during heat treatment under either isothermal or continuous heating conditions. Numerical models have been developed for the solution of the diffusion equations, which enable the prediction of austenite formation during heating of hypoeutectoid steels. In the present chapter, simulation of intercritical annealing is presented. The simulation was performed with the use of Dictra computational kinetics software, which employs a procedure for the numerical solution of the coupled diffusion equations involved, as well as mobility databases for the retrieval of the appropriate kinetic data. Simulation results, regarding the amount and composition of austenite, the rate of transformation and the effect of annealing temperature, are presented and discussed. It is concluded that the simulation can assist the design of the intercritical annealing in these steels.

5.2 The model

The starting microstructure of low-alloy TRIP steels consists of proeutectoid ferrite and pearlite. It is well established that austenite (γ) formation during heating of ferrite/pearlite microstructures proceeds in two steps. The first step is relatively rapid and involves the formation of high-C γ from pearlite. The second step is substantially slower and involves the growth of γ in expense of proeutectoid ferrite (α). Therefore, in the model employed here, the assumption was that pearlite transformation to austenite is completed in a negligible amount of time. The conditions at the end of the first step (i.e. volume fractions and compositions of phases) were considered as initial conditions for the second step. Consequently, the system was considered to initially consist of a high-C γ region (formed of pearlite) with width L_γ, and a proeutectoid α region with width L_α, Figure 47.

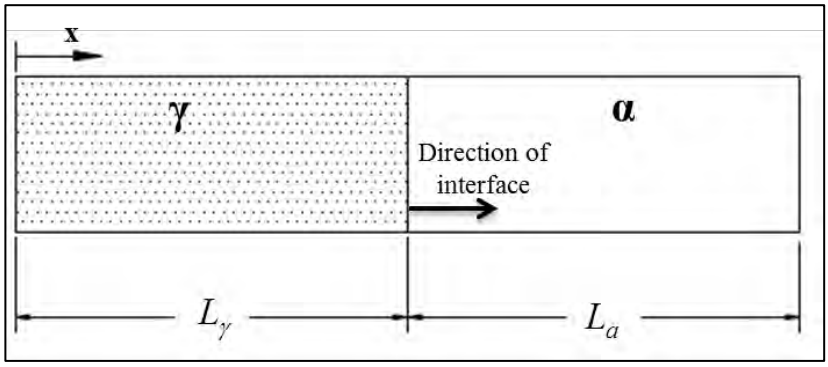

Figure 47: Geometrical model for austenite formation during intercritical annealing

The model is one-dimensional and a planar geometry is assumed. Thus, the initial widths of the two regions L_γ and L_α , can be directly related to the moles of the two phases, n_γ and n_α, calculated at a temperature T_s , which corresponds to the temperature where all pearlite has been dissolved and only γ and proeutectoid α remain in the system :

$$\frac{n_\gamma}{n_\alpha} = \frac{L_\gamma}{L_\alpha} \tag{5.1}$$

The moles n_γ and n_α are calculated with the aid of computational alloy thermodynamics software Thermo-Calc [53] at T_s, and consequently since L_α is known (proeutectoid ferrite grain-size measurement), then L_γ can be calculated by equation (5.1).

Under these conditions simulation of γ formation within the intercritical range (α+γ) can be performed by solving the coupled diffusion equations in the two phases involved. The evolution of concentration profiles of species k, as a function of time in each phase i, $c_k^i(x,t)$

is described by Fick's second law:

$$\frac{\partial c_k^i}{\partial t} = \frac{\partial}{\partial x}\left(D_k^i \frac{\partial c_k^i}{\partial x} \right) \tag{5.2}$$

where c_k^i is the concentration and D_k^i the diffusion coefficient of species k (C, Mn, Si or Al) in phase i (γ or α). The flux of atoms in a multicomponent system with n components is given by Onsager's extension of Fick's first law:

$$J_k^\gamma = -\sum_{j=1}^{n} D_{jk}^\gamma \frac{\partial c_j^\gamma}{\partial x} \tag{5.3}$$

in the austenite-γ region and

$$J_k^a = -\sum_{j=1}^{n} D_{jk}^a \frac{\partial c_j^a}{\partial x} \tag{5.4}$$

in the ferrite-α region. Onsager's law accounts for the diffusive flux of a species k, triggered by the existence of a concentration gradient of another species.

Calculation of the γ/α interface velocity, v, is achieved by applying a mass balance to the interface, which is given by the following equation:

$$v\left({}^{\gamma}c_k^{\gamma/\alpha} - {}^{\alpha}c_k^{\gamma/\alpha} \right) = D_k^a \left(\frac{\partial c_k^\alpha}{\partial x} \right)_{\gamma/\alpha} - D_k^\gamma \left(\frac{\partial c_k^\gamma}{\partial x} \right)_{\gamma/\alpha} \tag{5.5}$$

In equation (5.5), v denotes the velocity of the interface, while D_k^{γ} and D_k^{α} are the diffusion coefficients of species k in the two phases. The diffusion coefficients are temperature and concentration dependent and are calculated using the kinetic data available in Dictra, mob2. ${}^{\gamma}c_k^{\gamma/\alpha}$ and ${}^{\alpha}c_k^{\gamma/\alpha}$ are the concentration of k at the γ and α sides of the interface, respectively. These concentrations are calculated by Thermo-Calc using the SSOL2 database, under the assumption that the phases are in local thermodynamic equilibrium at the interface.
The system is considered not to exchange matter with the surroundings, resulting in the following boundary conditions:

$$\left.\frac{\partial c_k}{\partial x}\right|_{x=0} = 0 \tag{5.6}$$

$$\left.\frac{\partial c_k}{\partial x}\right|_{x=L_\gamma + L_\alpha} = 0 \tag{5.7}$$

Finally, the initial conditions express the concentration of solute atoms in γ and α at the starting temperature T_s, and are given by the following equations:

$$c_k^{\gamma}(x,0) = c_k^{\gamma}(T_s), \quad 0 \le x \le L_\gamma \tag{5.8}$$

$$c_k^{\alpha}(x,0) = c_k^{\alpha}(T_s), \quad L_\gamma \le x \le L_\gamma + L_\alpha \tag{5.9}$$

The initial concentrations $c_k^{\gamma}(T_s)$ and $c_k^{\alpha}(T_s)$ are calculated by Thermo-Calc, as mentioned earlier. The resulting 1-D moving-boundary diffusion problem can be solved by a numerical method for the solution of coupled diffusion equations developed by Ågren [70], which is incorporated in the Dictra computational kinetics software.
Additionally, regarding the annealing temperature T_T, it was considered steady and a little greater than the temperature where all pearlite has been dissolved T_s.

5.3 Results and discussion

Conventional TRIP steel compositions are usually based on the original 0.12–0.55 wt. % C 0.2–2.5 wt. % Mn 0.4–1.8 wt. % Si concept proposed by Matsumura et al [71]. The C content plays a key role in the composition. The typical Mn content in low-alloy TRIP steel is ~1.5% Mn, which is required to achieve hardenability. Mn, being an austenite stabilizer, lowers the temperature at which the cementite starts to precipitate. Mn also lowers the activity coefficient of C in ferrite and austenite and increases the C solubility in ferrite [72]. Si significantly increases the C activity coefficient in both ferrite and austenite and reduces the C solubility in ferrite. Si also

increases the temperature at which the cementite starts to precipitate in ferrite at a given aging time and inhibits the formation of cementite during the austempering stage. This is usually explained by the fact that Si has an extremely low solubility in cementite.

The evolution away from the conventional CMnSi composition is mainly driven by the requirement for continuous galvanizing of AHSS sheet steel for automotive applications: the high Si content results in film-forming surface oxides which prevent the formation of the inhibition layer during hot dip galvanizing [73]. This prevents the wetting of the sheet by the liquid Zn. CMnAl TRIP steels have also received much attention. Aluminum is known to have similar effects on the TRIP behavior as silicon, but giving a better finishing surface at the end of the cold rolling and more importantly accelerating the bainite formation [74]. The disadvantages of the use of Al are the lower solid solution hardening [75] and the fact that Al increases the Ms temperature considerably [73], i.e. Al destabilizes the austenite and moves the start temperature and the Ms –Mf range partly above room temperature.

Simulations of intercritical annealing were performed for the two different low-alloy TRIP steels shown in Table 12. Steel 1 has a typical low-alloy TRIP steel composition containing carbon, manganese and silicon as the major alloying elements. Steel 2 differs from the classical low-alloy TRIP composition as it contains aluminum in the place of silicon.

Table 12: Chemical composition (in mass %) of TRIP steels employed in simulations

Material	C	Mn	Si	Al
Steel 1	0.2	1.5	1.49	-
Steel 2	0.216	1.65	-	1.25

The initial intercritical austenite contains more C than the equilibrium C content of austenite in the intercritical range. The C reaches equilibrium partitioning between the ferrite and the austenite even for relatively short annealing times. The early stages of intercritical austenite formation are controlled by C diffusion, which is followed by the much slower process of Mn and Si diffusion. In industrial continuous annealing lines and in galvanizing lines, the partitioning of the substitutional elements Mn, Si, Al will never reach the equilibrium as the homogenization of the austenite and ferrite is controlled by sluggish substitutional diffusion processes. Figure 48 depicts concentration profiles for C, Mn, Si, Al in steel 1 and steel 2 across the austenite-ferrite phase boundary during intercritical annealing after 10s, 50s, 90s.

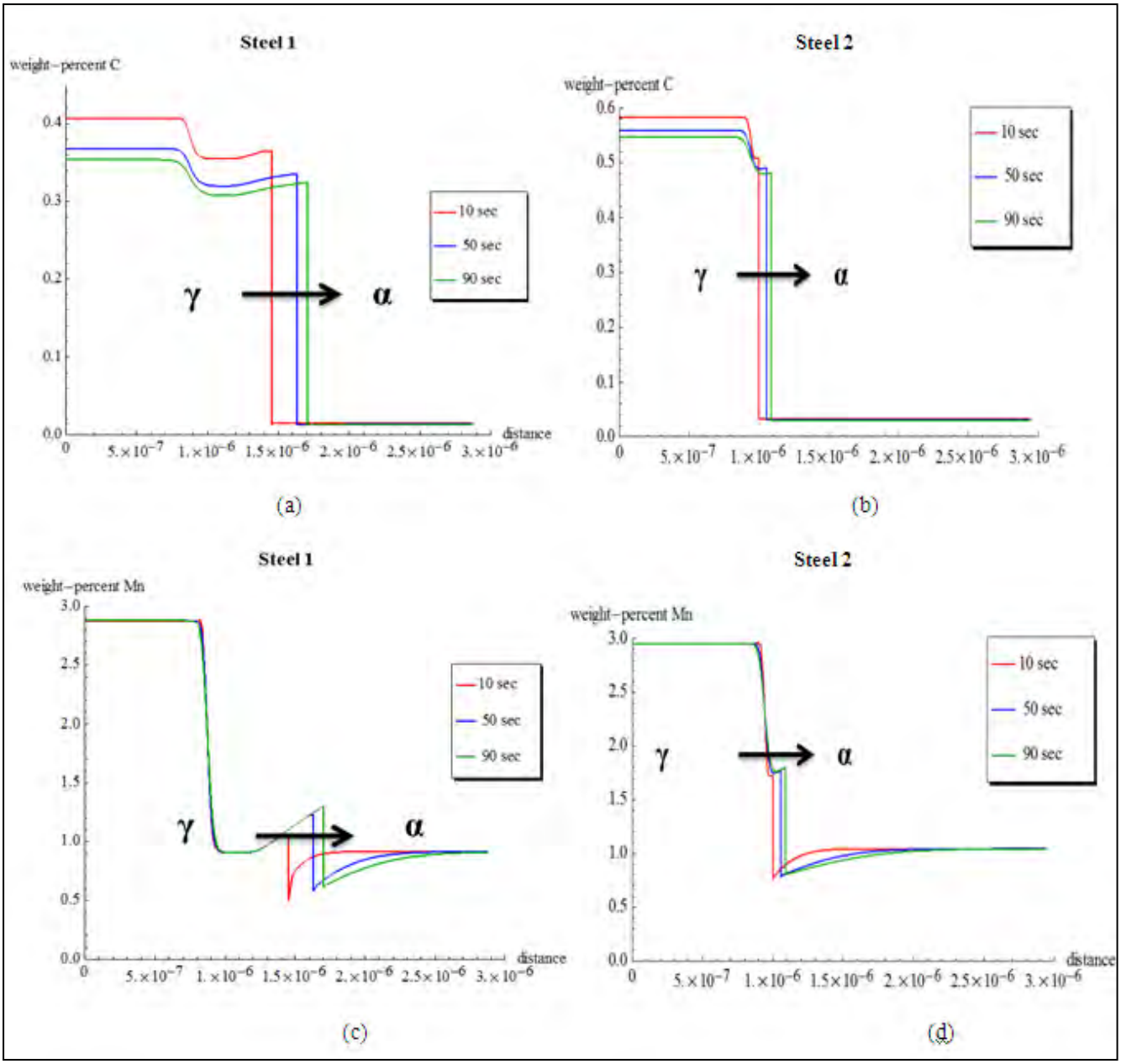

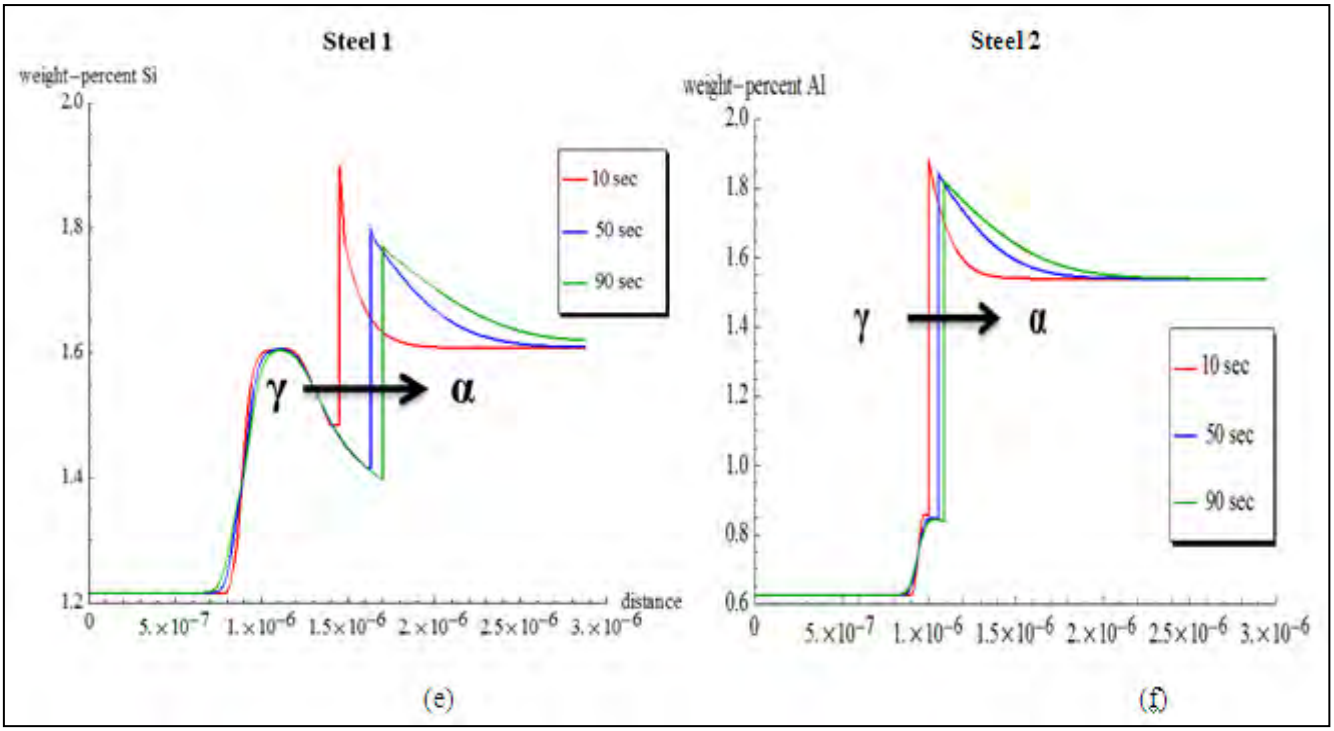

Figure 48: Concentration profiles for (a) C (c) Mn (e) Si in steel 1 , (b) C (d) Mn and (f) Al in steel 2 across the austenite-ferrite phase boundary during intercritical annealing after 10s, 50s, 90s at 817 ^{o}C. The arrow indicates the direction of movement of the phase boundary during intercritical annealing. Whereas the C is expected to reach equilibrium composition, the substitutional solutes are not

The volume fraction of austenite during intercritical annealing depends on the annealing temperature, the residence time at this temperature and the chemical composition of the steel. As it can be seen in Figure 49 which depicts the variation of volume fraction austenite with time for steel 1 and steel 2, annealed at 777 ^{o}C, 797 ^{o}C and 817 ^{o}C, the volume fraction increases with increasing intercritical annealing temperature. According to literature for the Al-TRIP steel, the volume fraction of retained austenite increases with increasing intercritical annealing temperature. However, for the Si-TRIP steel, the amount of retained austenite - i.e., nontransformed austenite - increases and then decreases with increased annealing temperature. At high temperatures, higher amounts of the initial austenite phase lead to greater nucleation of bainite at the isothermal holding temperature. Thus, at annealing temperatures near A_{c3} (temperature at which ferrite completes its transformation into austenite), it is expected that the amount of retained austenite is reduced. Conversely, at relatively low temperatures near A_{c1} (temperature at which austenite begins to form), the volume fraction of the retained austenite decreases due to the lower amount of austenite present at this temperature [76]. The optimum temperature for intercritical annealing has been reported by Chung [77] as:

$$\frac{A_{c1} + A_{c3}}{2} + 20^{o}C \qquad (5.10)$$

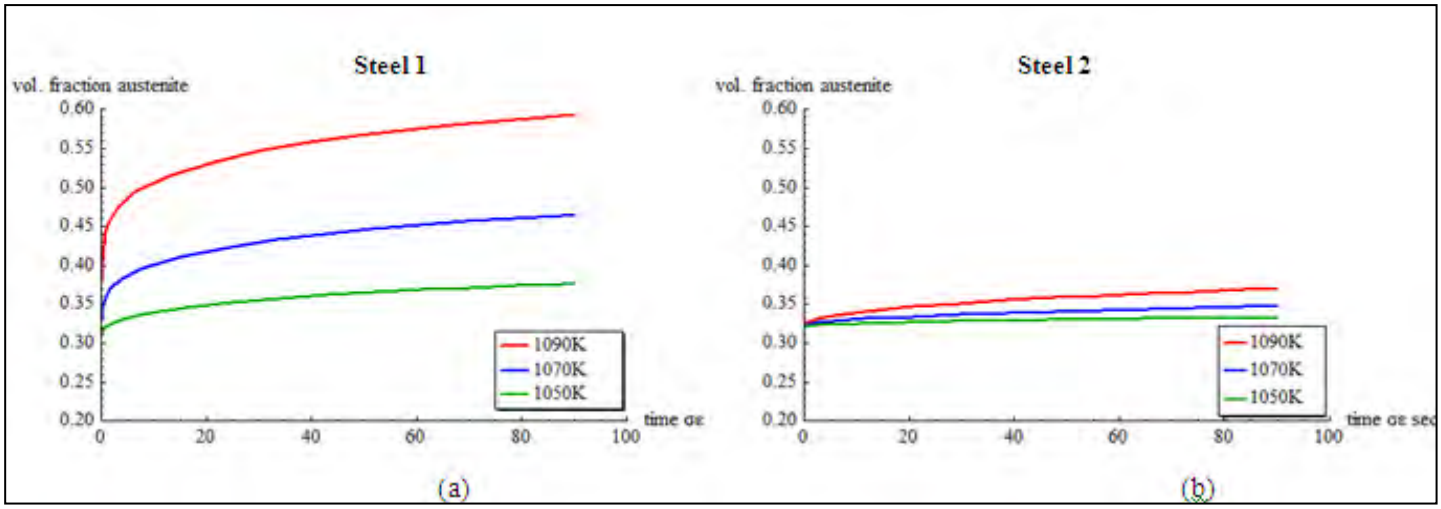

Figure 49: Austenite volume fraction as a function of annealing time for (a) steel 1and (b) steel 2 at 1050K (777 ^{o}C), 1070K (797 ^{o}C) and 1090K (817 ^{o}C)

Kinetics simulation offers a possibility to study the rate of transformation. This can be done by examining the velocity of the γ/α interface with respect to time. Figure 50 presents a typical diagram of v as a function of time, for steel 1 and steel 2 annealed at 817 ^{o}C. It can be seen that the interface velocity decreases rapidly since the annealing temperature is steady and according to literature interface velocity reaches a maximum value and when temperature stabilizes it decreases. This happens, because the driving force decreases as the transformation proceeds. Moreover, the velocity in steel 1 is much greater than the one in steel 2 which justifies the greater volume fraction of austenite as it can be seen in Figure 51 which depicts the variation of volume fraction austenite with time for steel 1 and steel 2, annealed at 817 ^{o}C. Figure 52 depicts the position of interface as a function of annealing time for steel 1and steel 2 at 817 ^{o}C.

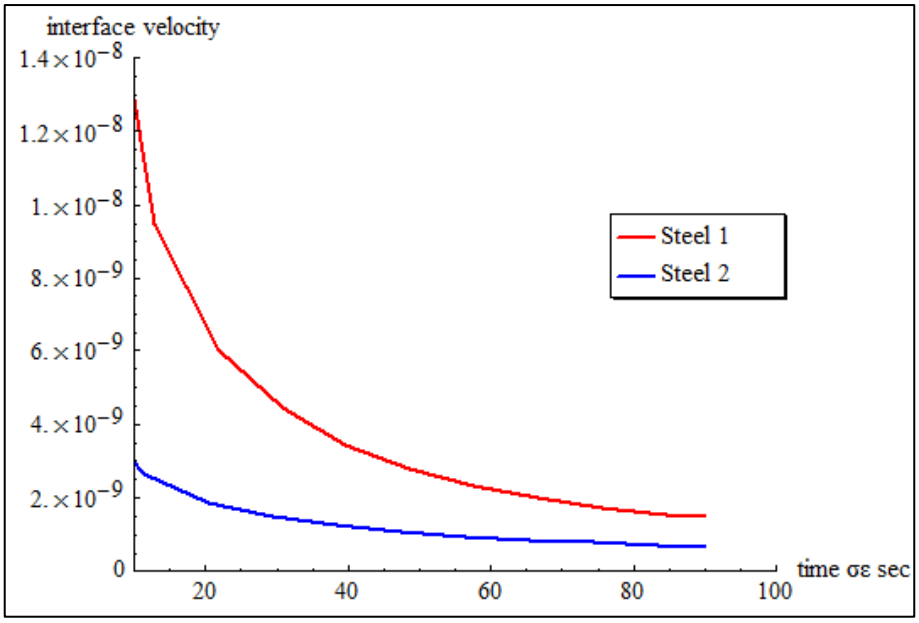

Figure 50: Interface velocity as function of annealing time for steel 1and steel 2 at 817°C

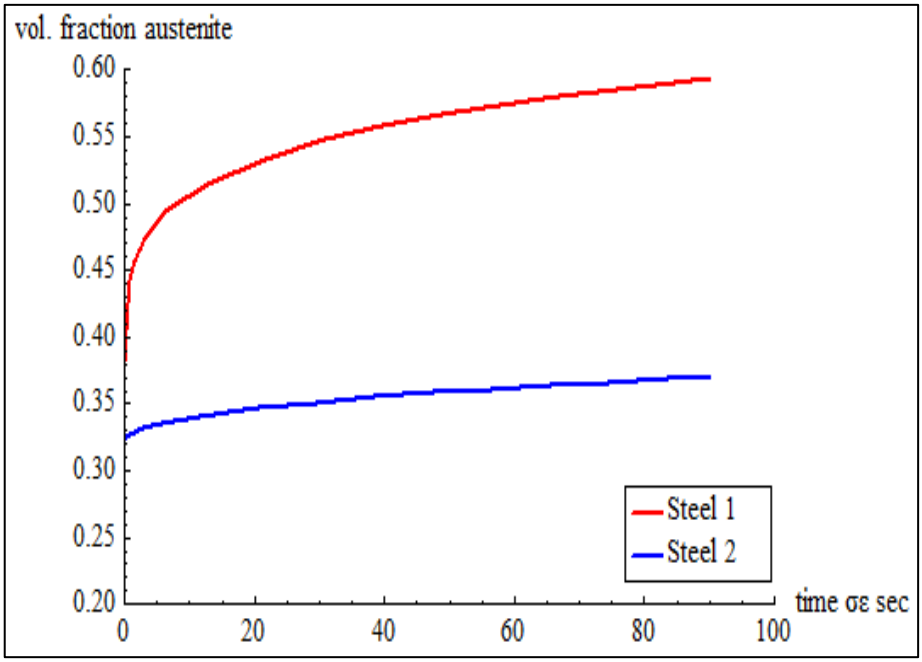

Figure 51: Austenite volume fraction as a function of annealing time for steel 1and steel 2 at 817°C

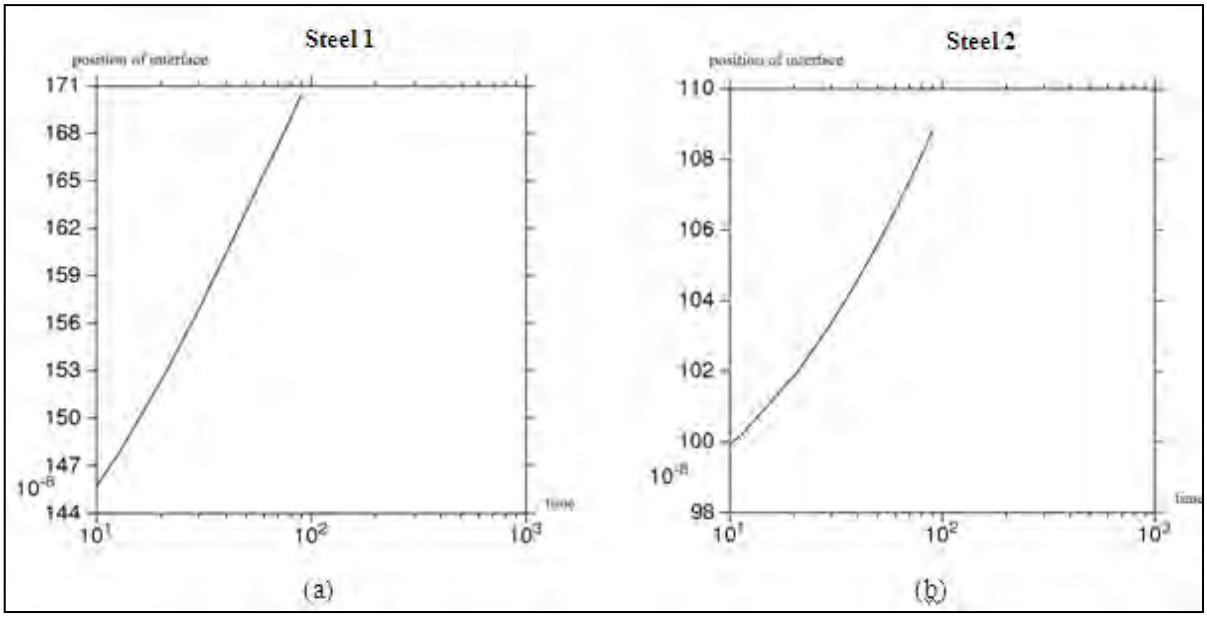

Figure 52: Position of interface as a function of annealing time for (a) steel 1and (b) steel 2 at 817^{o}C

Another interesting result of the kinetics simulation is the concentration profile diagrams, which show the redistribution of the alloying elements during the transformation. Figure 53a shows the concentration profile diagrams for C in steel 1 and in steel 2 annealed at 817 ^{o}C for 90s, while Figure 53b shows the corresponding diagrams for Mn. It can be seen that in steel 2 the formed austenite is more enriched in carbon and manganese, resulting in enhanced austenite stability. This can lead to more stable retained austenite at the final microstructure, i.e. after the isothermal bainite transformation step.

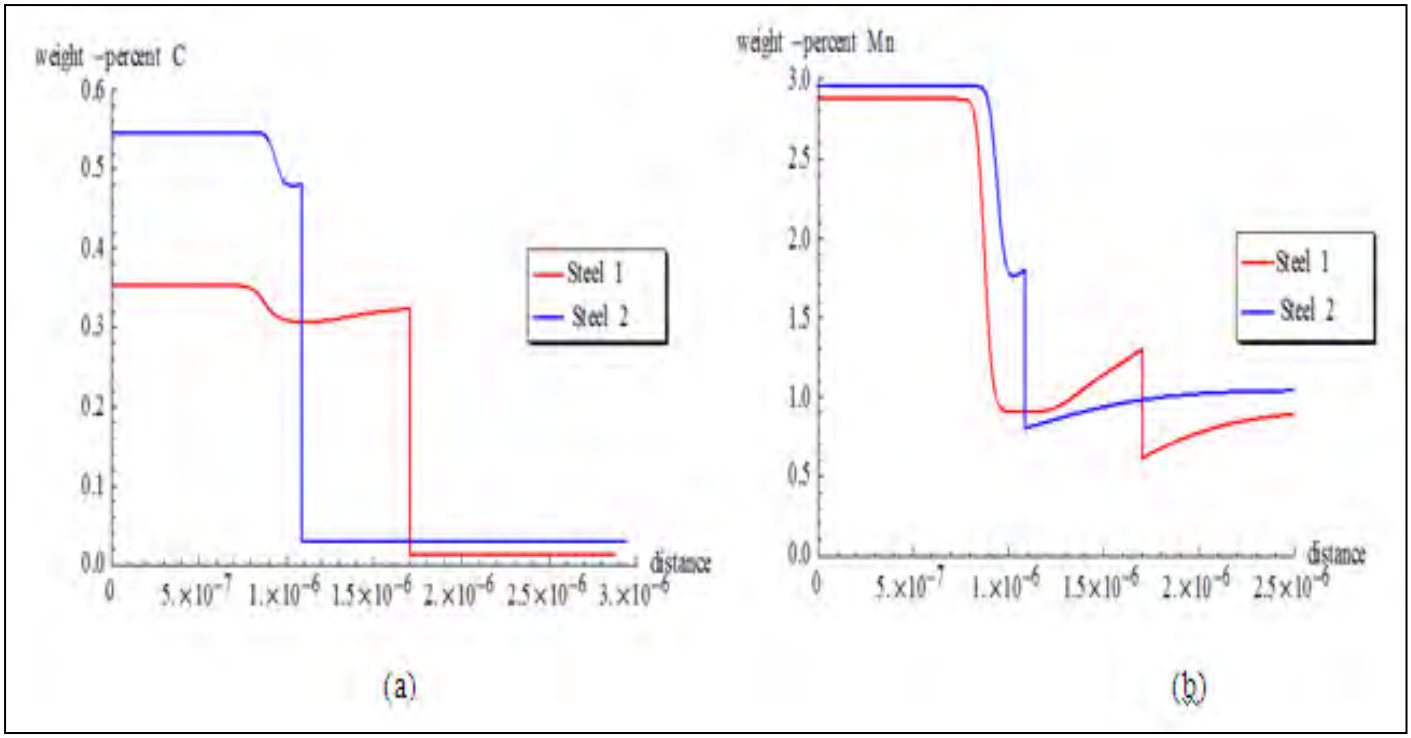

Figure 53: Concentration profiles for (a) C and (b) Mn mass contents in % in steel 1and steel 2, after annealing at 817°C for 90s

5.4 Conclusions

Computational kinetics modeling of austenite formation, during intercritical annealing of TRIP steels, leads to the following concluding remarks:

- The initial intercritical austenite contains more C than the equilibrium C content of austenite in the intercritical range due to the pearlite dissolution.
- The volume fraction of austenite during intercritical annealing depends on the annealing temperature, the residence time at this temperature and the chemical composition of the steel. The volume fraction increases with increasing intercritical annealing temperature and time and is greater for CMnSi TRIP steels
- Interface velocity decreases rapidly when temperature stabilizes. Moreover, the velocity is controlled by the component with the slower diffusion rate.
- In CMnAl TRIP steels the formed austenite is more enriched in carbon and manganese, resulting in enhanced austenite stability. This can lead to more stable retained austenite at the final microstructure, i.e. after the isothermal bainite transformation step.
- Computational kinetics modeling of austenite formation can be used as a powerful tool, for a more accurate design of the intercritical annealing treatment, during the processing of TRIP steels.

6 Conclusions and Suggestions for future work

6.1 Conclusions

A model that describes the kinetics of the evolution of martensite volume fraction during the strain-induced transformation of dispersed austenite in low-alloy TRIP steels has been developed. It is worthy of note that whereas all traditional mechanical constitutive equations do not have a "length scale", the present model introduces though v_p an intrinsic "material length", which is the austenite particle size that can be defined as $L = v_p^{1/3}$ or $R = \left(\frac{3 v_p}{4 \pi} \right)^{1/3}$. Aim of the work presented is to distinguish the individual effect of each one of the factors influencing the austenite stability. The model has been fitted to available experimental data regarding the evolution of martensite as a function of plastic strain for several steels containing austenitic dispersions. Uniaxial tensile tests were carried out and specific experimental procedures were adopted in order to investigate the evolution of mean austenite particle size during deformation. Finally simulation of the intercritical annealing of low-alloy TRIP steels has been carried out.

The experimental techniques and the simulations, which were utilized in the present study, enabled us to obtain a more representative picture of the strain-induced transformation kinetics. The results deducted from the present work are presented below:

- Several factors influence the austenite stability. Besides temperature, the chemical content and the size of the retained austenite are strong stabilizing factors. The chemical driving force ΔG_{ch} is a function of chemical composition and temperature. Especially carbon content has a very strong stabilizing impact. In addition, the transformation fraction increases with decreasing temperature due to the increase of the chemical driving force ΔG_{ch}. Stress triaxiality influences the transformation kinetics through the interaction with the transformation dilatation. It is important to note that the model predicts that the effect of stress triaxiality changes with the average austenite particle size. The effect of stress triaxiality according to the model is not as strong as the particle size effect. However, the stress state applied could become important in austenitic dispersions with high chemical stability.

- As mentioned, austenite particle refinement has a strong stabilizing influence by retarding the strain-induced transformation kinetics according to the model. The experimental results concerning the evolution of the mean austenite particle size during deformation indicate that with increasing plastic strain the martenstitic transformation rate initially increases. As the transformation continues the transformation rate $df / d\varepsilon$ becomes fairly constant and then at higher plastic strains the rate decreases. These results are in agreement with the results obtained by MFM measurements concerning the evolution of the mean

austenite particle size during deformation. The austenitic particles transform progressively. The mean austenitic grain size decreases with increasing plastic strain. At high strain rates the mean austenitic grain size reaches a quite constant value. The stabilizing impact of austenite particle size refinement is evident. Heat treatment, which leads to thinner austenite particle refinement in the final microstructure, enhances the stability of the retained austenite and therefore increases the strength of the steel.

- The transformation rate $df / d\varepsilon$ and the saturation level of the steels examined follow the stability of the retained austenite according to the model describing strain-induced transformation kinetics. The same holds for the stress-assisted portion of the transformation f_{SA}. The lower the stability of the retained austenite, the higher is the contribution of stress-assisted transformation relative to the strain-induced transformation. This is a very important result which indicates that in order to take advantage of the TRIP phenomenon, the design of the heat treatment should lead to optimal stability of the retained austenite. Austenite should transform progressively during deformation.

- The model predicts well the sigmoidal shape of the strain-induced transformation in all of the cases examined in the present work.

- The M_s^{σ} temperature can be used to characterize the stability of the retained austenite. The M_s^{σ} model presented in this thesis can be used as an approximate way to predict the carbon content of the retained austenite, given the fact that the M_s^{σ} temperature is known.

- Computational kinetics modeling of austenite formation, during intercritical annealing of TRIP steels have proved that the volume fraction of austenite depends on the annealing temperature, the residence time at this temperature and the initial chemical composition of the steel. With an increase in the intercritical annealing temperature and residence time, the volume fraction of the formed austenite increases. The initial intercritical austenite contains more C than the equilibrium C content of austenite in the intercritical range due to the pearlite dissolution.

The kinetic model described in this thesis can be used for the development of a constitutive model describing the three dimensional mechanical behavior of TRIP steels containing austenite dispersions. This model could be used for the microstructural design of low-alloy TRIP steels in order to achieve the desired mechanical behavior.

6.2 Suggestions for further work

Based on the work presented in this thesis there are several other aspects, which could be object of future research:

- The model describing the kinetics of evolution of martensite volume fraction during strain-induced transformation, which has been described in the present work, considers stable mean particle size v_p during the transformation. However, as the transformation proceeds the mean austenite particle size decreases. The mean austenite particle size is a function of plastic strain. An equation describing the evolution of the mean austenite particle size as a function of plastic strain could be developed. The implementation of this equation on the available model should not however change the sigmoidal shape of the curve describing the strain-induced transformation.

- The aforementioned constitutive model could be used in connection with the finite element method to predict, not only the tensile behavior, but the more complex stress states encountered in forming operations as well.

- Several other parameters influencing austenite stability could be taken into account by the model.

- Measurement of the C and the Mn content in the retained austenite with the implementation of electron microscopy.

- Further investigation of the intercritical annealing with the use of DICTRA computational software combined with experiments, in order to define the heat treatment, which leads to the optimal stability of the retained austenite.

References

[1] P. L. Kokkonidis, Relation of properties and microstructure in TRIP steels during deformation, PhD Thesis, NTUA, 2012.

[2] A.N. Vasilakos, J. Ohlert, K. Giasla, G.N. Haidemenopoulos, W. Bleck: Steel Research, 73 (2002) 249-252.

[3] Jacques, P.J., Allain, S., Bouaziz, O., De, a., a. F. Gourgues, Hance, B.M., Houbaert, Y., Huang, J., Iza-Mendia, a., Kruger, S.E., Radu, M., Samek, L., Speer, J., Zhao, L., and van der Zwaag, S. On measurement of retained austenite in multiphase TRIP steels -results of blind round robin test involving six different techniques. Materials Science and Technology, 25(5), (2009) 567–574.

[4] A.I. Katsamas, G. N. Haidemenopoulos, N. Aravas: Steel Research, 75 (2004) 737-743.

[5] F. Hassani, and S. Yue, 41st Mechanical Working and Steel Processing Conference Proceedings, Iron and Steel Society/AIME, USA, 37 (1999) 493.

[6] Bhadeshia, H. K. D. H. ISIJ International 42 (2002) 1059.

[7] S. Chatterjee, Transformations in TRIP-assisted Steels: Microstracture and Properties, PhD Thesis, Darwin College, University of Cambridge, 2006.

[8] A.Uenishi, Y. Kuriyama and Takahashi, M. Nippon Steel Technical Report (Japan) 81 (2000) 17.

[9] P. Hedström, Deformation and Martensitic Phase Transformation in Stainless Steels, PhD Thesis, Division of Engineering Materials, University of Luleå, 2007.

[10] G.B. Olson, M. Cohen, Dislocation Theory of Martensitic Transformations (1986) 297-403.

[11] G.N. Haidemenopoulos, Physical Metallurgy. Tziolas Publications.2007.

[12] G.B. Olson, M. Cohen. A mechanism for the strain-induced martensitic transformations*.Journal of the Less-Common Metals, 28, (1972), 107–118.

[13] G.B. Olson. Mechanically Induced Phase Transformations in Alloys (1986).

[14] G.N. Haidemenopoulos, A.N. Vasilakos, Steel Res. 67 (1996) 513-519.

[15] T. Angel, J. Iron Steel Inst., 177 (1954) 165-174.

[16] Mintz, B. Materials Science Forum, (2003) 426-432.

[17] F. B. Pickering, Physical Metallurgy and the Design of Steels, Applied Science Publishers Ltd, England, (1978).

[18] I. D. Choi, D. M. Bruce, S. J. Kim, C. G. Lee, S. H. Park, D.K. Matlock, and J. G. Speer, ISIJ International 42 (2002) 1483.

[19] A. Itami, M. Takahashi, K. Ushioda, ISIJ Int., 35 (1995) 1121-1127.

[20] J. Wang and S. Van Der Zwaag: Metall. Mater. Trans. A, 32A, (2001) 1527-39.

[21] R. E. Cech, D. Turnbull, Trans. AIME 206 (1956) 124-132.

[22] Y.Sakuma, O. Matsumara, and H.Takechi, Metallurgical and Materials Transactions A 22 (1991) 489.

[23] C.P. Livitsanos, P.F Thomson. The effect of temperature and deformation rate on transformation-dependent ductility of a metastable austenitic stainless steel. Material Science and Engineering, 30, (1977) 93-98.
[24] S.S. Hecker, M.G. Stout, K.P. Staudhammer and J.L. Smith. Effects of StrainState and Strain Rate on Deformation-Induced Transformation in 304 Stainless Steel: Part I. Magnetic Measurements and Mechanical Behavior. Metallurgical Transactions A, 13 (4), (1982) 619-626.
[25] K.I. Sugimoto, M. Kobayashi and S.I. Hashimoto Metallurgical and Materials Transactions A 23 (1992) 3085.
[26] J.R. Patel, M. Cohen, Acta Metall. 1 (1953) 531-538.
[27] G. B. Olson,and M. Azrin, Transformation Behavior of TRIP steels, Metall. Trans. A 9A (1978) 713-721.
[28] A.N. Vasilakos, Strain-induced transformation in low-alloy TRIP steels, PhD Thesis, University of Thessaly, 2000.
[29] T. Naturani, G. B. Olson, and M. Cohen, Constitutive flow relations for austenitic steels during strain-induced martensitic transformation, J. de Phys. 43 (1982) 429-434.
[30] G.N. Haidemenopoulos, A.T. Kermanidis, C. Malliaros, H.H. Dickert, P. Kucharzyk, W. Bleck, Mater. Sci. Eng. A 573 (2013) 7-11.
[31] R. Zhu, S. Li, I. Karaman, R. Arroyave, T. Niendorf, H.J. Maier, Acta Mater. 60 (2012) 3022-3033.
[32] J.H. Ryu, J.I. Kim, H.S Kim, C.-S. Oh, H.K.D.H. Bhadeshia, D.-W. Suh, Scripta Mater. 68 (2013) 933-936.
[33] C. Garcia-Mateo, F.G. Caballero, J. Mater. Sci. 44 (2009) 4617-4624.
[34] R. Zhu, S. Li, M. Song, I. Karaman, R. Arroyave, Mater. Sci. Eng. A 569 (2013) 137-143.
[35] Z.H. Cai, H. Ding, X. Xue, J. Jiang, Q.B. Xin, R.D.K. Mishra, Scripta Mater. 68 (2013) 865-868.
[36] Y.F. Shen, Y.D. Liu, X. Sun, Y.D. Wang, L. Zuo, R.D.K. Misra, Mater. Sci. Eng. A, 583 (2013) 1-10.
[37] L. Samek, E. De Moor, J. Penning, B.C. De Cooman, Metall. Mater. Trans. A, 37A (2006) 109-124.
[38] D.C. Ludwingston, J.A. Berger, J. Iron Steel Inst., 207 (1969) 63-69.
[39] O. Matsumura, Y. Sakuma, H. Takechi, Scripta Metall., 21 (1987) 1301-1306.
[40] J. Burke, Kinetics of Phase Transformations in Metals, Pergamon Press, Oxford, United Kingdom, 1965.
[41] N. Tsuchida, Y. Tomota, Mater. Sci. Eng. A, 285 (2000) 345-352.
[42] K. Sugimoto, M. Kobayashi, S. Hashimoto, Metall. Mater. Trans. A, 23A (1992) 3085-3091.
[43] G.B. Olson, M. Cohen, Metall. Trans. A, 6A (1975) 791-795, ISBN: 0-08-0431526.
[44] S. Zhang, K.O. Findley Acta Mater. 61 (2013) 1895-1903.
[45] Q. Zhou, L. Qian, J. Tan, J. Meng, F. Zhang, Mater. Sci. Eng. A 578 (2013) 370-376

[46] R. Blonde, E. Jimenez-Melero, L. Zhao, N. Schell, E. Bruek, S. van der Zwaag, N.H. van Dijk, Mater. Sci. Eng. A 594 (2014) 125-134.
[47] G.B. Olson, Effects of Stress and Deformation on Martensite Formation, Encyclopedia of Materials: Science and Technology, Elsevier Science Ltd, 2001, 2381-2384.
[48] G.B. Olson, M. Cohen, Metall. Trans. A, **7**A (1976) 1897-1904.
[49] G.B. Olson, M. Cohen, Metall. Trans. A, **7**A (1976) 1905-1914.
[50] G.B. Olson, M. Cohen, Metall. Trans. A, **7**A (1976) 1915-1923.
[51] M. Cohen, G.B. Olson, Martensitic Nucleation and the Role of the Nucleating Defect, Proc. First JIM International Symposium (JIMIS-1) Kobe, Japan. Suppl. *Trans. JIM* 17 (1976), 93-98, 1976.
[52] Y. Kuroda, Kinetics of Deformation-Induced Transformation of Dispersed austenite in Two Alloy Systems, SM Thesis, Massachusetts Institute of Technology, 1987.
[53] J.O. Anderson, T. Helander, L. Hoglund, P. Shi, B. Sundman, Calphad 26 (2002) 273-312.
[54] G.B. Olson, K. Tsuzaki, M. Cohen, MRS Proc. 57 (1987) 129-148.
[55] R. Labush, J. Phys. Stat. Solidi 41 (1970) 659-669.
[56] G.N. Haidemenopoulos, M. Grujicic, G.B. Olson M. Cohen, Acta Metall. 37 (1989) 1677-1682.
[57] I-Wei Chen, Y-H. Chiao, K. Tsuzaki, Acta Mater. 33 (1985) 1847-1859.
[58] R.H. Leal, J.R.C. Guimaraes, Microstructure evolution during mechanically induced martensitic-transformation in Fe–31-percentNi–0.1-percent-C. Mater. Sci. Eng. 48 , (1981) 249–254.
[59] W.C. Jeong, D.K. Matlock, G. Krauss, Observation of deformation and transformation behavior of retained austenite in a 0.14C–1.2Si–1.5Mn steel with ferrite bainite austenite structure. Mater. Sci. Eng. A. 165, (1993) 1–8.
[60] J.L. Gonzáles,R. Aranda, M. Jonapá, The Influence of Grain Size on the Kinetics of Strain Induced Martensite in Type 304 Stainless Steel. In: H.Nordberg, and J. Björklund, (Eds.). Applications of Stainless Steel '92, Stockholm, Sweden, (1992) 1009-1016.
[61] D.Q. Bai, A. Di Chiro, S. Yue, Stability of retained austenite in a Nb microalloyed Mn–Si TRIP steel. Mater. Sci. Forum (1998) 253–260.
[62] G. Reisner, E.A. Werner, F.D. Fischer, Micromechanical modeling of martensitic transformation in random microstructures, Int.J. Solids Struct. 35 (1998) 2457–2473.
[63] T. Iwamoto, T. Tsuta, Computational simulation of the dependence of the austenitic grain size on the deformation behavior of TRIP steels. Int. J. Plast. 16 (2000) 791–804.
[64] A. Perlade, O. Bouaziz, Q. Furne´mont, A physically based model for TRIP-aided carbon steels behaviour. Mater. Sci. Eng. A, 356 (2003) 145–152.
[65] E. Leunis, D.Hanlon, A. Rijkenberg, C.Scott, J. Drillet, R. Hackl,Quantitative phase analysis of multi-phase steels-PHAST, Technical steel research, Contract No 7210-PR/359 (2006).

[66] R.L.O Basso, V. L. Pimentel, S. Weber, G. Marcos, T. Czerwiec, I. J. R. Baumvol, Magnetic and structural properties of ion nitrided stainless steel, Journal of Applied Physics, 105(12), (2009) 124914. doi:10.1063/1.3153945.

[67] Q. Furne´mont, M. Kempf,P.J Jacques, M. Goken, F. Delannay, On the measurement of the nanohardness of the constitutive phases of TRIP-assisted multiphase steels, 328 (2002) 26–32.

[68] K. R. Gadelrab, L. Guang, M. Chiesa, S.Tewfik, Local characterization of austenite and ferrite phases in duplex stainless steel using MFM and nanoindentation, Journal of Materials Research, 27, (2012) 1573–1579.

[69] A.I Katsamas, A.N Vasilakos, G.N Haidemenopoulos, Simulation of intercritical annealing in low-alloy TRIP steels, Steel. Res., 71 (2000) 351-356.

[70] J. Ågren, A new numerical method to solve coupled diffusion equations intem. rep. ser. D. No 84, Institutionen för Metallografi, KTH, Stockholm, (1987).

[71] Matsumura O, Sakuma Y, Takechi H. Camp-ISIJ 1985-S1293, 89.

[72] S.J. Kim, C.G. Lee, I. Choi, S. Lee, Effects of heat treatment and alloying elements on the microstructure and mechanical properties of 0.15 wt pct C transformation-induced plasticity-aided cold rolled steel sheet, Metall Trans A, 32A(2001).

[73] J. Mahieu, S. Claessens, B.C. De Cooman, Galvanizability of high strength steels for automotive applications, Metall Mater Trans A, 32A (2001).

[74] C. Garcia-Mateo, F.G. Caballero, Bhadesia HKDH,Acceleration of low-temperature bainit.,ISIJ Int 43(2003).

[75] P.J. Jacques, E. Girault, A. Mertens, B. Verlinden, J. Van Humbeeck, F. Delannay, The development of cold rolled TRIP-assisted multiphase steels Al-alloyed TRIP-assisted multi-phase steels, ISIJ Int 41(2001).

[76] E. Emadoddin, A. Akbarzadeh, G.H. Daneshi, Effect of intercritical anneling on retained austenite characterization in textured TRIP-assisted steel sheet, Materials Characterization vol.57 (2006).

[77] J.H. Chung PhD thesis: Pohang University of Science Technology Pohang (1994).

[78] I. Papatriantafillou, M. Agoras, N. Aravas, G.N. Haidemenopoulos, Comput. Methods Appl. Mech. Engrg. 195 (2006) 5094-5114.

[79] G.B. Olson, M. Cohen. A mechanism for the strain-induced martensitic transformations*.Journal of the Less-Common Metals, 28, (1972), 107–118.

[80] J. Talonen, Effect of strain-induced α'-Martensite transformation on mechanical properties, PhD Thesis, Helsinki University of Technology, 2007.

[81] A.N. Vasilakos, K. Papamantellos, G.N. Haidemenopoulos, W. Bleck:Steel Research, 70 (1999) 466-71.

[82] G.N. Haidemenopoulos, A.N. Vasilakos, Journal of Alloys and Compounds 247 (1997) 128-133.

[83] G.N. Haidemenopoulos, N.Aravas, I. Bellas, Kinetics of strain-induced transformation of dispersed austenite in low-alloy TRIP steels, Mater. Sci. Eng. A 615 (2014) 416-423.

[84] A.G. Mamalis, G.N. Haidemenopoulos, Aspects of ductility, toughness and formability of steel sheet in relation to transformation plasticity, Journ.of Mater.Proces.Techn., 30 (1992) 211-230.

[85] O. Žáček, J. Kliber,I. Schindler, TRIP steel thermomechanical processing simulation and subsequent microstructure evaluation concepts, Acta Mater. 12 (2006) 454-461.